

NAVAL POSTGRADUATE SCHOOL Monterey, California

AD-A219 832



THESIS

DTIC
ELECTE
MAR 29 1990
S E D

A STUDY OF THE VELOCITY STRUCTURE NEAR
A COLD FILAMENT
FROM ADCP AND CTD MEASUREMENTS

by

Francis L. Daggett

September 1989

Thesis Advisor

Steven R. Ramp

Approved for public release; distribution is unlimited.

90 03 28 196

Unclassified

security classification of this page

REPORT DOCUMENTATION PAGE

1a Report Security Classification Unclassified			1b Restrictive Markings		
2a Security Classification Authority			3 Distribution Availability of Report Approved for public release; distribution is unlimited.		
2b Declassification Downgrading Schedule			5 Monitoring Organization Report Number(s)		
4 Performing Organization Report Number(s)			7a Name of Monitoring Organization Naval Postgraduate School		
6a Name of Performing Organization Naval Postgraduate School		6b Office Symbol (if applicable) 35	7b Address (city, state, and ZIP code) Monterey, CA 93943-5000		
6c Address (city, state, and ZIP code) Monterey, CA 93943-5000			9 Procurement Instrument Identification Number		
8a Name of Funding Sponsoring Organization		8b Office Symbol (if applicable)	10 Source of Funding Numbers		
8c Address (city, state, and ZIP code)			Program Element No Project No Task No Work Unit Accession No		
11 Title (include security classification) A STUDY OF THE VELOCITY STRUCTURE NEAR A COLD FILAMENT FROM ADCP AND CTD MEASUREMENTS					
12 Personal Author(s) Francis L. Daggett					
13a Type of Report Master's Thesis		13b Time Covered From To		14 Date of Report (year, month, day) September 1989	
				15 Page Count 123	
16 Supplementary Notation The views expressed in this thesis are those of the author and do not reflect the official policy or position of the Department of Defense or the U.S. Government.					
17 Cosati Codes			18 Subject Terms (continue on reverse if necessary and identify by block number)		
Field	Group	Subgroup	California Current, Filament Mapping, ADCP; <i>Military Thesis, (KT) a</i>		
19 Abstract (continue on reverse if necessary and identify by block number) CTD and ADCP data from the Coastal Transition Zone (CTZ) pilot cruise off Point Arena, California, during June 1987, were combined to make optimal estimates of the current velocity field. The region was characterized by upwelling over the shelf, a single strong offshore geostrophic jet to the north, and a meandering equatorward flow which advected upwelled water from the coastal region up to 150 km offshore. Geostrophic velocity profiles referenced to 500 dbar were adjusted to the ADCP-measured velocity in the 190-274 m layer. Comparison of the unadjusted and adjusted profile sets showed generally good agreement below 200 m but marked differences in several of the profiles above 200 m. Sections of geostrophic and ADCP velocity indicated that the flow in the region was highly geostrophic, but ageostrophic flow components were also present, particularly in the high velocity regions. Volume transport was computed for a portion of the survey area using the two velocity data sets and the Ekman transport, computed from the observed wind data. Transport in the chosen subregion was not balanced due to 1) rapid temporal changes in the meandering upwelling jet, and 2) the influence of high frequency variability which impacted both the CTD and the ADCP data. <i>Keywords: Cold filaments; Ocean currents;</i>					
20 Distribution Availability of Abstract <input checked="" type="checkbox"/> unclassified unlimited <input type="checkbox"/> same as report <input type="checkbox"/> DTIC users			21 Abstract Security Classification Unclassified		
22a Name of Responsible Individual Steven R. Ramp			22b Telephone (include Area code) (408) 646-3162		22c Office Symbol 68Ra

DD FORM 1473.84 MAR

83 APR edition may be used until exhausted
All other editions are obsolete

security classification of this page

Unclassified

Approved for public release; distribution is unlimited.

A Study of the Velocity Structure Near a Cold Filament
from ADCP and CTD Measurements

by

Francis L. Daggett
Lieutenant, United States Navy
B.A., Saint Joseph's College, 1980

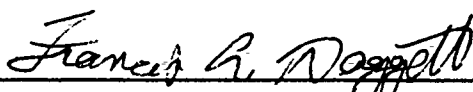
Submitted in partial fulfillment of the
requirements for the degree of

MASTER OF SCIENCE IN PHYSICAL OCEANOGRAPHY


from the


NAVAL POSTGRADUATE SCHOOL
September 1989

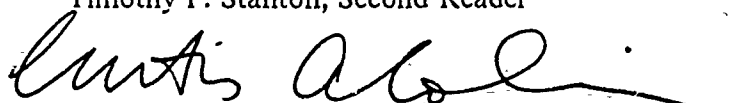
Author:


Francis L. Daggett

Approved by:


Steven R. Ramp, Thesis Advisor


Timothy P. Stanton, Second Reader


Curtis A. Collins, Chairman,
Department of Oceanography

ABSTRACT

CTD and ADCP data from the Coastal Transition Zone (CTZ) pilot cruise off Point Arena, California, during June 1987, were combined to make optimal estimates of the current velocity field. The region was characterized by upwelling over the shelf, a single strong offshore geostrophic jet to the north, and a meandering equatorward flow which advected upwelled water from the coastal region up to 150 km offshore. Geostrophic velocity profiles referenced to 500 dbar were adjusted to the ADCP-measured velocity in the 190-274 m layer. Comparison of the unadjusted and adjusted profile sets showed generally good agreement below 200 m but marked differences in several of the profiles above 200 m. Sections of geostrophic and ADCP velocity indicated that the flow in the region was highly geostrophic, but ageostrophic flow components were also present, particularly in the high velocity regions. Volume transport was computed for a portion of the survey area using the two velocity data sets and the Ekman transport, computed from the observed wind data. Transport in the chosen subregion was not balanced due to 1) rapid temporal changes in the meandering upwelling jet, and 2) the influence of high frequency variability which impacted both the CTD and the ADCP data.

Accession For	
NTIS GRA&I	<input checked="" type="checkbox"/>
DTIC TAB	<input checked="" type="checkbox"/>
Unannounced	<input type="checkbox"/>
Justification	
By _____	
Distribution/	
Availability Codes	
Dist	Avail and/or Special
A-1	



TABLE OF CONTENTS

I. INTRODUCTION	1
II. DATA AND METHODS	3
A. DATA COLLECTION AND PROCESSING	3
B. COMPARATIVE VELOCITY AND TRANSPORT	7
III. RESULTS	9
A. DESCRIPTION OF THE VELOCITY FIELD	9
B. COMPARISON OF ADCP AND GEOSTROPHIC VELOCITY PRO- FILES	12
C. COMPARISON OF VELOCITY SECTIONS	25
D. TRANSPORT COMPARISONS	37
IV. DISCUSSION	39
A. TRANSPORT IMBALANCE	39
B. DIFFERENCES IN ADCP AND GEOSTROPHIC SHEAR	43
V. CONCLUSIONS AND RECOMMENDATIONS	53
A. CONCLUSIONS	53
B. RECOMMENDATIONS	54
APPENDIX A. VERTICAL PROFILES OF HORIZONTAL VELOCITY CAL- CULATED FROM CTD DYNAMIC HEIGHT (REF TO 500 DBAR) AND ADCP DATA	55
APPENDIX B. PROFILES OF ADCP AND ADJUSTED GEOSTROPHIC VE- LOCITY	56
LIST OF REFERENCES	57
INITIAL DISTRIBUTION LIST	59

LIST OF TABLES

Table 1.	ADJUSTMENT LAYER VELOCITY DIFFERENCE STATISTICS FOR LINE 2	22
Table 2.	ADJUSTMENT LAYER VELOCITY DIFFERENCE STATISTICS FOR LINE 3	22
Table 3.	ADJUSTMENT LAYER VELOCITY DIFFERENCE STATISTICS FOR LINE 4	23
Table 4.	ADJUSTMENT LAYER VELOCITY DIFFERENCE STATISTICS FOR LINE B	23
Table 5.	ADJUSTMENT LAYER VELOCITY DIFFERENCE STATISTICS FOR LINE T	24
Table 6.	CROSS-SECTIONAL VELOCITY MAXIMA OF SIGNIFICANT FEATURES.	35
Table 7.	TRANSPORT (SV) THROUGH BOX SIDES (FROM SURFACE TO 274 M)	38

LIST OF FIGURES

Figure 1.	CTD station locations from Part I (June 16-20) of the CTZ pilot cruise	4
Figure 2.	Map of the CTD stations showing the subregion used for volume transport comparisons.	5
Figure 3.	Map of the sea surface dynamic height (dy m) off Pt. Arena during 16-20 June 1987, relative to 500 dbar	10
Figure 4.	Map of the sea surface temperature ($^{\circ}\text{C}$) during 16-20 June 1987	11
Figure 5.	Across-shore geostrophic velocity section, referenced to 500 dbar, for 16-20 June 1987	13
Figure 6.	Geostrophic velocity section, referenced to 500 dbar, for Line 3	14
Figure 7.	ADCP horizontal velocity at 7-23 m	15
Figure 8.	ADCP horizontal velocity at 50 m	16
Figure 9.	ADCP horizontal velocity at 100 m	17
Figure 10.	ADCP horizontal velocity at 150 m	18
Figure 11.	ADCP horizontal velocity at 200 m	19
Figure 12.	Vertical section of density anomaly from Line 3.	21
Figure 13.	Section of geostrophic velocity referenced to 500 dbar for Line 2	26
Figure 14.	Section of ADCP velocity for Line 2	27
Figure 15.	Section of adjusted geostrophic velocity for Line 2	29
Figure 16.	ADCP velocity section for Line 3	30
Figure 17.	Adjusted geostrophic velocity section for Line 3	31
Figure 18.	Geostrophic velocity section, referenced to 500 dbar, for Line 4	32
Figure 19.	ADCP velocity section for Line 4	33
Figure 20.	Adjusted geostrophic velocity section for Line 4	34
Figure 21.	Hourly averages of wind speed and direction	36
Figure 22.	ADCP u-components for station 35	40
Figure 23.	ADCP v-components for station 35	41
Figure 24.	ADCP velocity section for the north side of the box	42
Figure 25.	Ageostrophic velocity section for Line 2	45
Figure 26.	Ageostrophic velocity section for Line 3	46
Figure 27.	Ageostrophic velocity section for Line 4	47
Figure 28.	Time series of ADCP velocity in 50-102 m layer for Line 3 (3-min. averages).	48

Figure 29. Time series of ADCP adjustment (190 - 274 m) layer velocity for Line 3 (3-min. averages).	50
Figure 30. Time series of ADCP adjustment (190 - 274 m) layer velocity for Line 3 (86-min. averages).	51
Figure 31. Time series of ADCP velocity in 50 - 102 m layer (bins 13 - 25) for Line 3 (86-min. averages).	52

I. INTRODUCTION

A very interesting feature of the California Current System is the occurrence of upwelling filaments over and offshore of the continental shelf, from at least as far north as Cape Blanco, Oregon, to Point Conception, California. These cold filaments appear in late spring and summer, when the seasonal regime of steady northwest winds is established and the offshore Ekman transport results in a strong zone of upwelling along the coast (Brink, 1983). This cold upwelled water is advected from the coast to distances of up to several hundred kilometers offshore (Flament, 1985), forming the filaments. Though they are usually rooted at or near headlands, and recur in these locations during successive upwelling seasons, their relation to coastal topography is not well known (Brink, 1983). The irregularities of the coastline (Peffley and O'Brien, 1976; Narimousa and Maxworthy, 1987), variations in the bathymetry of the continental shelf (Preller and O'Brien, 1980; Brink, 1987; Narimousa and Maxworthy, 1985), alongshore variation of the wind stress (Batteen *et al.*, 1989), and wind stress curl (McCreary *et al.*, 1987) are influences which have been theorized as affecting the mesoscale variability along the coast of California and Oregon. Known variously as tongues, plumes, and squirts, filaments may be a significant mechanism in the exchange of coastal upwelled water with the open North Pacific. Comprehension of the dynamics of these filaments is important not only to the understanding of the physical oceanography of the region, but to the study of the biosphere and the meteorology along the coast as well.

The Coastal Transition Zone (CTZ) program, sponsored by the Office of Naval Research, seeks to understand the dynamics and kinematics of this complex and important region. A pilot study was conducted in 1987. As part of that study, a hydrographic cruise was conducted by the R/V POINT SUR near Point Arena, California, from 15 to 28 June 1987. The purpose of the cruise was to create quasi-synoptic three-dimensional maps of the hydrographic and velocity fields in the vicinity of a pronounced cold filament which was observed in the NOAA-9 AVHRR sea surface temperature imagery for 11 June. Guided by this and other imagery, relayed to the vessel in near real time by the Scripps Institution of Oceanography, a survey was conducted using several sensors, including conductivity, temperature and depth (CTD), acoustic Doppler current profiler (ADCP), expendable bathythermograph, thermosalinograph, instrumented drifters, and shipboard meteorological instruments.

The present work examines the velocity structure of the filament from CTD and ADCP measurements taken during 16-20 June 1987. Vertical profiles, horizontal maps, and vertical sections of ADCP and geostrophic velocity were produced.

The velocity fields computed by the geostrophic method differed significantly from the ADCP velocity fields. The causes and magnitude of these differences was of specific interest to this study and is of general interest in physical oceanography. Since neither the CTD nor ADCP data alone are capable of furnishing a completely accurate depiction of the ocean flow, it is desirable to use both together in order to best capitalize on the advantages of each, and to overcome their independent disadvantages. While the modern CTD can be used to obtain quite precise information about the thermohaline circulation, it cannot detect motion which is not density-driven, such as wind-induced currents and certain long-wave motions which play major roles in the ocean circulation. The ADCP, while it can quickly collect velocity data with greater horizontal resolution, is range-limited, and in the shipboard configuration cannot penetrate the deep ocean. Further, ADCP surveys alone cannot resolve the thermohaline component of the circulation. Together, or with other sensors, a much more detailed and accurate description of oceanic flow fields can be obtained. The purpose of this thesis was twofold: 1) to describe the velocity field observed during the cruise using the ADCP and CTD data, and 2) to test a method for combining ADCP and CTD measurements to get an improved estimate of the actual velocity.

The combination method was as follows: First, geostrophic velocity was computed using an arbitrary reference level, in this case no motion at 500 decibars. Next, vertical profiles of cross-sectional velocity obtained from CTD and ADCP data were compared on a station by station basis. The geostrophic velocity profiles were then adjusted to agree with the ADCP profiles in the 190-274 meter depth range. Transport was calculated using the adjusted profiles and compared with the unadjusted and ADCP values and with the Ekman transport calculated from wind data. Velocity sections were produced using the adjusted and unadjusted geostrophic velocity fields and the ADCP velocity measurements. Sections of the ageostrophic velocity component were also produced. Finally, explanations of the differences between the ADCP and adjusted geostrophic velocity field were sought, and several possibilities examined.

II. DATA AND METHODS

A. DATA COLLECTION AND PROCESSING

During Part I of the cruise, which lasted from 16 to 20 June, 53 casts were made with a Neil Brown Mark III-B CTD at approximately 15-kilometer intervals to a maximum depth of 500 meters. Conductivity, temperature, and pressure measurements were sampled at 0.1 m intervals and averaged to 1 m intervals. Locations of the CTD stations are shown (Figure 1) superimposed on NOAA-9 AVHRR sea surface temperature imagery for 16 June. Three sections were made across the cold filament visible in the satellite imagery; these are referred to herein as Line 2 (stations 22-31), Line 3 (stations 33-43), and Line 4 (stations 47-54) (Figure 2). The ship steamed northwest along Lines 2 and 4 and southwest along Line 3, occupying each station in numerical order. However, all sections for these segments are displayed looking offshore, with northwest to the right and southeast to the left.

The temperature, conductivity, and pressure sensors on the CTD were calibrated following the cruise. The pressure calibration used a Chandler Engineering dead weight tester as a standard. At 10 equally spaced pressures from 50 to 500 dbar, indicated pressures from the standard and the CTD sensor were recorded. The differences between recorded values were within the stated accuracy of the sensor (± 1.6 dbar), so no pressure correction was applied.

The temperature calibration was made with a Seabird temperature sensor as a standard. This standard is recalibrated by the manufacturer about every six months. An insulated temperature controlled bath of 70 - 80 liters of fresh water was used to compare the standard and sample sensors at 1 °C increments from 0 - 20 °C. Thirty data points were collected at each temperature and then averaged to yield a single value for each sensor. A regression analysis was run on the 21 data points revealing a linear difference between the standard and sample sensors. The coefficients for the correction to the CTD temperature sensor were 1.00020 (slope) and +0.02361 (intercept).

The conductivity calibration used a Guildline Model 8400 Autosol as a standard. The standard and sample sensor conductivities were compared at five different conductivity levels. Ten samples were taken at each conductivity level and averaged to yield a single value for each sensor at each level. Regression analysis was run comparing the sample cell conductivity with the standard sensor conductivity. A linear correction

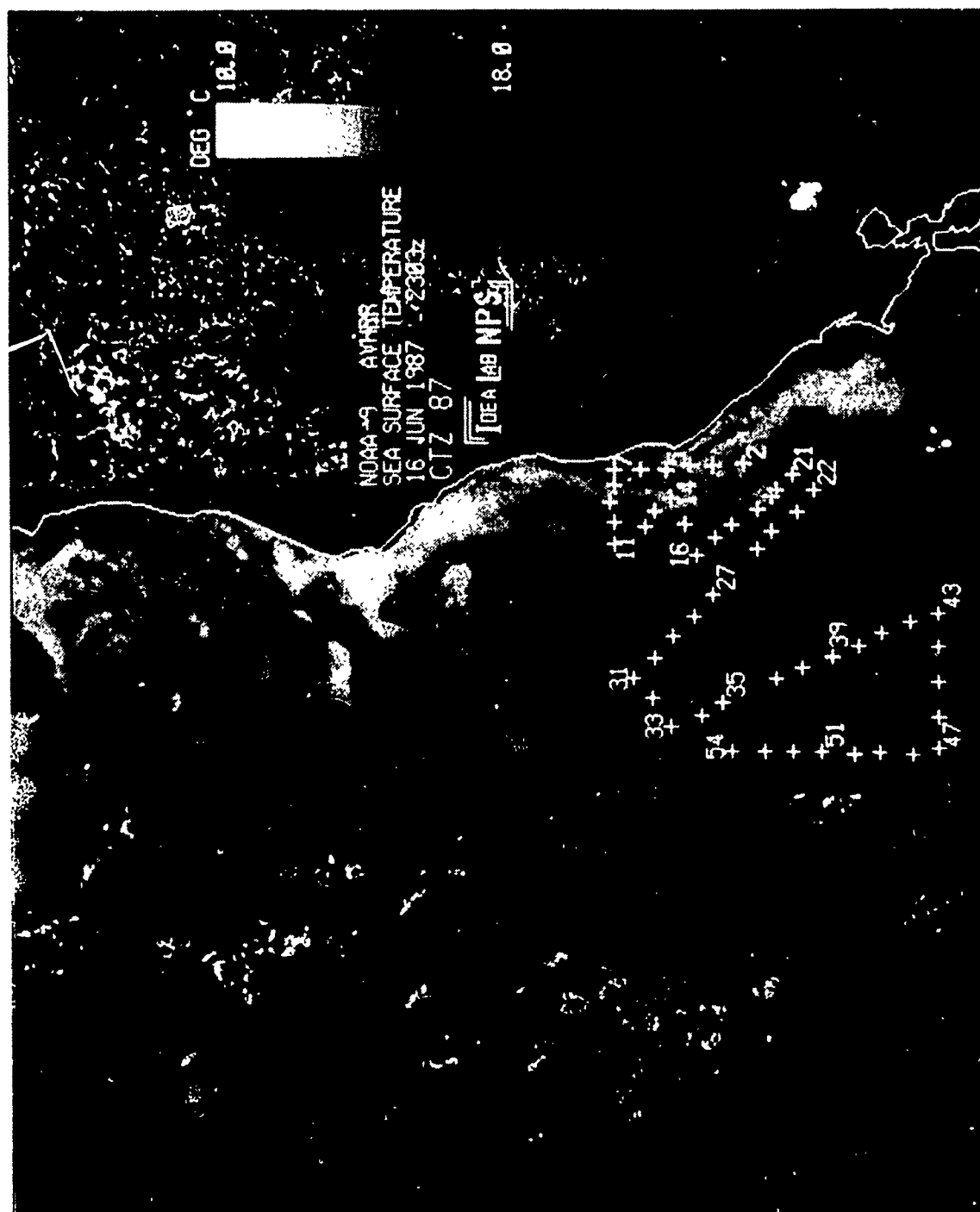


Figure 1. CTD station locations from Part I (June 16-20) of the CTZ pilot cruise: superimposed on AVHRR SST imagery for 2303 UT 16 June 1987 (From Best, 1989).

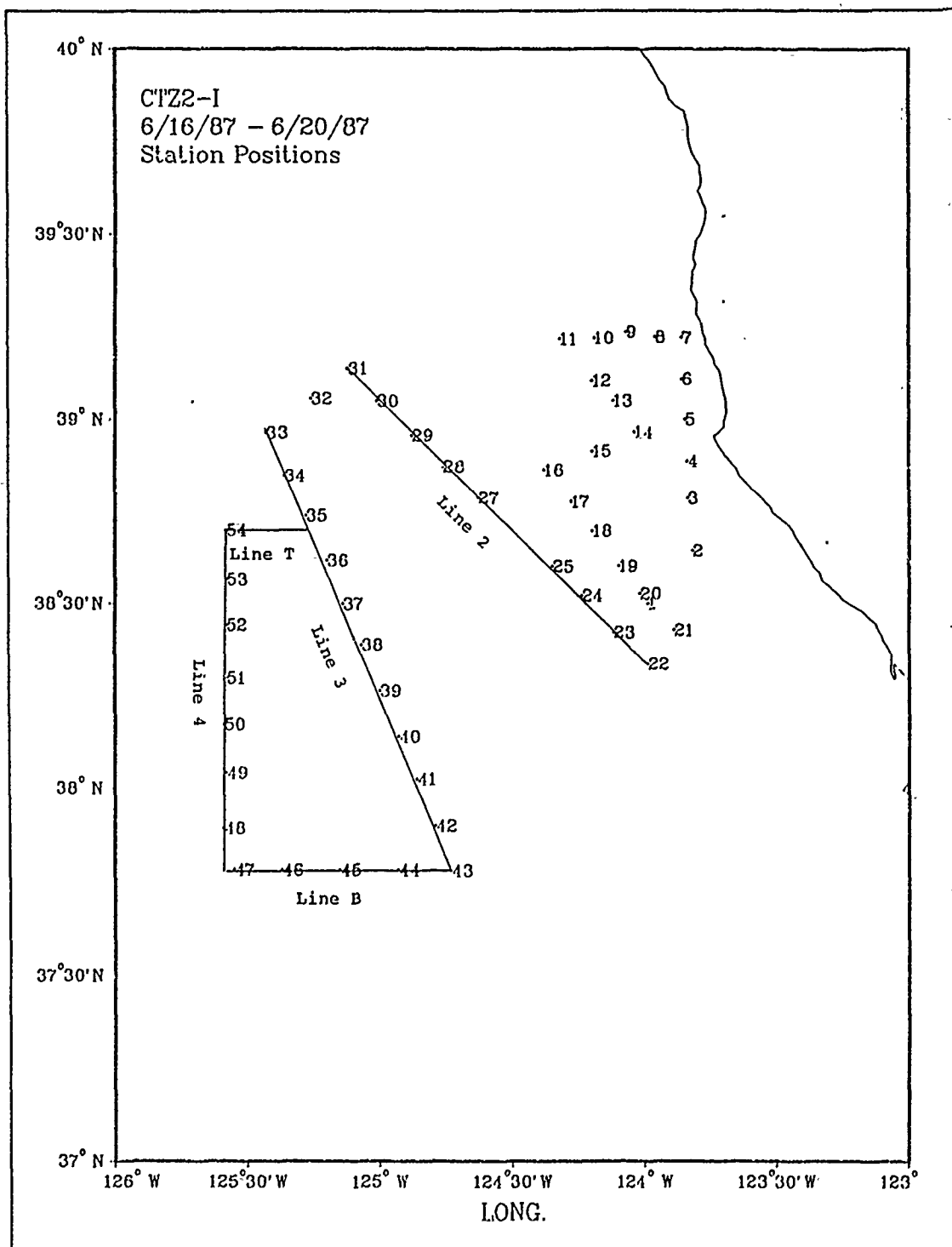


Figure 2. Map of the CTD stations showing the subregion-used for volume transport comparisons.

was found for the CTD sensor with coefficients of 1.001487 (slope) and -0.034173 (intercept).

A total of 42 water samples were taken at seven CTD stations for post-cruise calibration. The CTD pressure, conductivity and temperature were noted as each sample was taken. These numbers, after applying the calibration coefficients, were used to calculate salinity and the results compared with the water sample salinities calculated using the Autosal in the laboratory. In order to avoid erroneous comparisons due to ship roll in areas of high vertical salinity gradients, samples were eliminated from consideration if the salinity within 2 m of the nominal sample depth changed more than 0.01 PSU, reducing the number of comparable points to 32. The mean difference between the Autosal-calculated salinities and those from the CTD was +0.005, with a range of -0.077 to +0.025. No further adjustments were made to the CTD conductivities based on water bottle sample comparisons (Jessen, Ramp and Clark, 1989).

Acoustic Doppler velocity was obtained by using an RD Instruments ADCP mounted in the POINT SUR's seachest, operating on a nominal frequency of 150 kHz. Relative velocities from each acoustic pulse or "ping" were averaged over three minutes for storage, along with vessel motion information from the ship's LORAN-C and Sperry gyrocompass. Data were collected in 4 m vertical bins to an average of 380 m depth, ranging from a minimum of 172 m in heavy seas to 464 m when the ship was stopped. The navigation input introduced the greatest error into the final ADCP velocities.

For each three-minute averaged profile, a reference layer was chosen in which it was assumed that the water velocity was constant for the duration of the averaging period. The absolute velocity of this layer was calculated by subtraction of the ship's velocity, then low-pass filtered with a Hamming window filter having a cutoff period of 25 minutes. The relative ADCP profiles were then adjusted to the filtered reference layer velocity, thus producing three-minute profiles of absolute u , v , and w . Vertical velocities were considered to be below the instrumental noise level for a shipboard ADCP and were not used in this study. Detailed discussion of the accuracy of ADCP measurements can be found in Kosro (1986), Firing *et al.* (1988), and Chereskin *et al.* (1989). For this study the noise level of the ADCP absolute velocity was assumed to be on the order of $5 - 10 \text{ cm s}^{-1}$ for 15 minute averages.

These ADCP profiles were further averaged before analysis began. The averaging interval was chosen according to the type of presentation desired. For plan views of horizontal velocity vectors, a 30-minute time interval was used to filter higher frequency oscillations. For profiles of cross-sectional velocity and comparison with geostrophic

profiles, the ADCP data was spatially averaged over the corresponding distance between CTD stations, which was approximately 15 km. This resulted in a minimum of 25 3-minute ADCP profiles being averaged for each CTD station pair. For contoured velocity sections, a 12.5 km spatial filter gave greater resolution than the 15 km CTD station spacing but eliminated overlapping of the averaging intervals, based on a maximum ship speed of 9 knots. In all cases the ADCP velocity was vertically averaged over four bins (16 m).

B. COMPARATIVE VELOCITY AND TRANSPORT

To compare geostrophic and ADCP velocities, geostrophic velocity was calculated for each station pair using 500 decibars (the deepest level sampled) as the level of no motion. Geostrophic velocity was computed by the dynamic height method at four meter intervals using the program GEOVEL on the IBM mainframe computer at the Naval Postgraduate School.

ADCP velocity profiles were produced by calculating cross-sectional velocity averaged over the distance between CTD stations using the program TRANSPRT on the NPS Oceanography Department IBM PC network. The zonal and meridional components of velocity were converted into across-track velocities, and all three-minute absolute velocity profiles within the specified time period were spatially averaged to produce a single profile of the cross-sectional velocity in 16-meter vertical bins. Actual station spacing was calculated for each station pair for input as the spatial averaging interval.

For the Ekman transport calculations, relative wind data, measured at 10 m height, was recorded by the SAIL (Serial ASCII Instrumentation Loop) Data Acquisition System and processed with the ship's velocity and heading information from LORAN-C and gyrocompass to obtain true wind data which was spatially averaged over each CTD station interval. The averaged winds were rotated from a u, v , coordinate system into an along-track (v_{AL}) and across-track (v_{AC}) coordinate system.

A drag coefficient was calculated (after Large and Pond, 1981) from the spatially averaged wind speed by

$$c_D = 1.14 \times 10^{-3}, W < 10 \text{ m s}^{-1}, \text{ or}$$

$$c_D = 0.49 \times 10^{-3} + (0.065 \times 10^{-3} \times W), W > 10 \text{ m s}^{-1}.$$

The along-section wind stress was then computed as

$$\tau_{AL} = \rho_a c_D |v| v_{AL},$$

where ρ_a is the density of air and v_{AL} is the along-track wind velocity. The Ekman transport normal to the transect was calculated as

$$T_E = \frac{\tau}{\rho_w f} S,$$

where ρ_w is the density of seawater, f is the Coriolis parameter, and S is the distance between stations.

The aforementioned programs, as well as those used to produce vertical sections and horizontal vector maps, were written by Mr. P. Jessen at NPS.

III. RESULTS

A. DESCRIPTION OF THE VELOCITY FIELD

A map of the dynamic height at the surface relative to 500 dbar (Figure 3) shows a meandering flow centered near $38^{\circ} 15' \text{ N}$, $124^{\circ} 45' \text{ W}$. The southward flow nearshore at the northern edge of the survey area turns sharply near Point Arena and flows westward to an offshore distance of about 150 km, then recurves to return shoreward to the south. Both offshore and onshore flows are indicated, with weak flow inside the meander. Another strong flow appears to the north of the filament, indicated by the 0.84 - 0.88 dynamic height isopleths, flowing southwestward through the survey area, entering between stations 29 and 30 and exiting near stations 52 and 53. This flow can be observed visually in the SST imagery (Figure 1) as a second cold filament, which seems to be rooted in the north near Cape Mendocino, and is being advected southward and offshore along the inshore edge of a warm, anticyclonic eddy. The dynamic height field was well correlated with the sea surface temperature field shown in the NOAA-9 AVHRR image (Figure 1) and in the map of sea surface temperature (Figure 4). Cold ($< 12^{\circ} \text{C}$) upwelled water from along the coast is advected offshore in the meander; to the north and south in the survey region, strong flows indicated by closely spaced dynamic height contours correspond to surface thermal gradients (Figures 3 and 4).

Alongshore and cross-shore geostrophic velocity sections (Figure 5 and Figure 6) show the vertical structure of the flow. The cross-shore section shows that there was a strong ($> 35 \text{ cm s}^{-1}$) equatorward jet over the slope, associated with the sharp temperature gradient along the offshore edge of the upwelling region. A second, weaker equatorward flow was located further offshore; this corresponds to the strong flow north of the meander. In this section the flow appears diffused due to the wide station spacing; note also that this section was non-synoptic; the interval from station 7 to 54 was 3.5 days. Stations 7-11 were occupied over a four-hour interval, from 1810 to 2217 UT on 16 June. Station 29 was occupied at 1418 UT on 18 June, station 34 at 2256 UT on 18 June, and station 54 at 0613 UT on 20 June. The alongshore section was continuously occupied, with about 1.4 hours between each station. The northern geostrophic offshore flow was approximately 60 km wide and extended well below 200 m. The offshore flow ascribed to the meander was located just to the south, was about 35 km wide, and extended below 300 m. The onshore flow was broader, and though its southernmost extent

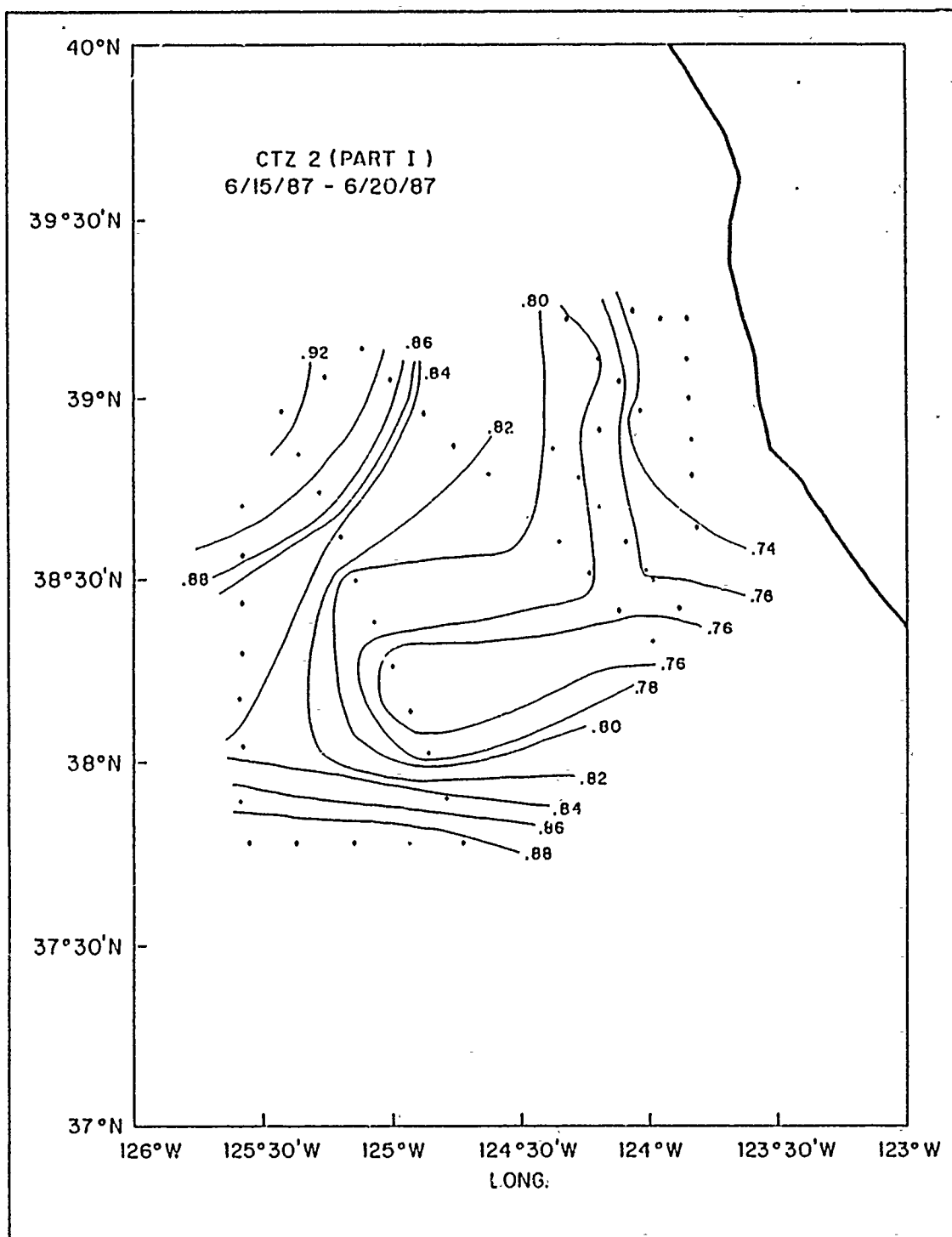


Figure 3. Map of the sea surface dynamic height (dy m) off Pt. Arena during 16-20 June 1987, relative to 500 dbar

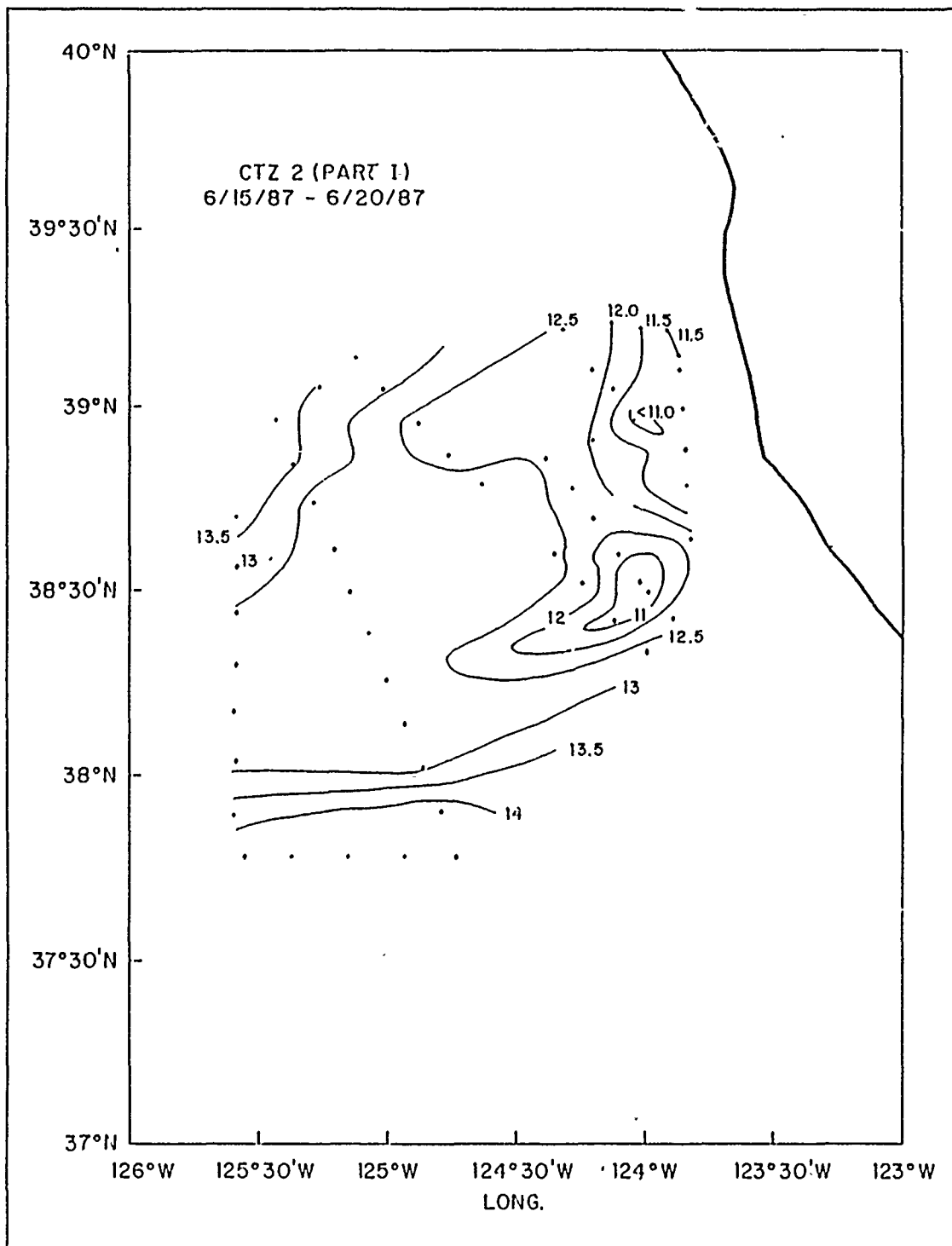


Figure 4. Map of the sea surface temperature (°C) during 16-20 June 1987.

was not surveyed it was at least 60 km wide, with flow over 5 cm s^{-1} below 300 m. The geostrophic section shows the offshore flow of the meander was weaker across this line than the onshore flow.

These main features were also apparent in the horizontal ADCP velocity vector maps (Figures 7 - 11). These show 30-minute average velocity vectors, plotted at 8 km intervals. From these it can be seen that the meandering current structure extended quite deep, with the meandering pattern still evident at 200 m offshore. The geostrophic jet to the northwest seems to increase in depth as it flows seaward; it was not evident at the 150 m or 200 m levels where it entered the survey region, but was evident where it departed to the west. The good qualitative agreement, in regions of high velocity, between the dynamic height field and the shallow ADCP vectors indicates that the flow in the region was highly geostrophic.

The ADCP, contrary to the geostrophic flow, shows stronger offshore flow along this line and weaker onshore return flow. This was consistent with the sign of the Ekman transport (discussed in more detail later). Other studies of similar features near Point Arena have found the offshore flow of the meander to be of higher velocity than the onshore flow. Flament *et al.* (1985) inferred velocity by tracking distinctive features in satellite images during July 1982. ADCP surveys conducted by Kosro and Huyer (1986) and Jessen and Ramp (1989) found stronger offshore flow and weaker return flow in meanders off Point Arena in July 1981 and 1982 for the former (the 1982 feature being the same as in Flament *et al.*, 1985) and in July 1988 for the latter.

Away from high velocity zones agreement is degraded, as for example near the middle of Line 4. Here the dynamic height gradient was small, and the Ekman transport and other ageostrophic velocity components may dominate the velocity field. In areas where the actual flow was very weak, such as below 150 m, the noise level of the ADCP measurements ($5\text{-}10 \text{ cm s}^{-1}$) became a problem, indicating deep velocity structure not indicated by geostrophy and which does not necessarily reflect the true oceanic flow.

B. COMPARISON OF ADCP AND GEOSTROPHIC VELOCITY PROFILES

Profiles of the cross-sectional component of absolute ADCP velocity and geostrophic velocity relative to 500 dbar were plotted for each station pair along the three cross-filament sections, Lines 2, 3, and 4 (Appendix A). In general, the ADCP profiles showed greater velocity in the direction of flow than geostrophy. Where the flow was strongly offshore, as between stations 34 and 35 or stations 53 and 54, ADCP velocity was generally greater in the offshore direction by 4 to 40 cm s^{-1} , though an ex-

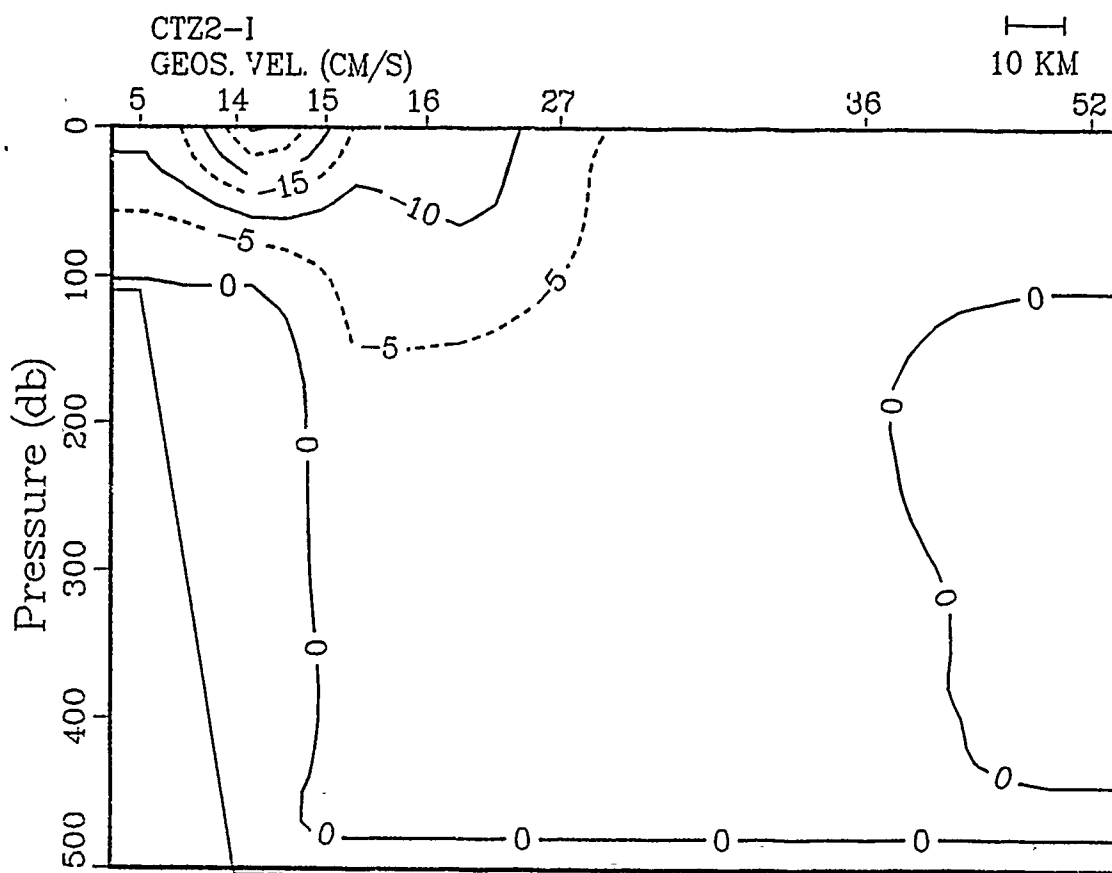


Figure 5. Across-shore geostrophic velocity section, referenced to 500 dbar, for 16-20 June 1987: The view is looking northward, with the coast on the right. Positive velocity is poleward (into the page), and negative velocity equatorward (out of the page).

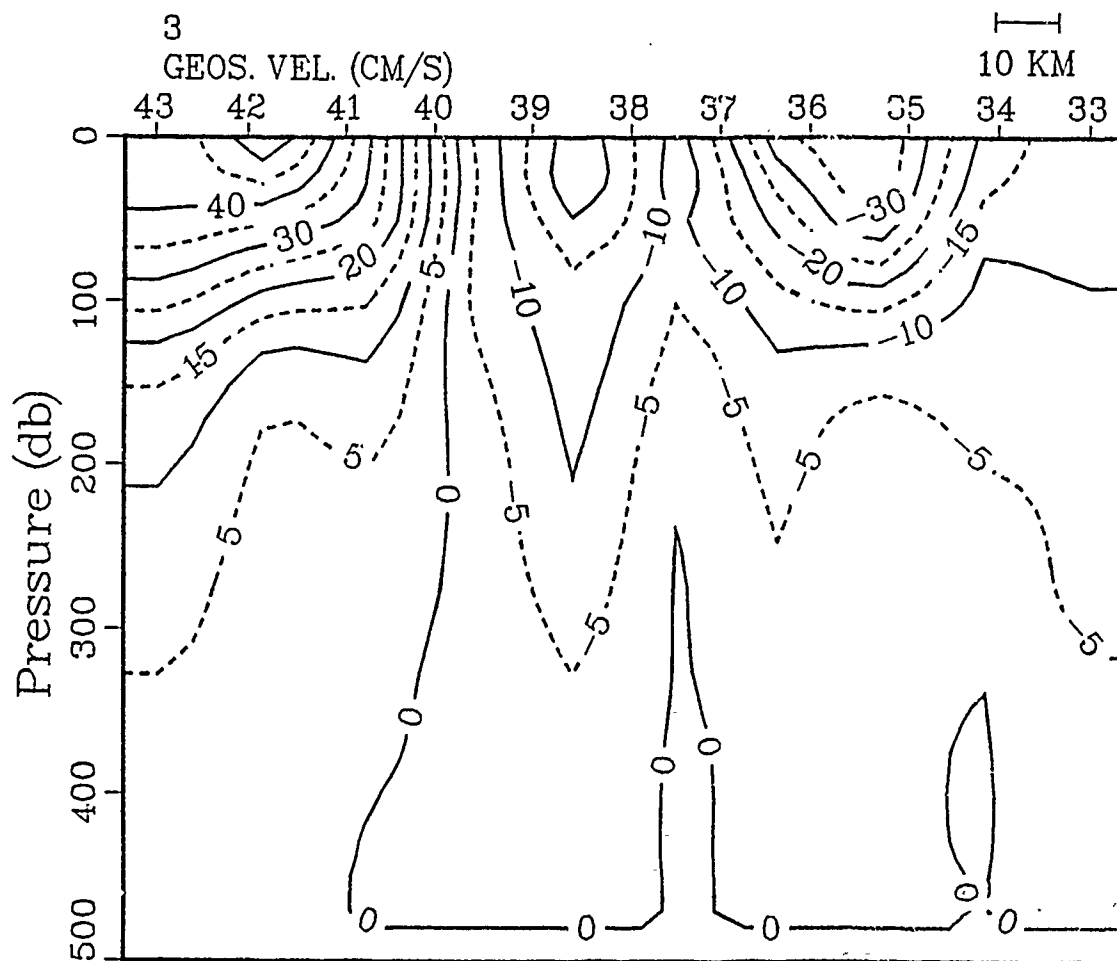


Figure 6. Geostrophic velocity section, referenced to 500 dbar, for Line 3: The view is looking offshore, with northwest to the right. Positive velocities are onshore (out of the page), and negative velocities offshore (into the page).

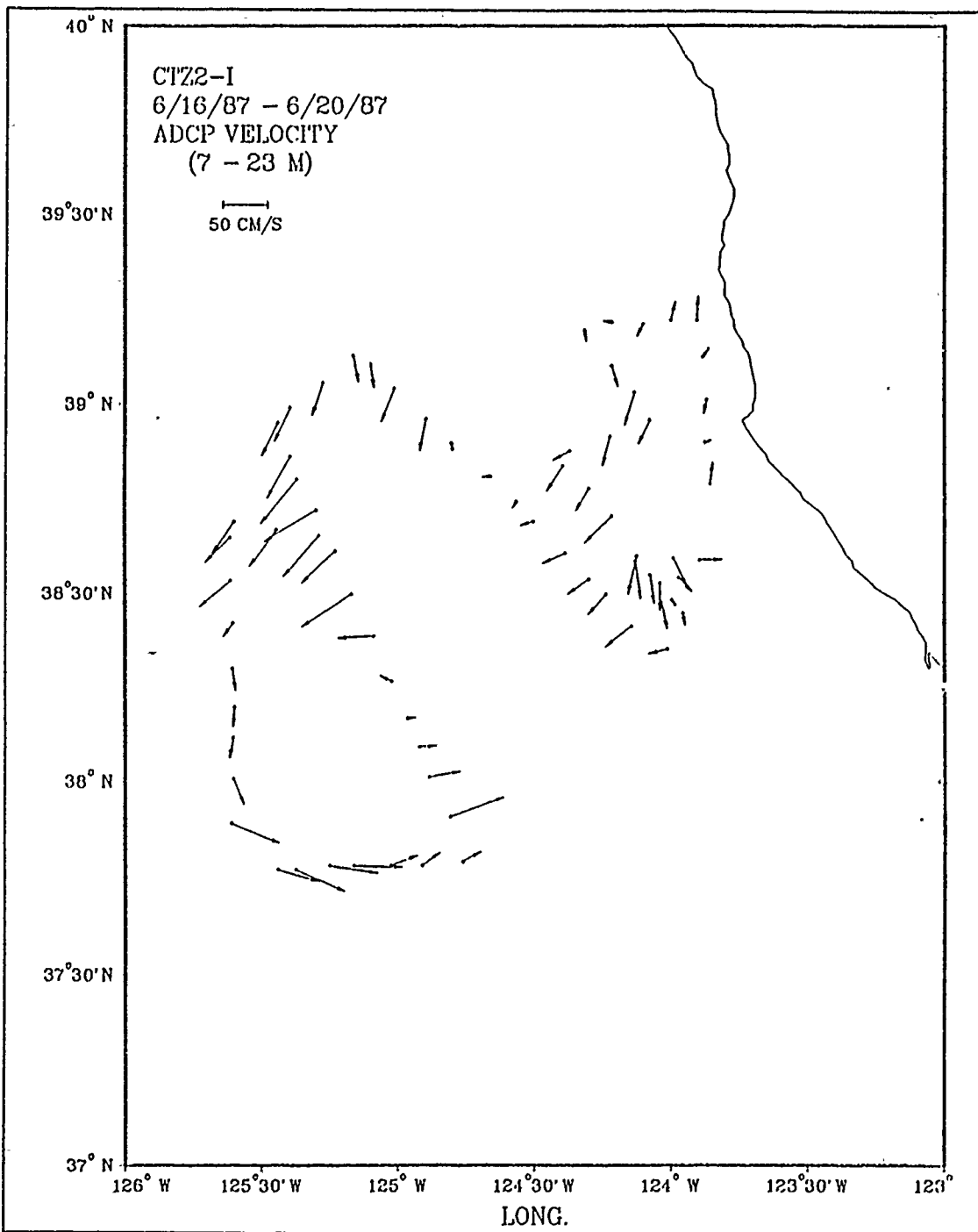


Figure 7. ADCP horizontal velocity at 7-23 m: Horizontal velocity vectors for bins 2-5 temporally averaged over 30 min. and plotted at 8 km intervals.

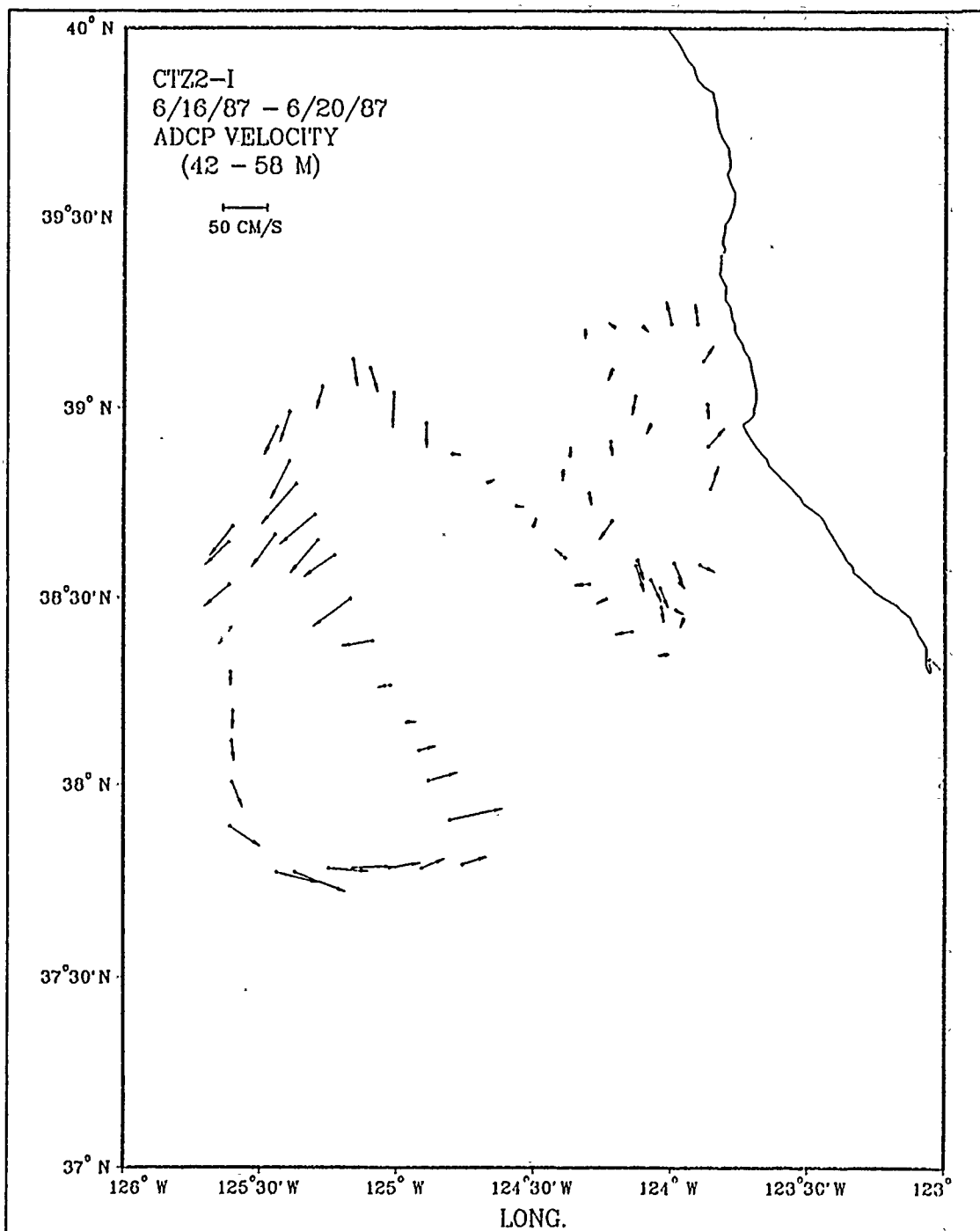


Figure 8. ADCP horizontal velocity at 50 m: Horizontal velocity vectors for bins 11-14 temporally averaged over 30 min. and plotted at 8 km intervals.

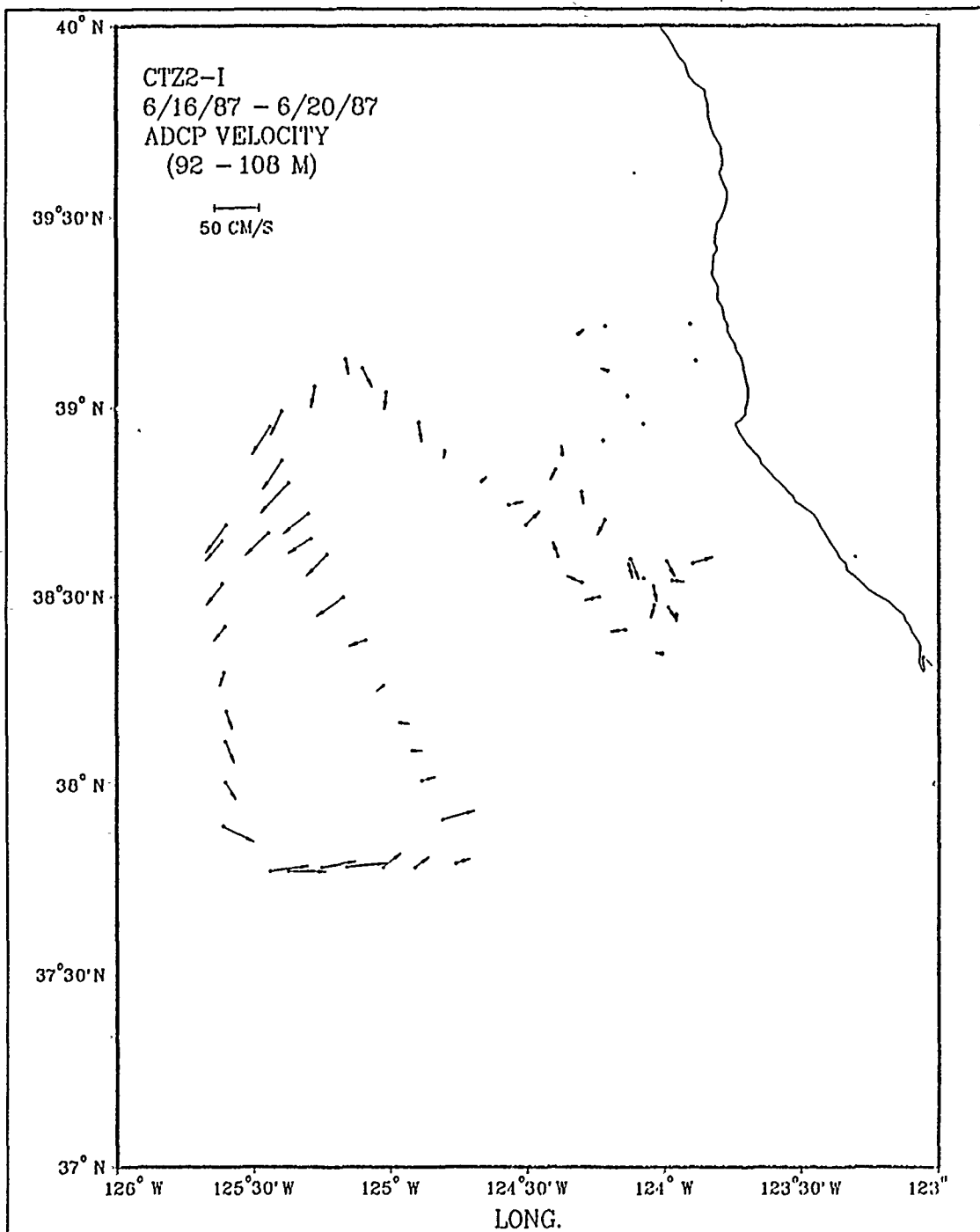


Figure 9. ADCP horizontal velocity at 100 m: Horizontal velocity vectors for bins 23-27 temporally averaged over 30 min. and plotted at 8 km intervals.

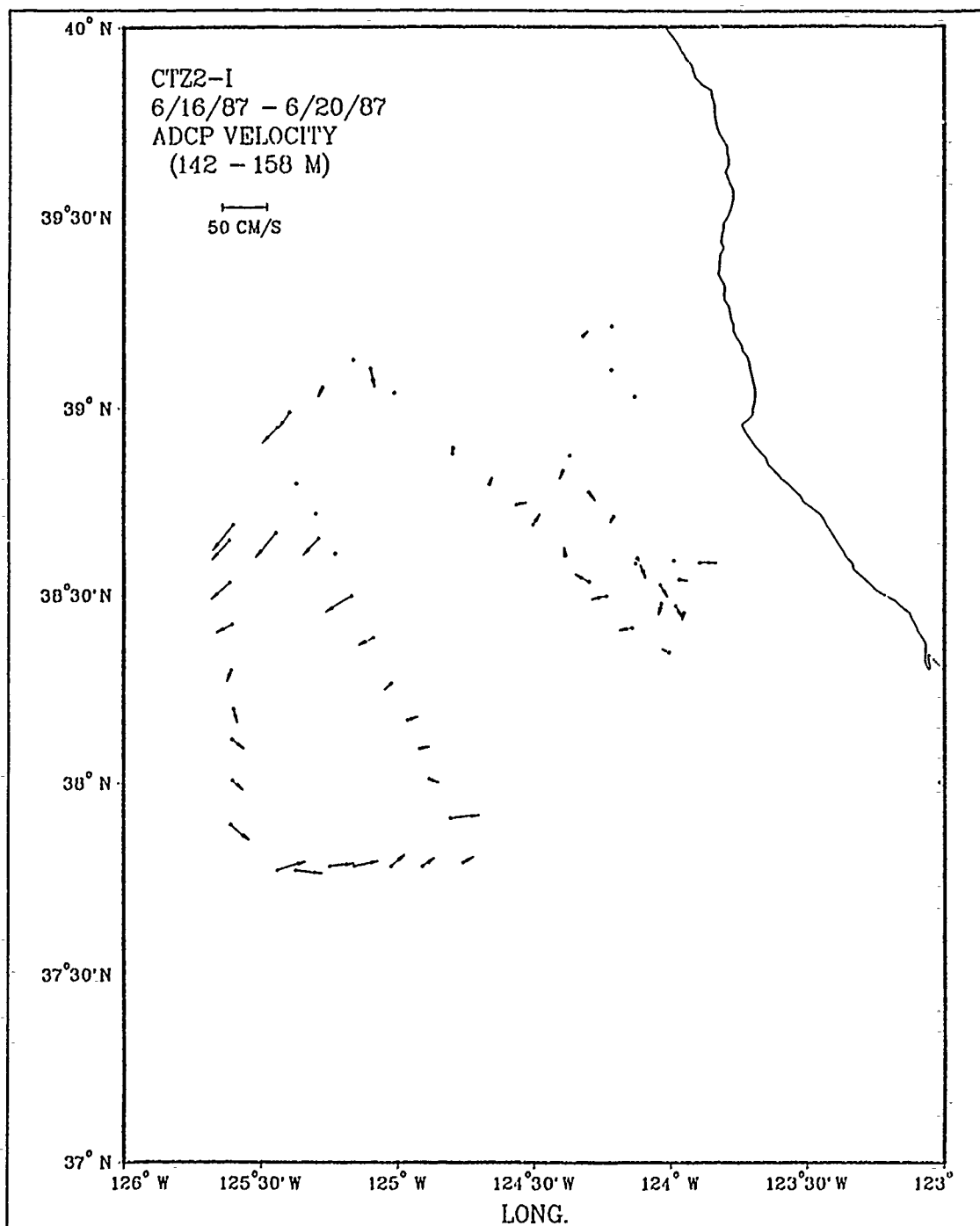


Figure 10. ADCP horizontal velocity at 150 m: Horizontal velocity vectors for bins 36-39 temporally averaged over 30 min. and plotted at 8 km intervals.

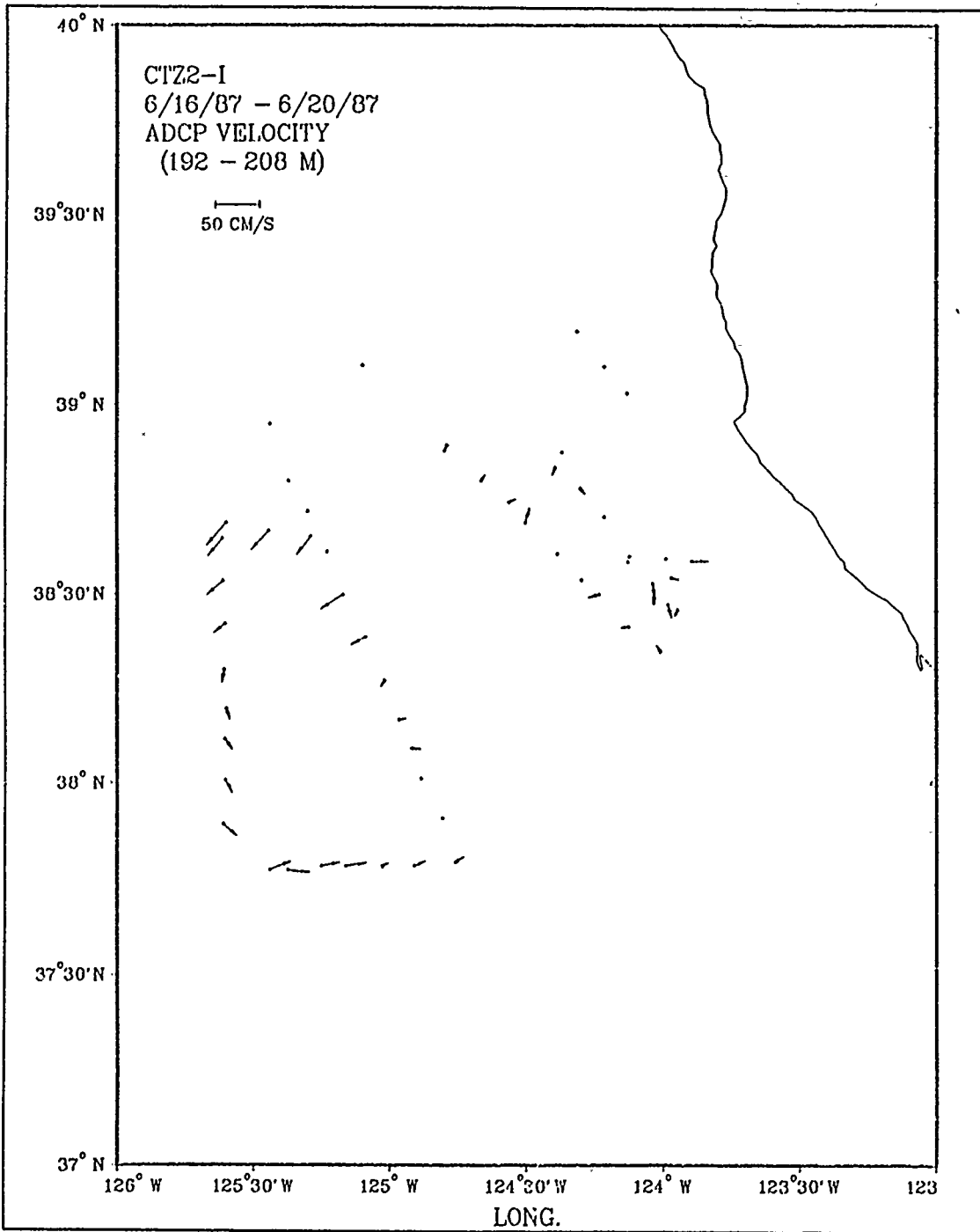


Figure 11. ADCP horizontal velocity at 200 m: Horizontal velocity vectors for bins 48-52 temporally averaged over 30 min. and plotted at 8 km intervals.

ception occurred between stations 29 and 30, where the ADCP velocity maximum was less than geostrophic by 9.6 cm s^{-1} . Conversely, where the flow was strongly onshore, as at stations 41-42 and stations 48-49, ADCP velocity was generally greater in the onshore direction, though the difference was smaller, generally less than 12 cm s^{-1} . Most of this difference is due to the choice of the level of no motion. Although 500 dbar was chosen, the isopycnals were still sloped at this level (e.g., Figure 12), so the assumption was known to be a poor one. Since the casts were only made to 500 m, there was no better alternative. Regardless of the choice of reference level, the geostrophic profile is simply a profile of the relative shear, and hence the shape of the profile will not change if the reference level is varied, though the magnitude of the velocity obtained is dependent on the reference level. This principle was later used to adjust the geostrophic profiles to a new reference level determined from the ADCP profiles.

Where the density surfaces were more nearly level, as for example in the center of the meander, the geostrophic and ADCP velocity magnitudes were in closer agreement. Thus at stations 22-23 and 38-39, all within the filament, the ADCP and geostrophic velocities were in close agreement below 100 meters. Stations 51-52, outside the filament to the northwest, also agreed to within $5\text{-}7 \text{ cm s}^{-1}$ throughout most of the depth range.

Another interesting feature of these profiles is that there appears to be more vertical structure on the 30-50 meter scale in the ADCP profiles than in the geostrophic. The amplitude of these features is less than 5 cm s^{-1} , which is within the noise band of the measurements. The typical station-to-station time interval includes about 30 three-minute averaged profiles. Averaging over a greater distance, as between stations 25 and 27, separated by 30 km, seems to smooth the vertical structure. Averaging over longer time intervals might also smooth the vertical structure; unfortunately, the available data set does not allow testing this hypothesis, since increasing the time interval any further would increase the spatial interval to beyond the CTD station spacing. It is curious, however, that the observed structure appears on vertical scales of 30 to 50 meters, the equivalent of two to three 16-meter bins, despite heavy averaging.

For the majority of the profile pairs there was a layer within which the slope of each velocity profile, and hence the vertical shear, was similar, so that there was a nearly constant velocity offset between the ADCP and relative geostrophic velocity through this layer. It was assumed that within this layer the predominant motion was governed by geostrophy, and therefore that the velocity measured by the ADCP would closely represent the true (absolute) velocity in the layer. The velocity difference between the two profiles was calculated for the layer from 190 to 274 meters, vertically averaged over

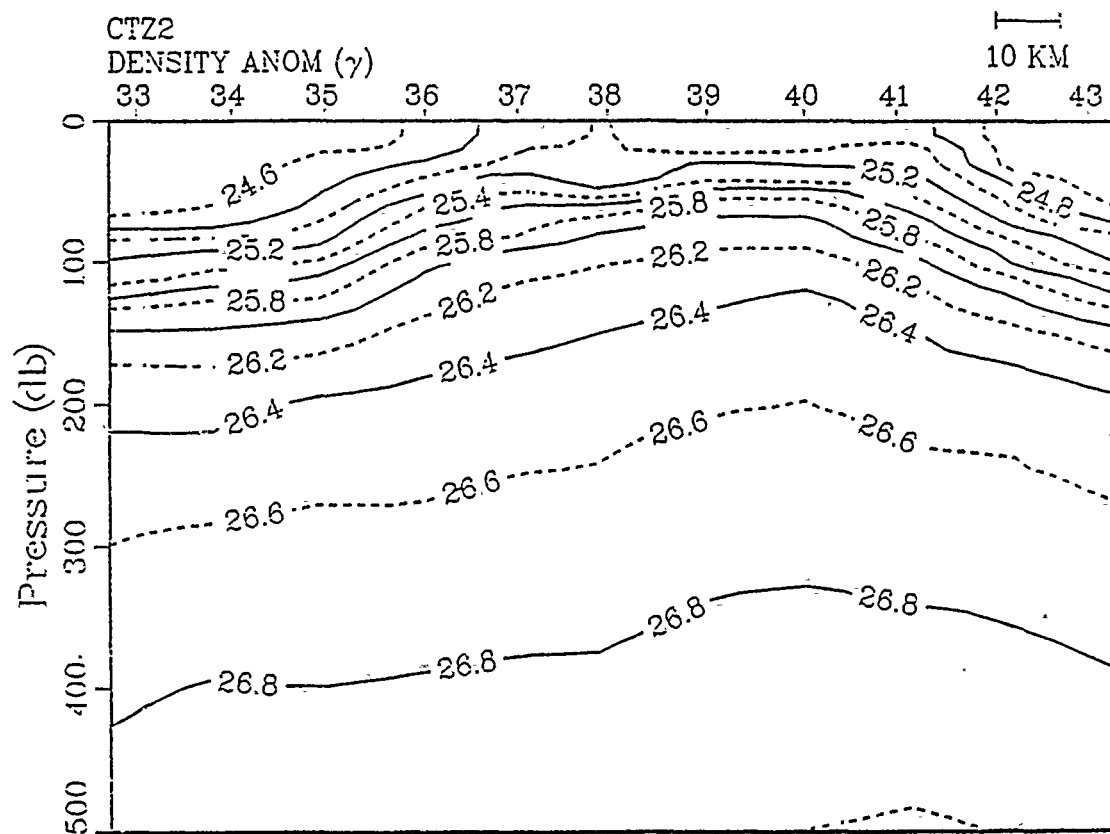


Figure 12. Vertical section of density anomaly (kg m^{-3}) from Line 3.

20 ADCP bins. This level was chosen empirically as the "quietest" layer available wherein the ADCP data was still shallow enough to be reliable. Shallower layers were contaminated by the Ekman velocities and differing profile slopes in the main thermocline. Tables 1 through 5 list the mean velocity difference and standard deviation for each station pair for which the profiles were compared. From these tables it can be seen again, though more succinctly, that the ADCP velocity was higher in the direction of flow. For example, Line 3 crossed the offshore jet and the northern (offshore) branch of the filament, a quiescent area, and then the southern (onshore) branch of the filament. The velocity differences were large and negative (indicating more offshore flow in ADCP measurements) to the north, small near the center, and large and positive (onshore) to the south. This pattern is repeated along Line 4, further seaward, and in the northern part of Line 2, further inshore. The standard deviations were quite small (less than 0.40 cm s⁻¹), showing that the velocity offsets through this depth range were quite constant.

Table 1. ADJUSTMENT LAYER VELOCITY DIFFERENCE STATISTICS FOR LINE 2: The mean and standard deviation of velocity differences between the ADCP and geostrophic (relative to 500 dbar) profiles from 190 to 274 m. Positive differences indicate greater onshore flow in the ADCP measurements.

Sta. Pair	$\overline{\Delta v}$	$\sigma_{\Delta v}$
30-31	-8.00	.38
29-30	-10.66	.28
28-29	-0.86	.22
27-28	2.13	.13
25-27	7.66	.25
24-25	-8.95	.18
23-24	-0.53	.16
22-23	2.69	.17

Table 2. ADJUSTMENT LAYER VELOCITY DIFFERENCE STATISTICS FOR LINE 3: The mean and standard deviation of velocity differences between the ADCP and geostrophic (relative to 500 dbar) profiles from 190 to 274 m.

Sta. Pair	$\overline{\Delta v}$	$\sigma_{\Delta v}$
33-34	-16.34	.40
34-35	-21.22	.39
35-36	-23.38	.38
36-37	-21.36	.28
37-38	-21.51	.20
38-39	2.52	.27
39-40	9.21	.07
40-41	3.2	.26
41-42	18.36	.36
42-43	7.26	.36

Table 3. ADJUSTMENT LAYER VELOCITY DIFFERENCE STATISTICS FOR LINE 4: The mean and standard deviation of velocity differences between the ADCP and geostrophic (relative to 500 dbar) profiles from 190 to 274 m.

Sta. Pair	$\overline{\Delta v}$	$\sigma_{\Delta v}$
53-54	-13.49	.08
52-53	-11.10	.14
51-52	-4.24	.23
50-51	8.16	.05
49-50	7.38	.08
48-49	9.13	.11
47-48	6.02	.69

Table 4. ADJUSTMENT LAYER VELOCITY DIFFERENCE STATISTICS FOR LINE B: The mean and standard deviation of velocity differences between the ADCP and geostrophic (relative to 500 dbar) profiles from 190 to 274 m. Positive velocity difference indicates more poleward flow in ADCP.

Sta. Pair	$\overline{\Delta v}$	$\sigma_{\Delta v}$
43-44	2.76	.19
44-45	9.25	.14
45-46	-1.3	.17
46-47	7.81	.15

Table 5. ADJUSTMENT LAYER VELOCITY DIFFERENCE STATISTICS FOR LINE T: The mean and standard deviation of velocity differences between the ADCP and geostrophic (relative to 500 dbar) profiles from 190 to 274 m.

Sta. Pair	$\overline{\Delta v}$	$\sigma_{\Delta v}$
54-35	-22.89	.16

The geostrophic profile for each station pair was then adjusted by the mean velocity difference to bring it into agreement with the (assumed correct) ADCP profile in the 190-274 m adjustment velocity layer. In effect, the geostrophic reference level is redefined, so that instead of a level of no motion, the relative velocity profile is matched to a level of known motion, as defined by ADCP measurements. It is obvious from the tables that an independent adjustment was required for each CTD station pair. The adjusted profiles are contained in Appendix B. Of course, this method is subject to the limitations inherent in the assumption that the flow is predominantly geostrophic in the adjustment layer; these limitations will be discussed later.

The adjusted geostrophic profiles generally agreed well with the ADCP profile below 200 meters, except in some cases where a divergence occurs in the very deepest ADCP bins. No geophysical explanation was sought for this feature, which occurs near 400 m in many profiles, with velocity differences on the order of 10 cm s⁻¹. This divergence between the two profiles appears at the limit of good ADCP data return, and is most likely due to the increasingly noisy acoustic Doppler velocity estimates near the noise

floor of the ADCP. No more detailed analysis of this result was attempted, and this part of the profile was ignored for the remainder of the study. For later transport comparisons, a maximum depth of 274 m was used.

Above 200 m, there were some quite significant differences between the ADCP and adjusted geostrophic profiles. These differences often extended in depth to 200 m, well below the typical Ekman layer depth of about 50 m. Moreover, the direction of the difference was not constant, nor related to the flow features in any consistent way. The variation of these differences in direction and magnitude suggested the influence of some type of wave motion in the velocity field. These differences are considered in greater detail in section IV B.

C. COMPARISON OF VELOCITY SECTIONS

Velocity sections were produced using the geostrophic profiles referenced to the 500 dbar level of no motion, the adjusted geostrophic profiles corrected station pair by station pair to the ADCP adjustment velocity layer, and the ADCP data using a 12.5 km spatial averaging. The shorter horizontal distance was chosen to capitalize on the higher horizontal resolution of the acoustic doppler instrument compared with the 15 km station spacing.

The geostrophic velocity section for Line 2, referenced to 0 velocity at 500 dbar (Figure 13), shows little flow below 200 m. A single offshore jet appears in the north of the section, near station 30, corresponding to the jet observed to the north of the filament, and the offshore flow associated with the filament itself appears weakly between stations 23 and 24. The jet associated with the filament penetrates much deeper than the one to the north. Weak ($< 5 \text{ cm s}^{-1}$) onshore flow was present below 100 m between stations 24 and 28. The same flow patterns appear in the ADCP section (Figure 14), but the velocity magnitudes are much greater. The offshore flow of the filament penetrates to below 400 m; likewise for the jet to the north, which slopes northward with depth in the acoustic doppler section.

The section prepared by using the geostrophic velocity profiles adjusted to the 190-274 m ADCP velocity reference layer (Figure 15) closely agreed with the velocity magnitudes of the ADCP section below 50 m. There is greater shear in the upper 50 m of the ADCP section (and the corresponding profiles) than in the sections produced from geostrophic profiles. In the offshore filament flow, the ADCP velocity is higher than the adjusted geostrophic, consistent with the sign of the Ekman transport, which is also offshore. This is also true of the jet to the north. The core of this jet is shifted

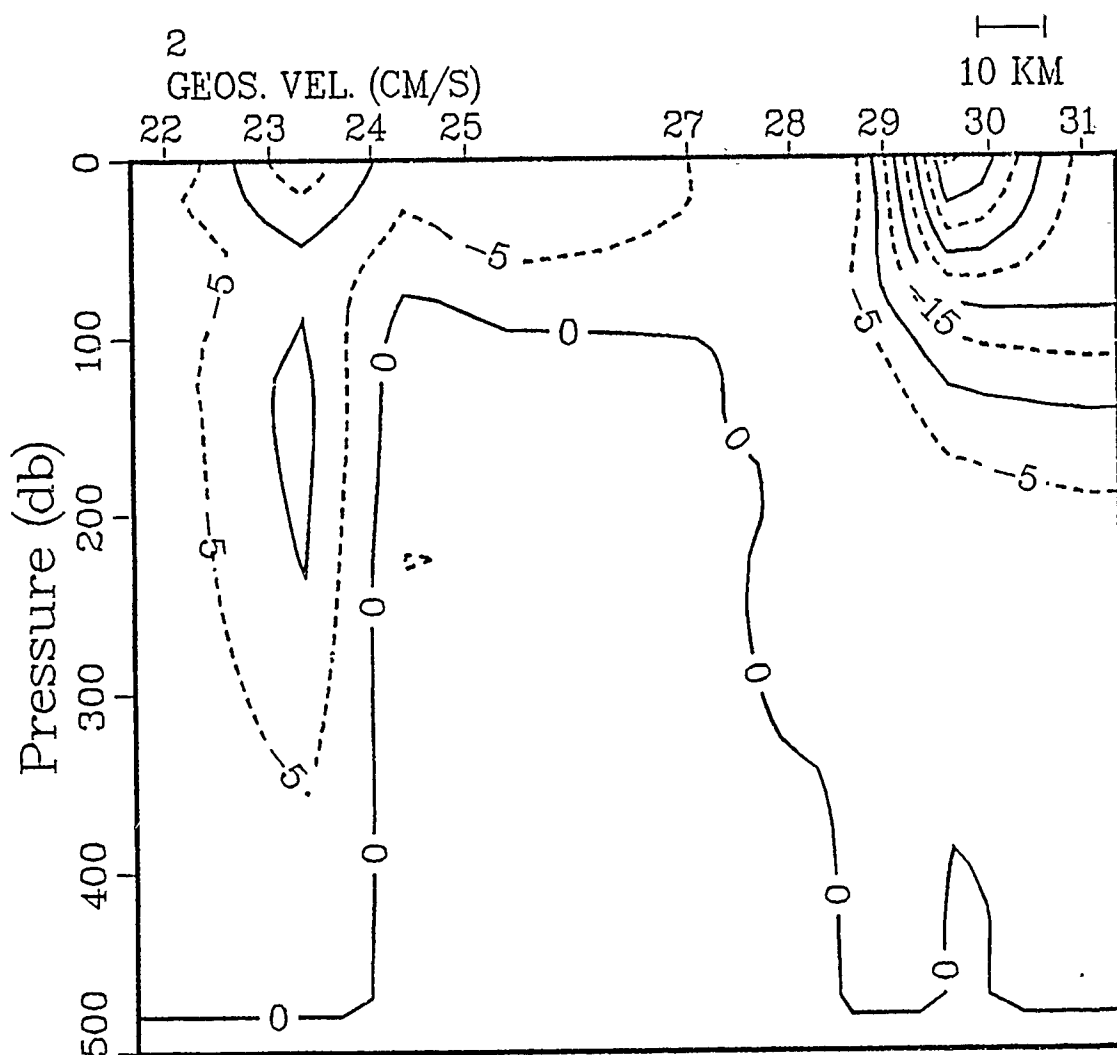


Figure 13. Section of geostrophic velocity referenced to 500 dbar for Line 2: The view is offshore, with northwest to the right. Positive velocities are onshore (out of the page), and negative velocities offshore (into the page).

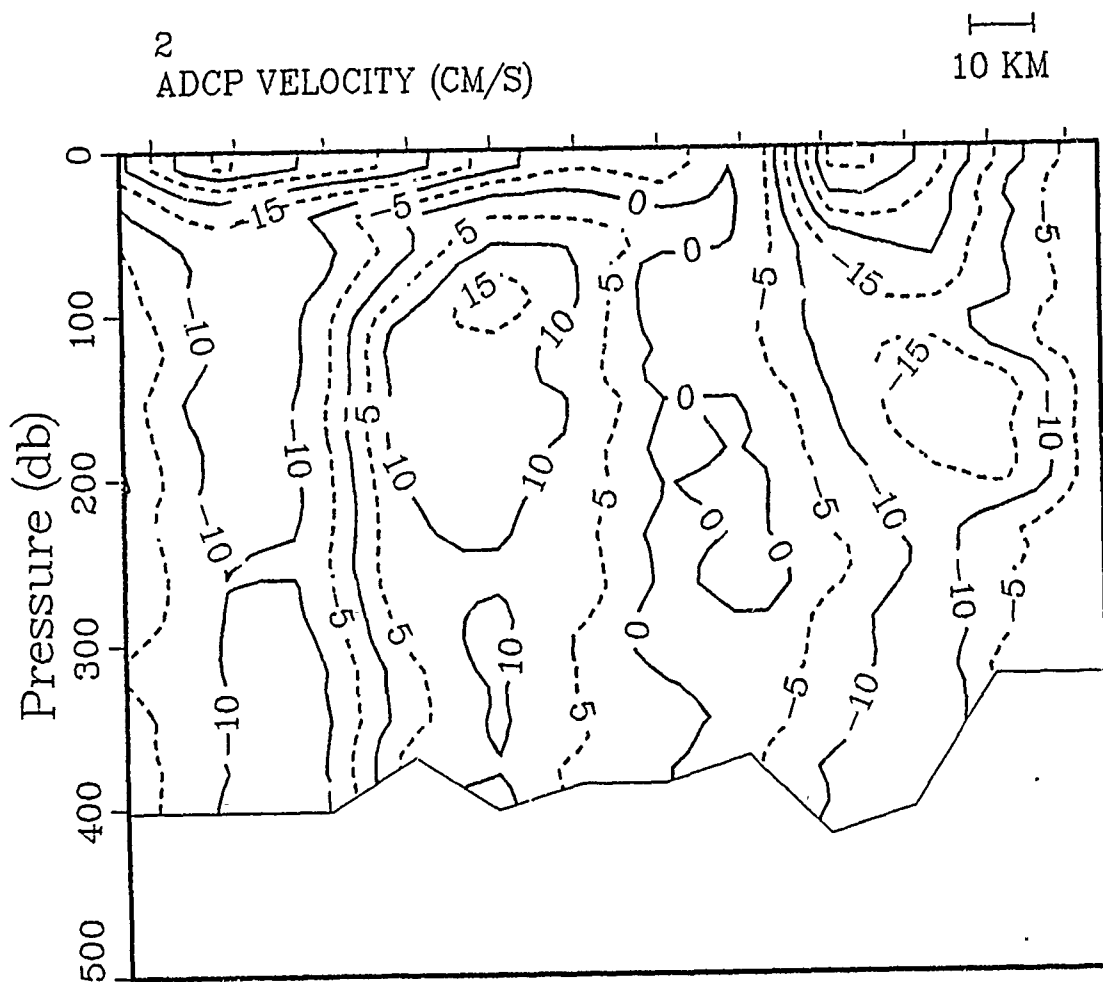


Figure 14. Section of ADCP velocity for Line 2: The view is offshore, with northwest to the right. Positive velocities are onshore (out of the page), and negative velocities offshore (into the page).

northward in the adjusted geostrophic section from its position in the ADCP and unadjusted geostrophic sections, by over 25 km.

Turning to the geostrophic velocity section for Line 3 (Figure 6), the two offshore jets seen in Line 2 continued further seaward. The offshore flow of the meander in Line 3 was slightly stronger than across Line 2. The return flow of the filament cut across the southern part of Line 3, and is much more vigorous than the offshore flow. This differs from the ADCP velocity section (Figure 16), in which the onshore maximum was less than the offshore maximum by 15 to 20 cm s^{-1} . The two offshore flows have nearly merged in the ADCP section, but two distinct maxima of greater than 50 cm s^{-1} are still distinguishable. The difference between the geostrophic and ADCP velocity was likely due to the near surface Ekman transport. The prevailing winds were from the northwest at about 10 m s^{-1} , almost parallel to Line 3, which reinforced the offshore flow but retarded the onshore flow. The ADCP also indicated significant velocity below 300 meters. This was reflected in the adjusted geostrophic section (Figure 17), although the 30 cm s^{-1} maxima at 350 m at the southern end of the ADCP section does not appear in the adjusted geostrophic section. This deep maxima in the ADCP is a manifestation of the divergence of the ADCP and adjusted geostrophic profiles at the bottom of the ADCP profile, noted earlier. At the surface, the onshore jet maximum was highest in the adjusted geostrophic velocity section, with a peak of 75 cm s^{-1} . The two offshore jets merged together in the adjusted section.

At Line 4, some 170 km offshore, the seaward flow of the filament has become quite weak. The flow bifurcated near $38^{\circ} 40' \text{ N}$, $125^{\circ} 15' \text{ W}$ (Figure 3), and the cross-sectional component of the geostrophic flow is low. The northern jet was still quite strong ($> 30 \text{ cm s}^{-1}$) (Figure 18), and the onshore flow south of the cold filament was also fairly strong ($> 30 \text{ cm s}^{-1}$). The ADCP velocity section is not markedly different, except again for the greater flow at depth (Figure 19), with the ADCP section showing 10-15 cm s^{-1} where the geostrophic section shows less than 5 cm s^{-1} . Note that while there was little flow in the region of the offshore portion of the filament visible in the sections, the ADCP measurements indicate that much of the flow at Line 4 was along the section (Figure 7), with southward flow as great as 36 cm s^{-1} . The adjusted geostrophic velocity section (Figure 20), except for the magnitudes of the deep velocities, was quite similar to the other two sections for Line 4. Unlike the previous two lines, the differences between ADCP and adjusted geostrophic surface maxima are not consistent with the sign of the Ekman transport, which was weaker along Line 4. The absolute differences were small, however ($\sim 6 \text{ cm s}^{-1}$).

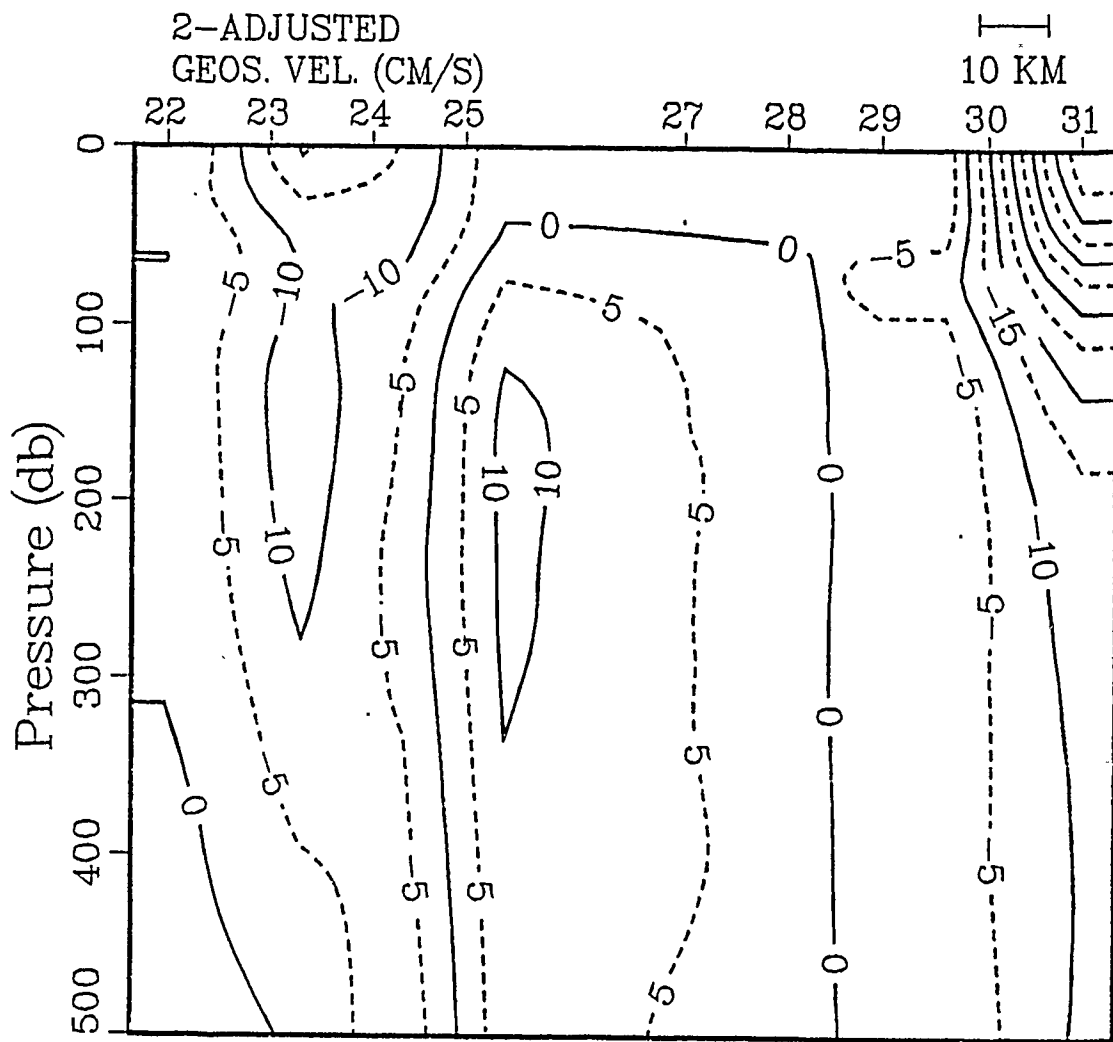


Figure 15. Section of adjusted geostrophic velocity for Line 2: Geostrophic velocity section referenced to the 190-274 m ADCP adjustment layer. The view is offshore, with northwest to the right. Positive velocities are onshore (out of the page), and negative velocities offshore (into the page).

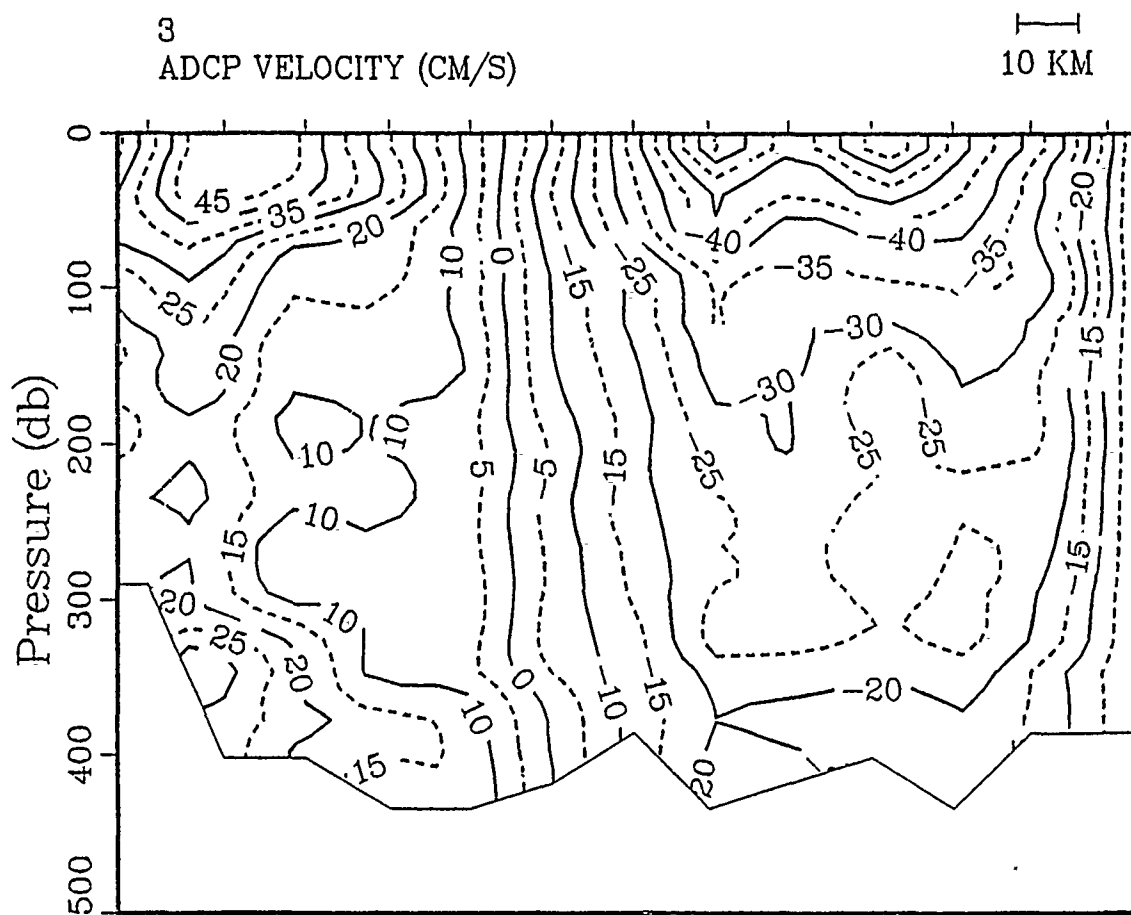


Figure 16. ADCP velocity section for Line 3: The view is offshore, with northwest to the right. Positive velocities are onshore (out of the page), and negative velocities offshore (into the page).

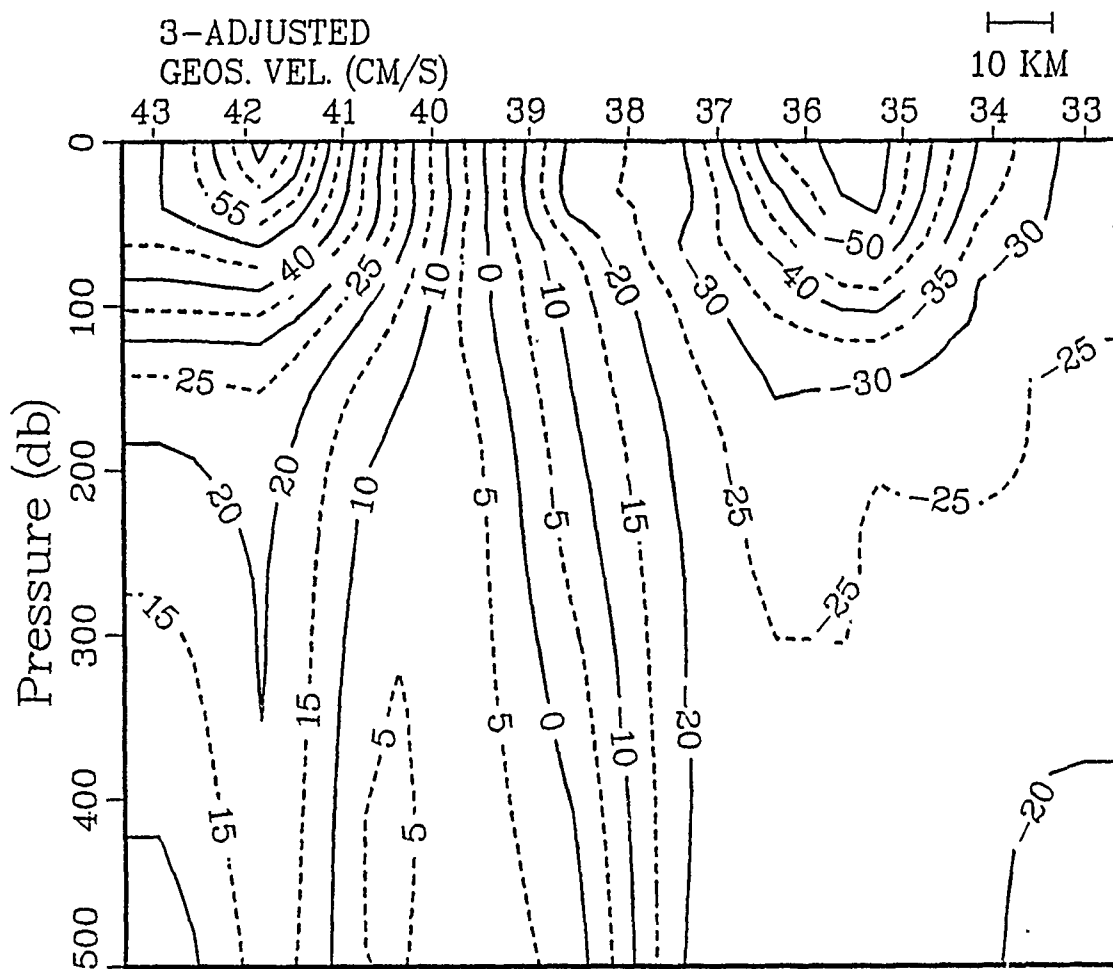


Figure 17. Adjusted geostrophic velocity section for Line 3: The view is offshore, with northwest to the right. Positive velocities are onshore (out of the page), and negative velocities offshore (into the page).

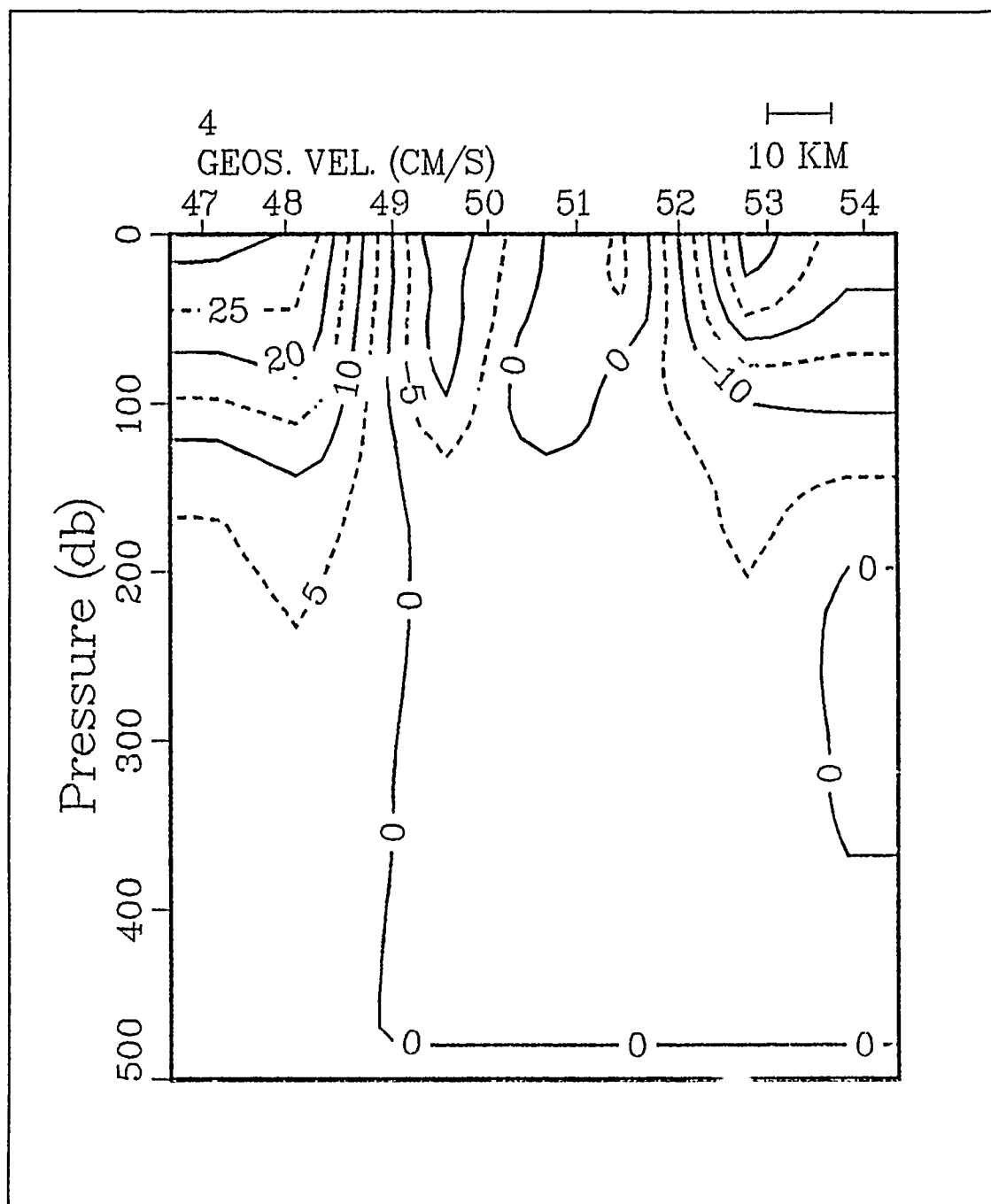


Figure 18. Geostrophic velocity section, referenced to 500 dbar, for Line 4: The view is offshore, with northwest to the right. Positive velocities are onshore (out of the page), and negative velocities offshore (into the page).

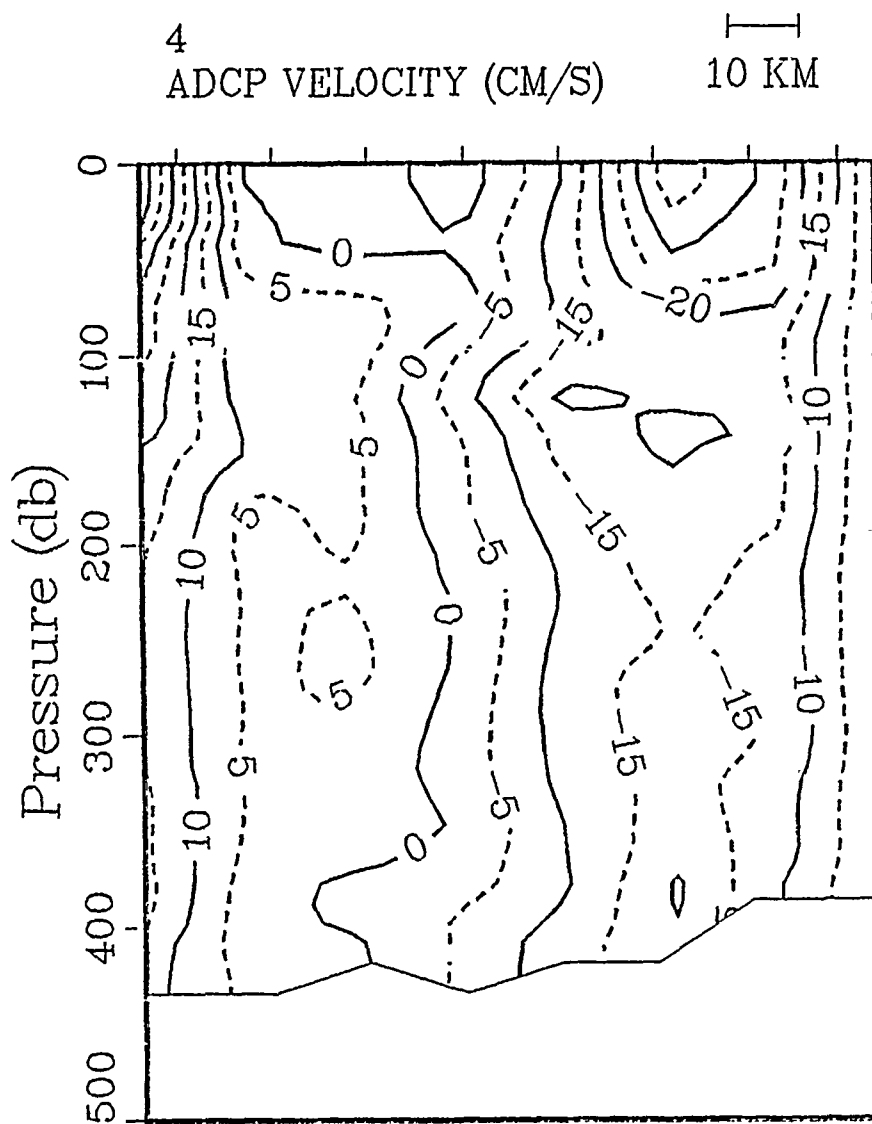


Figure 19. ADCP velocity section for Line 4: The view is offshore, with north-west to the right. Positive velocities are onshore (out of the page), and negative velocities offshore (into the page).

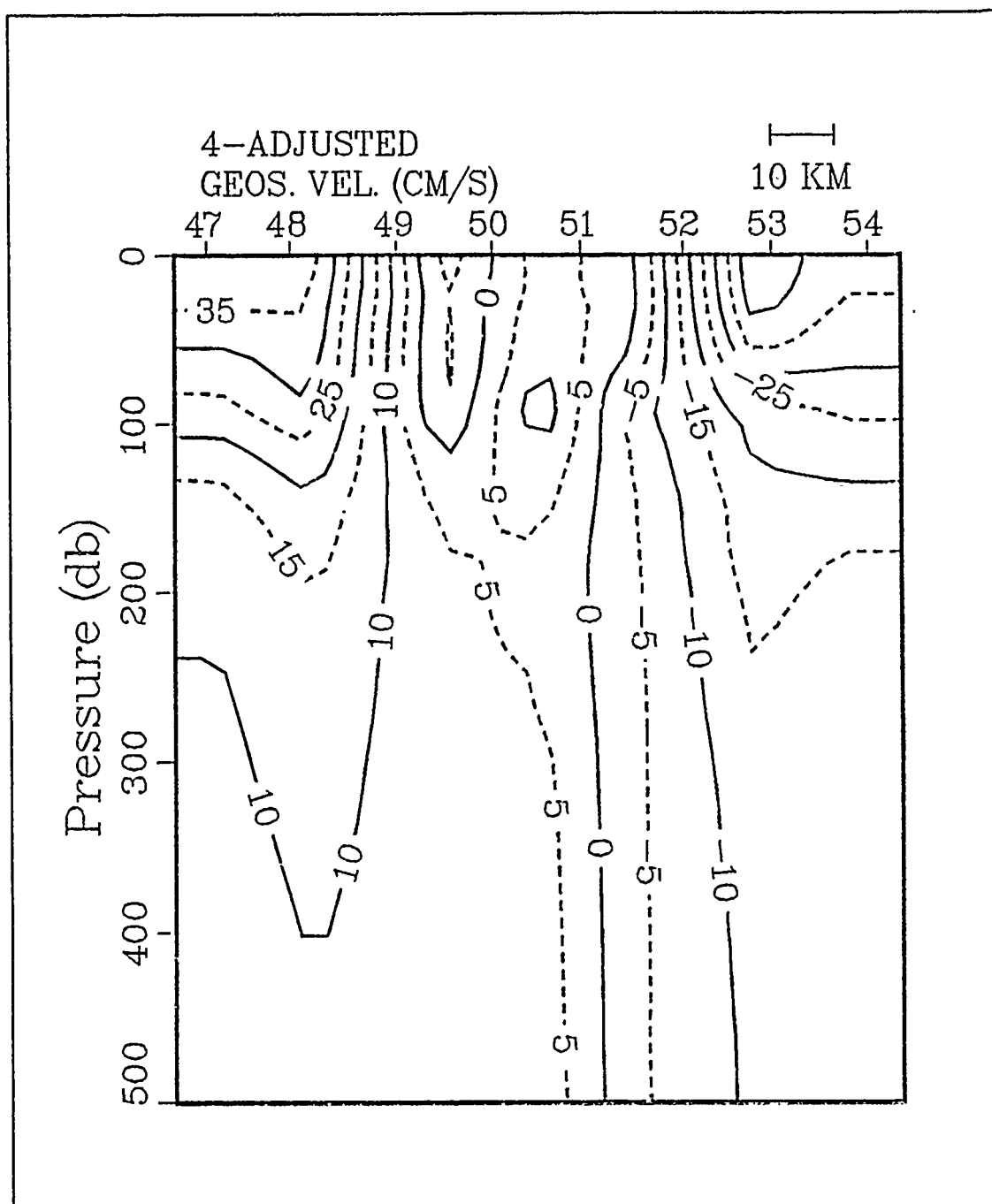


Figure 20. Adjusted geostrophic velocity section for Line 4: The view is offshore, with northwest to the right. Positive velocities are onshore (out of the page), and negative velocities offshore (into the page).

The velocity maxima of the features discussed above, as well as for Lines B and T, the southern and northern boundaries of the box used for transport comparisons, are summarized in Table 6. The major flow features were found to be in general qualitative agreement in the ADCP, the adjusted, and the unadjusted geostrophic sections, in terms of their sign and geographical location. However there were quantitative differences in the velocity maxima of several features, as well as in the deep flow in the ADCP (and hence the adjusted geostrophic) sections. Differences in near-surface velocity along Lines 2 and 3 were consistent with the sign of the Ekman transport across those lines, but Ekman transport was less across Line 4 due to lighter winds, (Figure 21) and did not significantly impact the surface velocity.

Table 6. CROSS-SECTIONAL VELOCITY MAXIMA OF SIGNIFICANT FEATURES.: (in cm s⁻¹)

	ADCP	Geostrophic	Adjusted Geostrophic
LINE 2 (Sta. 22-31)			
N offshore jet	39.3	48.9	31.6
Offshore filament jet	36.8	20.4	20.9
Onshore (deep)	19.3 at 96m	---	11.5 at 165m
LINE 3 (Sta. 33-43)			
N offshore jet	70.4	42.0	65.3
Offshore filament jet	65.7	24.8	(single jet)
Onshore jet (surface)	48.3	56.4	74.7
LINE 4 (Sta. 47-54)			
Offshore jet (single)	38.6	33.6	44.6
Onshore jet (surface)	44.6	32.2	38.2
LINE B (Sta. 43-47)			
Northward max	12.0	8.3	14.7
Southward max	20.9	15.3	7.8
LINE T (Sta. 54 & 35)			
Southward max	50.4	9.5	32.4

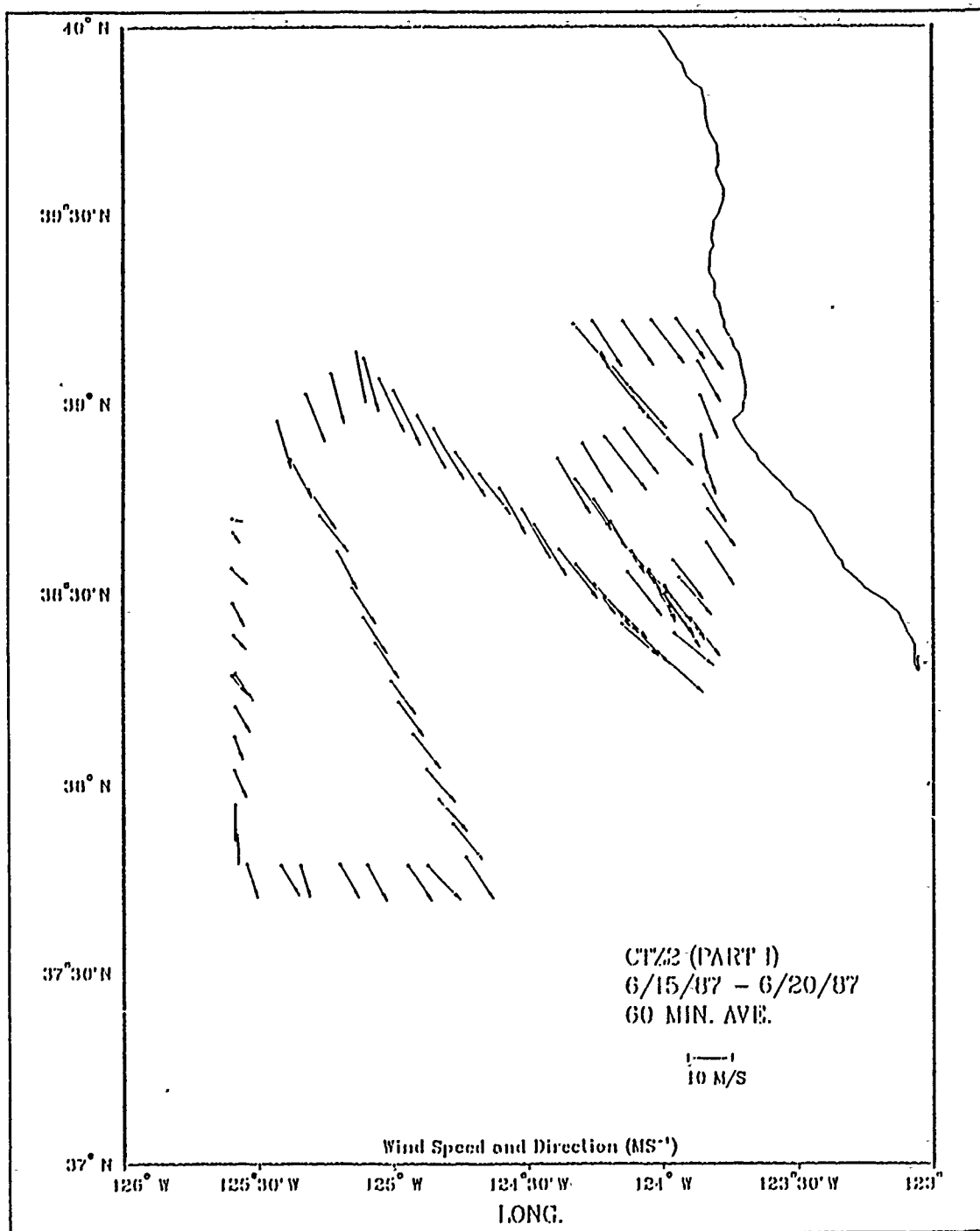


Figure 21. Hourly averages of wind speed and direction: Measured by an anemometer at approximately 10 m height on the mast of the R/V POINT SUR.

D. TRANSPORT COMPARISONS

Volume transports were calculated and compared for each of the three velocity fields. A box was defined such that if the measurements were accurate and the survey was synoptic, the transport through the sides of the box would balance. Vertical velocities through the bottom of the box were assumed insignificant compared to horizontal advection. The sides of the box were defined by the ship's track from stations 35 to 54 and its departure track to the east from station 54 to 1.8 km south of station 35 (Figure 2). The depth of the box was defined as 274 m, which was the maximum depth to which reliable ADCP data was available for the entire circumference of the box. The east side of the box, corresponding to CTD stations 35 to 43 along Line 3, was 118 km long; the south side, formed by CTD stations 43 through 47 (Line B), was 72 km long; and the west side, along Line 4 (stations 47 to 54), was 102 km long. The north side, Line C, differed slightly between the ADCP and geostrophic calculations. For the geostrophic method, stations 54 and 35, separated by 27 km, were used. The actual ship's track on a course due east after leaving station 54 brought it across Line 3 at a point approximately 1.8 km to the south of station 35. Since the entire circuit took 36 hours to complete, the geostrophic velocity section for stations 54 and 35 was non-synoptic. The consequences of this are discussed later.

Using recorded wind data, averaged over the distance between each station pair, the cross-sectional component of the Ekman transport was computed. The winds during Part I of the cruise (Figure 21) were fairly steady from the northwest at 10 to 15 m/s for most of the survey, which resulted in the winds being approximately parallel to Lines 2 and 3, and more perpendicular to the south side of the box. Along the west side, the winds began to diminish and back from northwest to west.

The volume transport was computed for each side using each velocity data set and the Ekman transport calculations. The Ekman transport values were subtracted from the ADCP totals. If the flow was predominantly geostrophic, with the only significant departure from geostrophy being in the Ekman transport, then this difference should agree with the transport calculated from the adjusted geostrophic velocity. The results of these computations are given in Table 7. The transport into and out of the box was not in balance. Over the box as a whole, the Ekman transport was not significant; it contributed substantially only on the east side, where the wind was strong and parallel to the section. On that side, subtraction of the Ekman component from the ADCP value brought the transport into quite close agreement with the adjusted geostrophic transport.

Table 7. TRANSPORT (SV) THROUGH BOX SIDES (FROM SURFACE TO 274 M): Positive values indicate net transport into box.

Side	Geostrophic	ADCP	Ekman	ADCP-Ekman	Adj. geos.
East	0.44	1.55	0.17	1.38	1.39
West	0.015	-0.69	-0.05	-0.65	0.13
South	-0.03	0.50	-0.03	0.53	0.86
North	0.05	2.10	0.003	2.05	1.70
TOTAL	0.47	3.46	0.09	3.31	4.08

By its absolute magnitude in comparison with the ADCP and adjusted geostrophic transport values, the unadjusted geostrophic transport appears to be in near balance; however, in relation to the small magnitudes of the transport through each side, this too is far from being balanced. The transport through the unadjusted geostrophic sections was small compared to the ADCP sections, and this difference is largely due to the choice of reference level. By constraining the velocity to go to zero at 500 dbar, even when there was significant slope in the isopycnals at that depth, much of the geostrophic velocity was suppressed.

Across the southern boundary, both the geostrophic and ADCP observed flows were weak. There was greater net transport observed using adjusted geostrophy than using the ADCP data alone. Across the western boundary, the transport was nearly balanced for all methods of determination. Unfortunately, this reveals little about the meandering upwelling jet, since the dominant offshore flow across this section was due to the jet north of the filament, and there was very little offshore flow in the filament itself at Line 4, because it was turning to the south along the section. The close proximity of the two offshore jets on Line 3 made it difficult to separate the two features and compute the transport balance in the meander alone with any reasonable assurance.

IV. DISCUSSION

A. TRANSPORT IMBALANCE

The observed transport imbalance in the box was quite large: 3.31 Sv in the ADCP data with the Ekman component removed, and 4.08 Sv in the adjusted geostrophic computation. Temporal changes over the time required for the ship to complete its circumnavigation of the box may be too rapid for the survey to be sufficiently synoptic. Although only one CTD cast was made at station 35, the northeast corner of the box and the terminus of the circuit, the continuously operating ADCP offers the opportunity to assess the magnitude of the temporal change in this area. Figure 22 and Figure 23 on page 42 show the u and v components averaged over 30 minutes centered on the time of arrival at station 35 and on the time that the ship crossed south of station 35 to close the box. These profiles show, in the upper 100 m, that the flow direction became more southward over the 36 hour time interval, causing the zonal and meridional components to vary as much as 10 cm s^{-1} . The ADCP velocity section across the north side of the box, (Figure 24), shows a southerly jet of 50 cm s^{-1} peak velocity entering the box. This is most likely the jet north of the filament which was located just south of station 35 at the beginning of the transit around the box. Satellite imagery taken on 20 June tends to support this interpretation that the flow re-oriented itself during the time required to make the survey. This would be quite similar to the relaxation observed during the 1988 CTZ survey (Stanton, *et al*, 1989) between 1988 Grids 4 and 5. If the jet changed position and direction, perhaps as a result of the relaxation of the wind, then essentially the jet would have been counted twice. This would of course seriously impact the transport balance, since the flow across the north side was the largest net inflow of any side, accounting for nearly half the imbalance in the adjusted geostrophic transport and nearly two-thirds of the imbalance in the ADCP transport. This high transport did not appear in the 500 dbar-referenced geostrophic section (Line T) across the north side of the box. If the jet moved as postulated, then both stations 35 and 54 would have been taken in nearly the same location with respect to the jet, and the geostrophic velocity calculated between these two stations would thus be small.

Another factor contributing to the transport imbalance in the ADCP data may be the presence of ageostrophic velocity components other than the Ekman velocities. The ageostrophic flow in the sections for Lines 3 and 4 (Figures 26 and 27) was mostly into

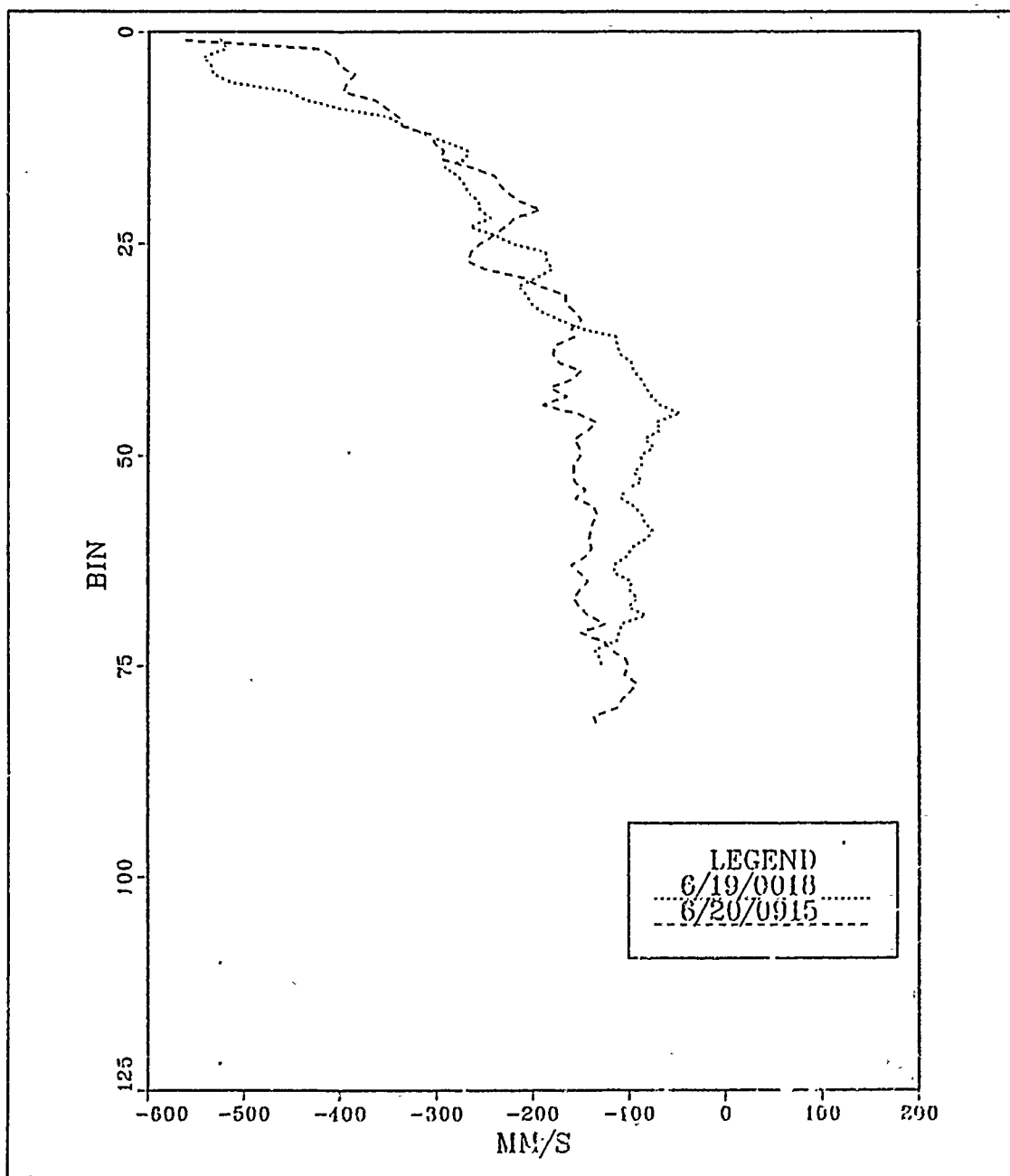


Figure 22. ADCP u-components for station 35: Zonal velocity component measured by the ADCP for two 30-minute intervals centered on 1) time of arrival at CTD station 35; and 2) time at which vessel crossed the previous track near station 35 to close the box. The vertical averaging interval is 4 m.

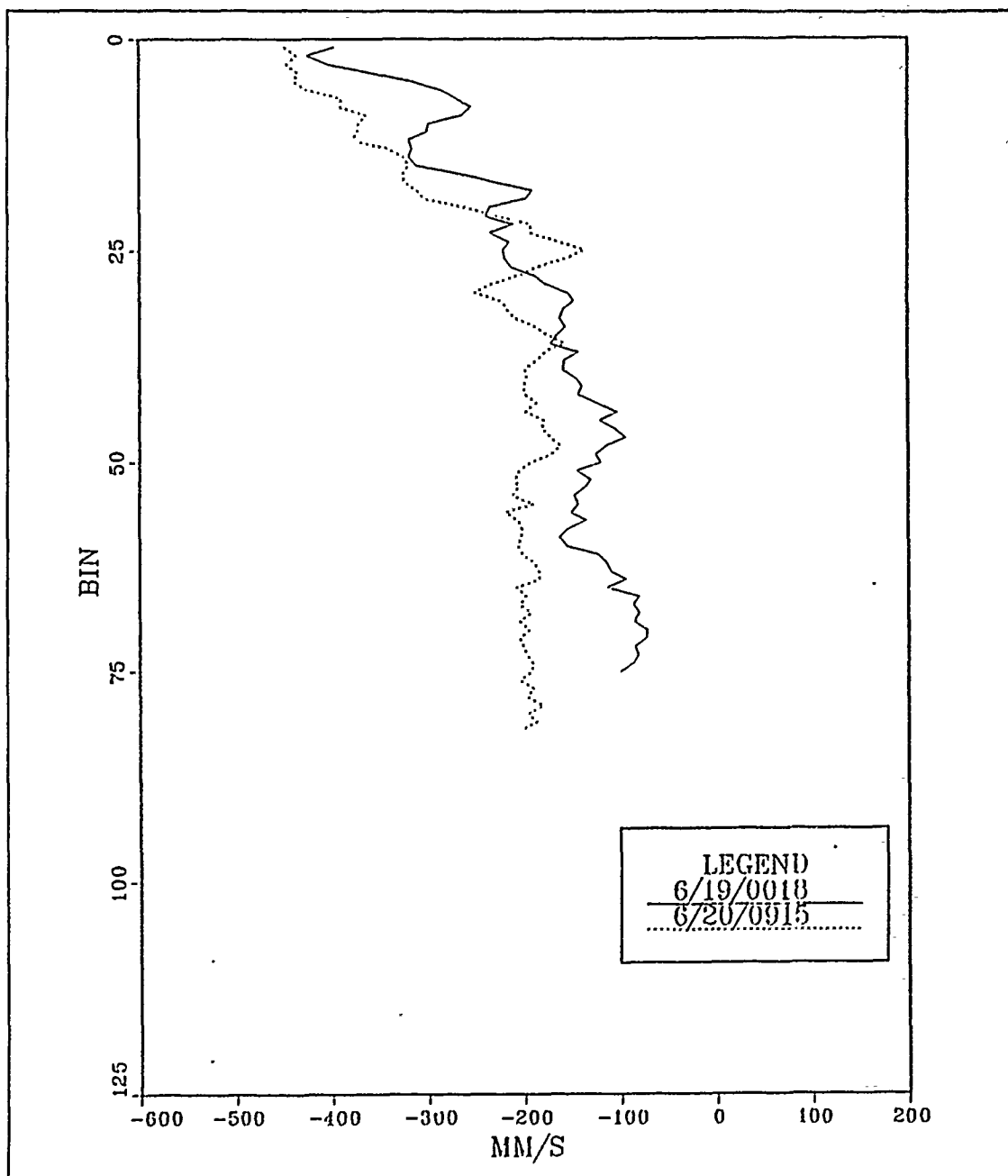


Figure 23. ADCP v-components for station 35: Meridional velocity component measured by the ADCP for two 30-minute intervals centered on 1) time of arrival at CTD station 35; and 2) time at which vessel crossed the previous track near station 35 to close the box. The vertical averaging interval is 4 m.

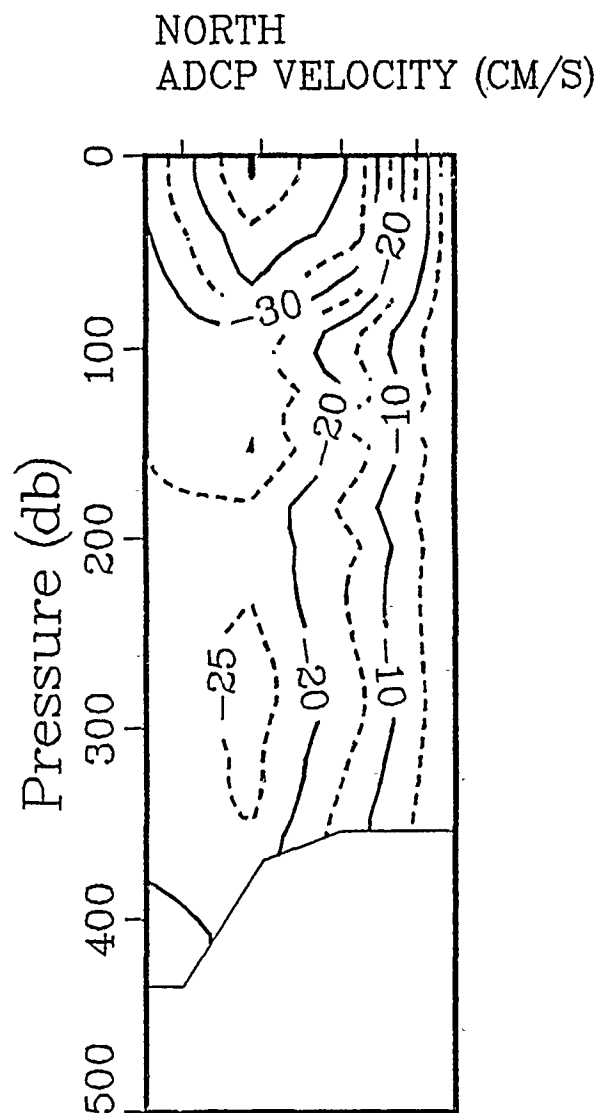


Figure 24. ADCP velocity section for the north side of the box: The view is northward, with negative velocities southward (out of page).

the box (offshore flow through the east side and onshore flow through the west side), also in agreement with the sign of the imbalance. These differences between the ADCP and geostrophic velocities are the subject of the next section.

B. DIFFERENCES IN ADCP AND GEOSTROPHIC SHEAR

As stated earlier, adjusting the relative geostrophic profiles to agree with the ADCP profiles in the 190-274 m adjustment layer did not remove all the differences in the profiles, with significant differences in shear apparent in the upper 200 m. At stations 39-40, for example (Appendix B), there was good agreement between the adjusted geostrophic and ADCP profiles below 200 m, but above this depth the ADCP profile exhibits much different shear, with a resultant velocity difference of 9-10 cm s^{-1} more onshore flow in the ADCP data than in the adjusted geostrophic flow in a layer extending from the surface to over 180 m. At stations 38-39, the ADCP data showed less offshore velocity in the upper 50 m, though the sign of the Ekman transport was in the opposite direction. At stations 42-43, there is pronounced shear in the upper 200 m in both profiles, but more shear in the geostrophic profile, so that ADCP velocity is less by 15 cm s^{-1} near the surface. Such large differences in shear may indicate the presence of small scale eddies or fronts not resolved by the 15 km CTD station spacing, the presence of other than density-driven motions, or be a product of instrument noise. One component already discussed is the wind-induced Ekman transport. With northwest winds along the sections, there should be marked shear in the Ekman layer, indicating greater offshore velocity. This was observed in all the profiles along Line 2 and Line 3. It was not observed along Line 4, where the wind was weak.

For 10 m s^{-1} winds, the typical wind speed observed, the corresponding Ekman layer depth assuming thorough mixing is about 55 m. Ekman dynamics does not explain the differences observed below this depth, nor does it explain the variation in the sign of the differences. Other dynamical effects were apparently operating to contribute to the observed ageostrophic shear.

The adjusted geostrophic velocity profiles were subtracted from the station averaged ADCP profiles and the resulting ageostrophic velocity sections were plotted (Figures 25 - 27). In these sections, 274 meters was chosen as the deepest ADCP bin common to the set of station pairs examined. These sections revealed a strong (about 10 cm s^{-1}) shoreward ageostrophic component acting against the northern jet as it crossed each section. In the offshore flow of the filament, the ageostrophic component accelerated the flow across Lines 2 and 3. In the onshore filament flow, the ageostrophic compo-

ment was in the direction of flow across Line 4 but in opposition to the flow across Line 3. Ekman dynamics do not explain the shoreward ageostrophic components nor do they explain the existence of strong ageostrophic velocity below the typical Ekman layer depth, for example the greater than 10 cm s^{-1} maxima at 100 m near stations 47 and 49 on Line 4.

Interpretation of these results requires assessment of whether the observed ageostrophic component was due to an actual geophysical phenomenon or whether it was due to some measurement error or instrument bias. Since the sign of the ageostrophic component is not always in the same direction relative to the flow, it does not appear that the ADCP consistently overestimates or underestimates the flow relative to geostrophy. Further, the ageostrophic component does not seem to favor one side of the ship, which would suggest a bias due to a transducer alignment error. Lines 2 and 4 were made along a northerly course, while Line 3 was made as the ship tracked southward. The sign of the ageostrophic component in a specific feature is consistent across the sections except in the case of the onshore flow of the filament.

Centripetal acceleration is not a likely candidate. Scaling with $\frac{u^2}{L}$, for the region under consideration could account for at most 5 % of the observed departure from the geostrophic velocity, which scales as fU ; i.e., less than 4 cm s^{-1} for the maximum observed velocity and less than 2 cm s^{-1} for more typical velocities. Differences of 10 cm s^{-1} were commonly observed in regions of low velocity and very large radius of curvature, e.g., stations 38-39 and 49-50.

The varying sign of the velocity differences suggests wave motion. Profiles of the Brunt-Väisälä frequency were plotted for each CTD station. These showed high stratification near 50 m depth at many of the stations. The large shear difference in the upper 200 m occurred only where the stratification was sharp, but did not appear at all stations with highly stratified layers. This, plus the change of the sign of the velocity difference suggested a rapidly time-varying effect related to the density profile, i.e., internal waves. A space-time plot (Figure 28) of the zonal and meridional components of ADCP velocity averaged from 50 to 102 meters, below the Ekman layer and in the region where large velocity differences were observed shows that a fluctuation with a period of around 1.4 hours and an amplitude of 15 cm s^{-1} was clearly superimposed on the general trend of the synoptic flow. The period is only an estimate since the ship was steaming while this time series was being made, but the plot suffices to show that high frequency noise, possibly introduced in the navigation, remains a problem when attempting to determine the mean flow from ADCP data.

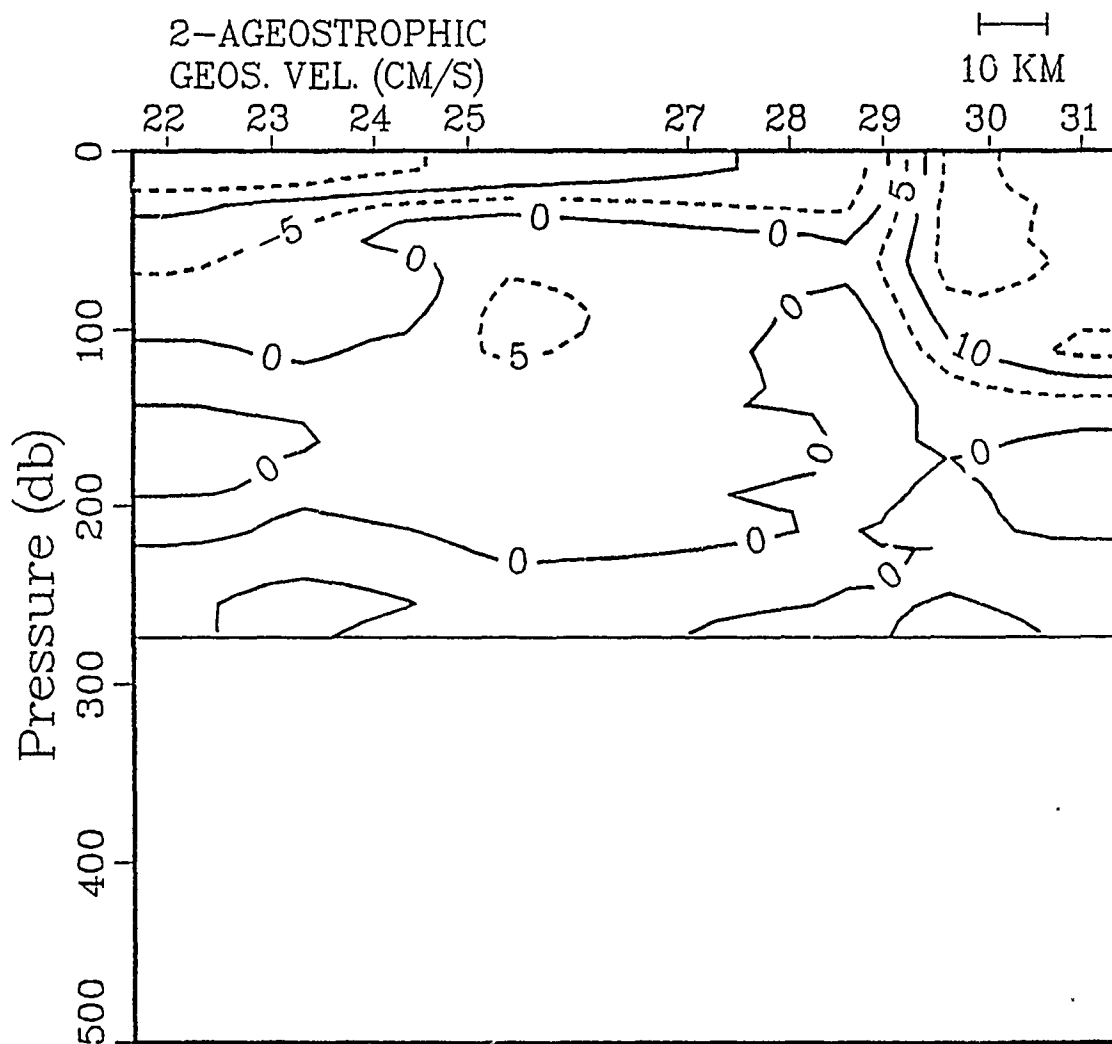


Figure 25. Ageostrophic velocity section for Line 2: Looking offshore, with northwest to the right. Positive velocities indicate onshore flow (out of the page), and negative velocities offshore (into the page).

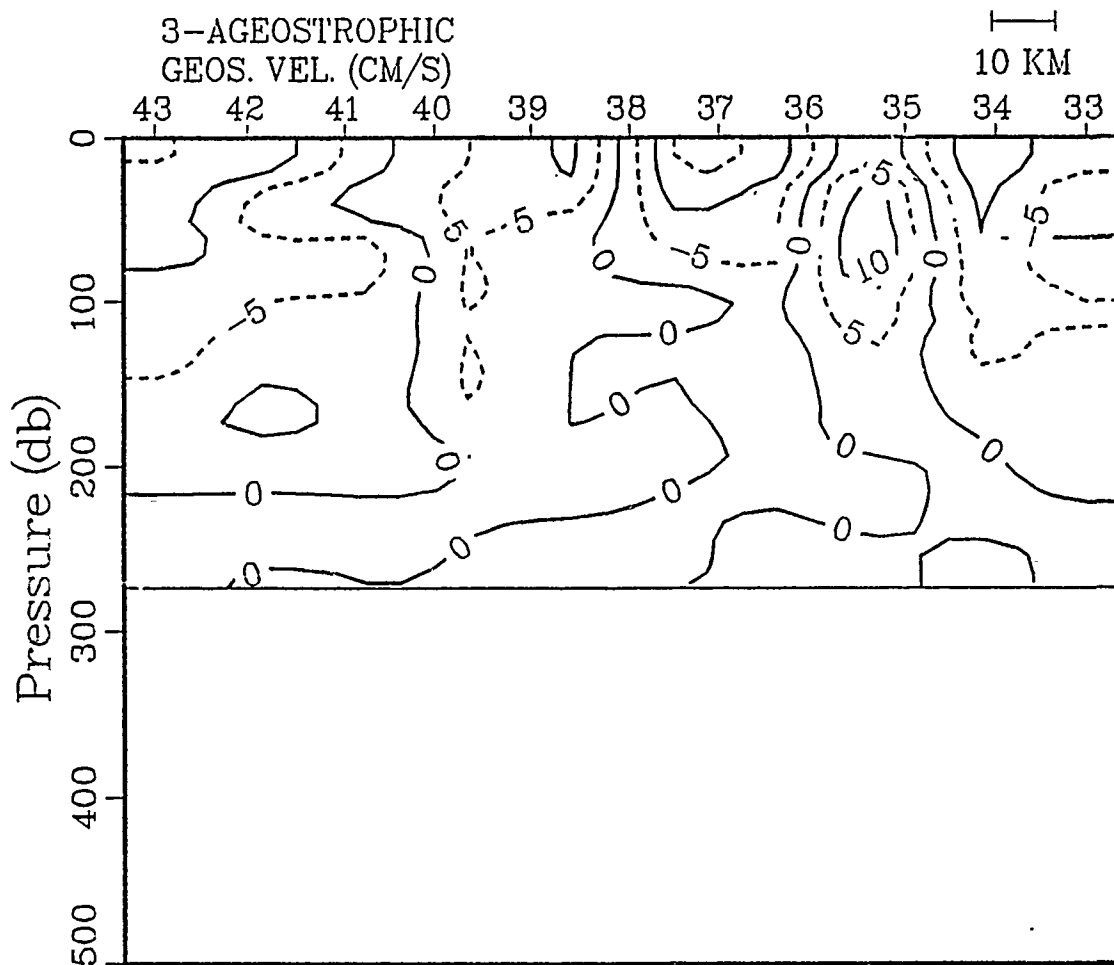


Figure 26. Ageostrophic velocity section for Line 3: Looking offshore, with northwest to the right. Positive velocities indicate onshore flow (out of the page), and negative velocities offshore (into the page).

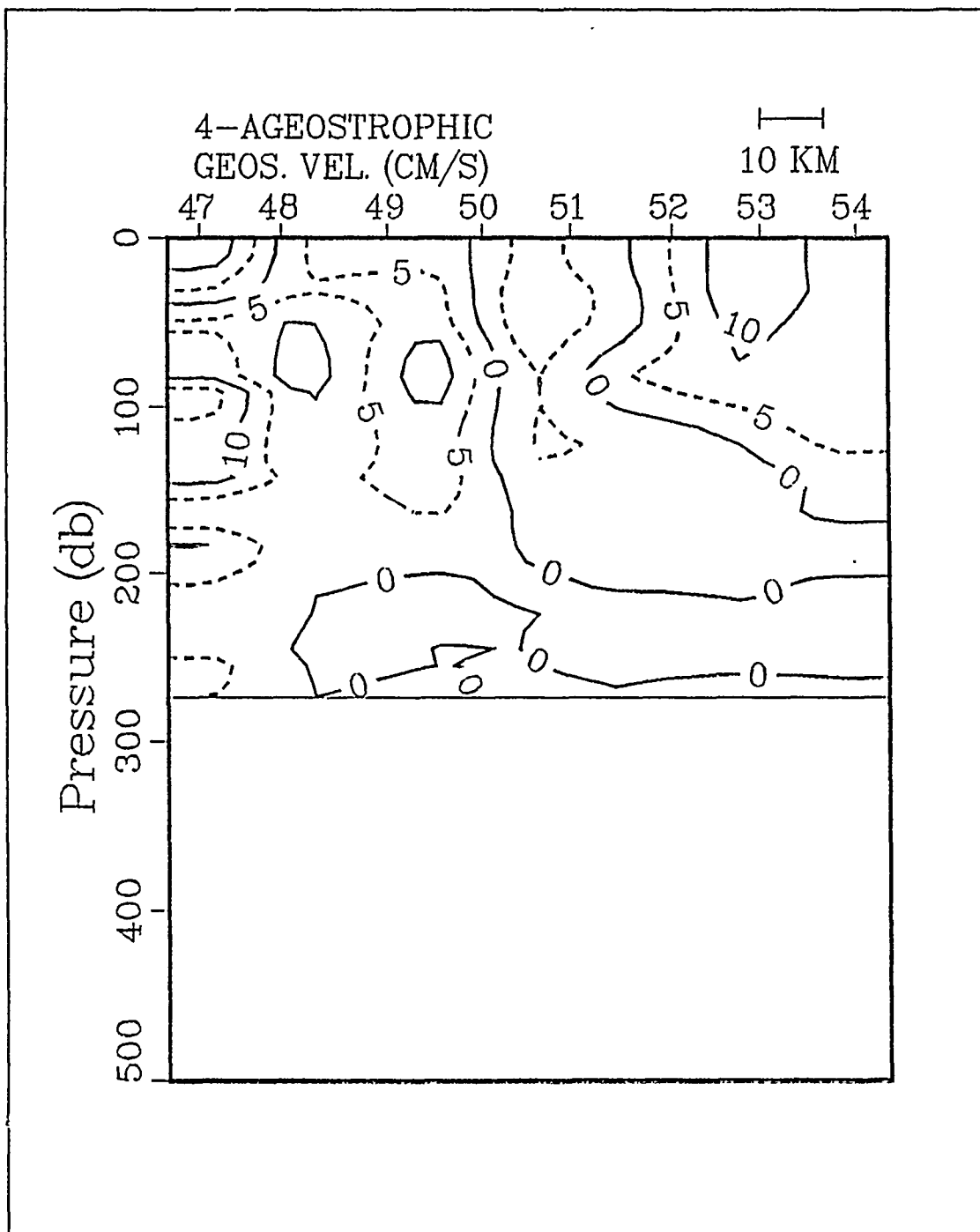


Figure 27. Ageostrophic velocity section for Line 4: Looking offshore, with northwest to the right. Positive velocities indicate onshore flow (out of the page), and negative velocities offshore (into the page).

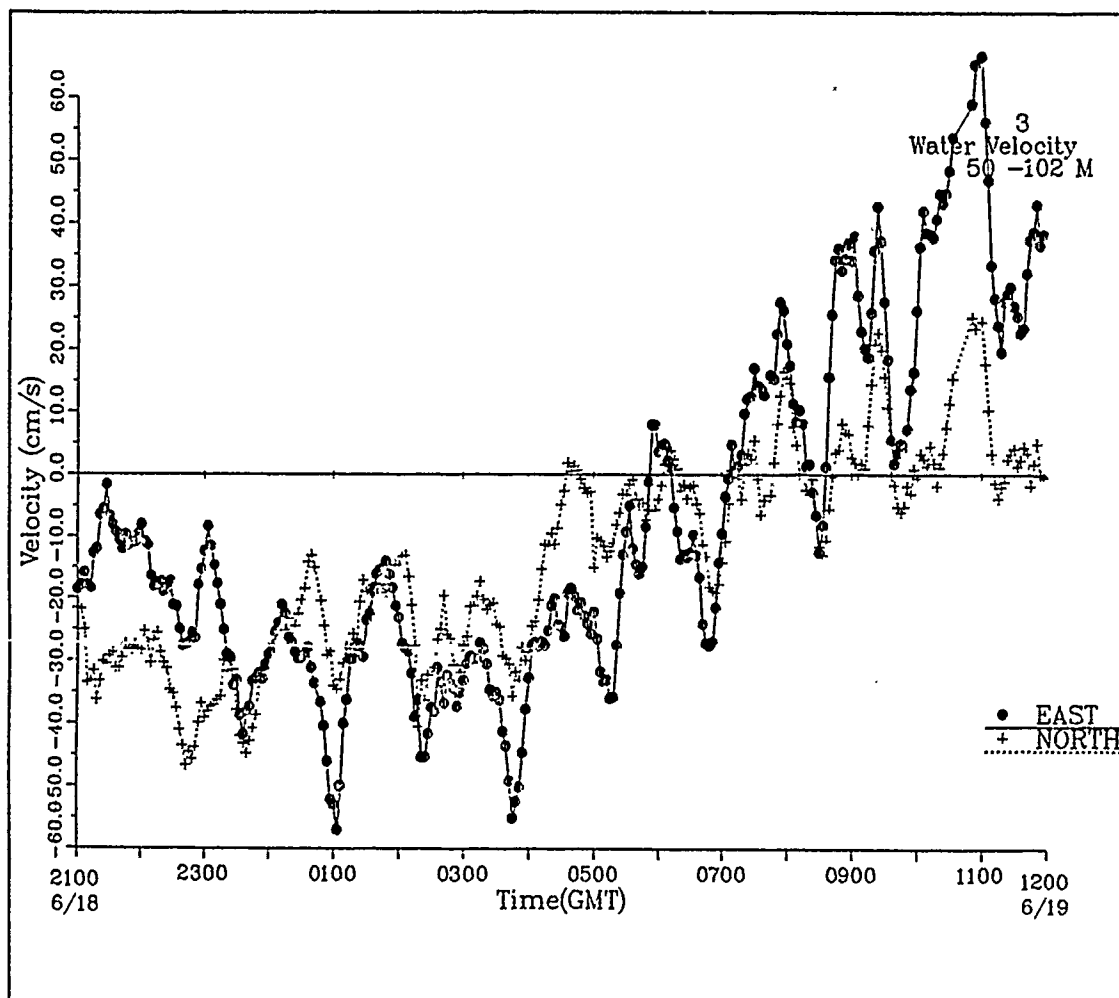


Figure 28. Time series of ADCP velocity in 50-102 m layer for Line 3 (3-min. averages).

If high frequency variability was present, the next question concerns its effect at greater depth, specifically, in the reference layer used to adjust the geostrophic profiles. The same high frequency variation appeared in the zonal and meridional components of ADCP velocity averaged over the adjustment layer (Figure 29), in phase with the fluctuation in the shallow plot but with slightly reduced amplitude, about 12 cm s^{-1} in the deep layer. However, a plot of the adjustment velocity layer averaged over the mean time interval between stations (86 minutes, Figure 30) indicates that the high frequency variability was filtered by averaging over the time between stations. That is, though high frequency variation, here with a period of approximately 1.4 hours, did influence the

velocity in the adjustment layer, the time interval of the station to station averaging was apparently sufficient to suppress the high frequencies and to yield a smooth adjustment layer velocity which was not contaminated by the higher frequencies.

The effect of the high frequency variation might not, however, be entirely removed from the upper portion of the profiles. Internal waves propagating through the survey area would influence the geostrophic profile as well as the ADCP. The slope of the isopycnals would be influenced according to the vertical amplitude and phase of the waves, and the response in the geostrophic velocity would not necessarily be the same as in the ADCP velocity. Several factors could account for this difference. First, the CTD cast takes a finite time to profile the density at a station; this time is relatively long compared to the period of the variation, approaching about one-third of a period. Second, the CTD temporal resolution is much less than in the ADCP data, yielding only one velocity profile approximately every 86 minutes. In contrast, ADCP profiles are taken at a rate of over 100 per minute, then averaged into three minute mean profiles and later over the interval between stations. The u , v components of ADCP velocity for 50 - 102 m resulting after this averaging was performed (Figure 31) show that the high frequencies are filtered from the ADCP profiles. Thus the ADCP data would be less susceptible than the CTD data to aliasing. Further study of the high frequency variability and internal wave generation and propagation in this region is required before their effects on CTD and ADCP velocity measurements can be resolved.

Pierce and Joyce (1988) applied an inversion technique to CTD, ADCP, and oxygen measurements to obtain velocity and transport estimates across the Gulf Stream near Cape Hatteras. Applying geostrophy and using the ADCP velocity at 100 dbar as the reference, they obtained a transport balance within the bounds of the noise level of their measurements. In contrast with the present study, the area surveyed was a region of strong signal (Gulf Stream core velocities of $120\text{-}130\text{ cm s}^{-1}$), relatively simple structure (a single strong jet, with no eddies impacting the transects), different scale and different geometry. A triangular region (one side bounded by the continental shelf) with one side over 500 km long was used. Temporal changes were not as rapid or were not as significant over the large region, and the manner of sampling made the survey more synoptic than the box used herein. The region off Point Arena was much more complex, with several jet-like features and strong temporal and spatial variability, and with relatively low signal, i.e., lower velocity flows, so that noise, both instrumental and geophysical, were more troublesome off California than in the Gulf Stream.

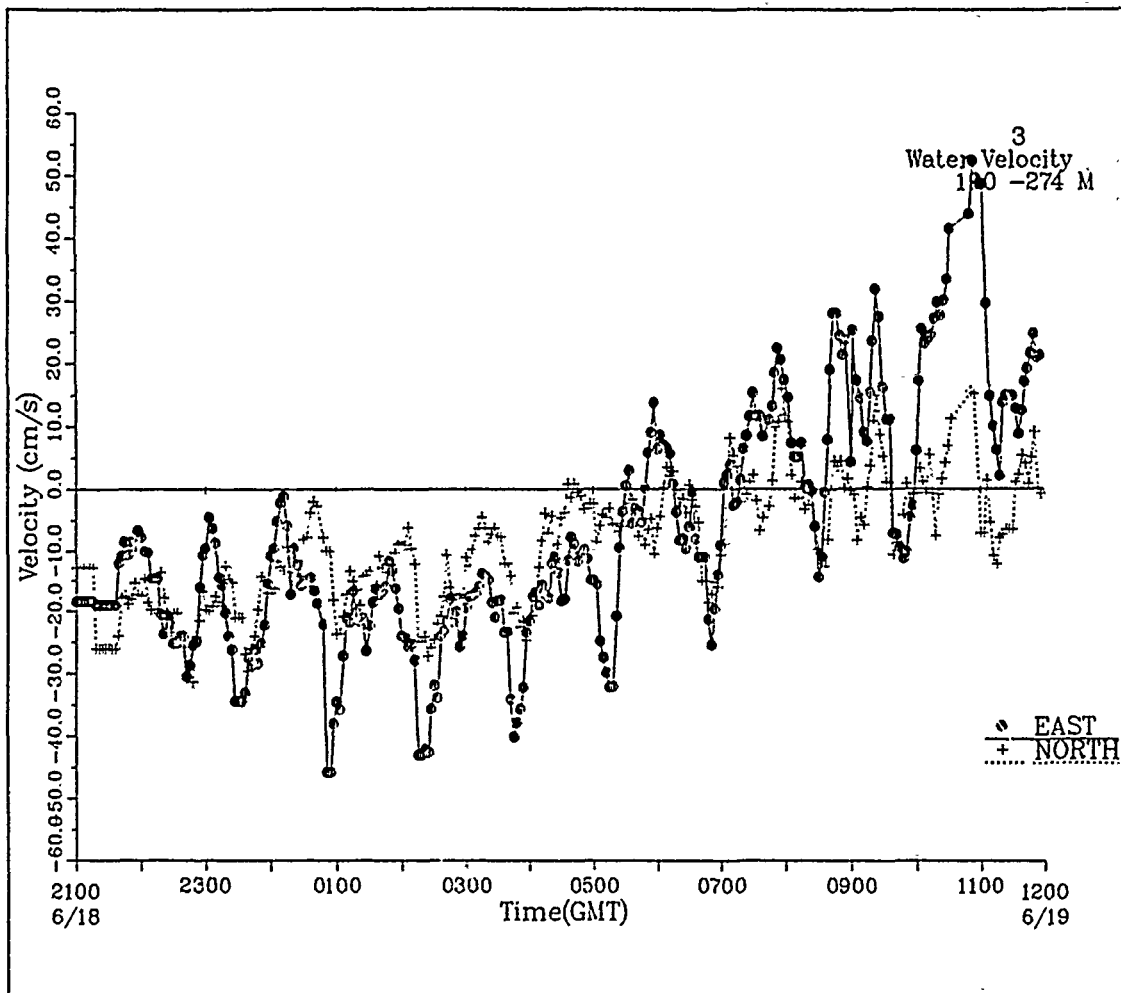


Figure 29. Time series of ADCP adjustment (190 - 274 m) layer velocity for Line 3 (3-min. averages).

Huyer and Kosro (1987) compared vertical shear as determined from CTD and ADCP measurements over the continental shelf and slope near Point Arena during the Coastal Ocean Dynamics Experiment (CODE) in 1981 and 1982. Averaging six synoptic surveys, they found significantly more shear in the upper 40 m in the ADCP data than in the geostrophic calculations, and attributed this difference to the Ekman velocity. This is consistent with the results of this study; average winds for their study were strong from the northwest. When strong winds prevailed, as along Lines 2 and 3 of this study, the Ekman transport was significant, and the corresponding shear was observed in the profiles.

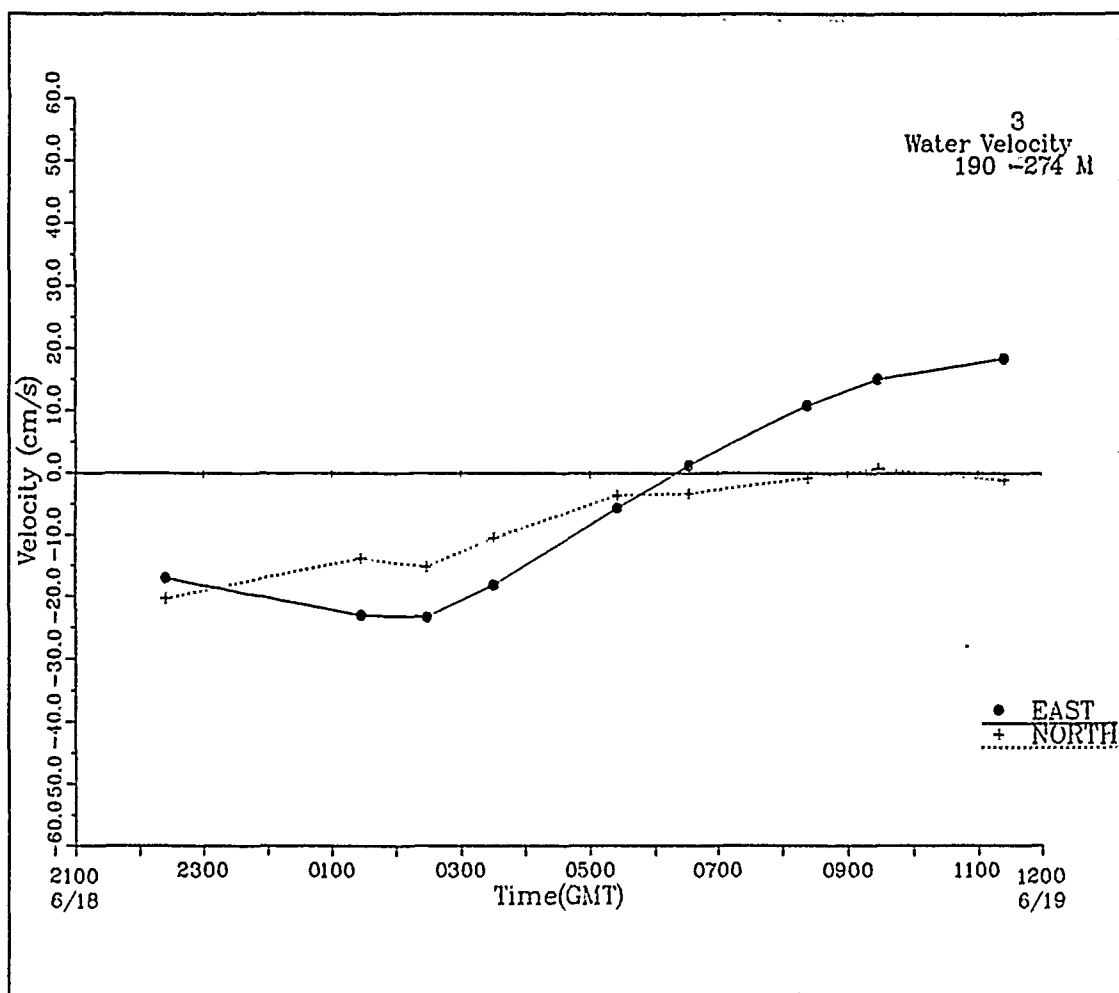


Figure 30. Time series of ADCP adjustment (190 - 274 m) layer velocity for Line 3 (86-min. averages).

The differences in shear due to high frequency variability observed in the present work were not observed in either of the aforementioned studies, most likely because 1) for the Gulf Stream study the spatial averaging was greater (40 km between stations) and the mean flow velocity was greater, and 2) the CODE data was more heavily smoothed, averaging the data from six synoptic surveys before shear comparisons were made. There is also the possibility that the high frequency motions observed in this survey were not present in the Gulf Stream region or are not a constant feature off Point Arena.

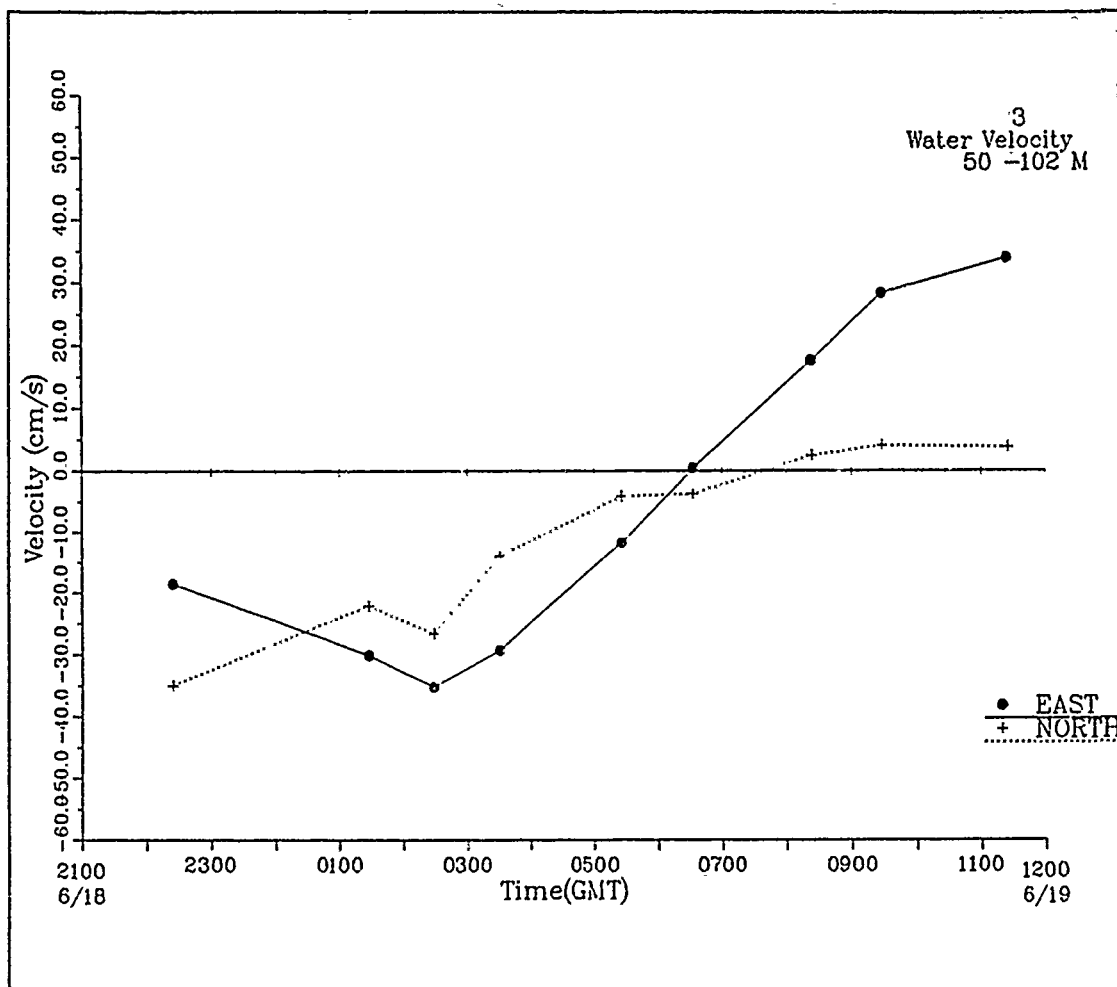


Figure 31. Time series of ADCP velocity in 50 - 102 m layer (bins 13 - 25) for Line 3 (86-min. averages).

V. CONCLUSIONS AND RECOMMENDATIONS

A. CONCLUSIONS

In the survey region off Point Arena during June 1987, geostrophy accounted for the major features observed in the CTD and ADCP data. Additionally, however, there were significant ageostrophic motions which variously impacted the velocity and transport measured by the two systems. The method of using an ADCP adjustment layer to calculate improved geostrophic velocity profiles achieved best results where the signal of interest, geostrophic flow, was strongest, but was degraded by noise, especially internal waves, where the flow was weak. The adjustment layer chosen for this study was apparently influenced by high frequency internal waves, but the influence was removed in the station to station averaging of the ADCP data. Internal waves, through deflection of the isopycnals, still contaminates the CTD data. In this study there was evidence that such contamination did occur, with the most notable effect being in the upper 200 m in regions of high stratification. One principle result of this study is that the choice of a reference layer for geostrophic profile adjustment based on ADCP measurements is not in itself sufficient to resolve the differences between the two instruments, particularly in the upper ocean and in regions of low geostrophic flow. Whether the remaining differences in the profiles after adjustment and after Ekman transport has been accounted for are due to internal waves, navigation errors, or to lower frequency ageostrophic effects could not be determined.

Using ADCP data to reference geostrophic velocity profiles is a method which must be applied discriminately, taking full account of the relative magnitude of the ageostrophic components of the flow, particularly internal waves. In areas of weak flow, internal waves may contaminate the ADCP data, adversely affecting the steadiness of the reference level. Averaging adjustment layer velocity over the period of the observed internal waves would remove this contamination. In this study, the vertical sections of velocity produced using geostrophic profiles adjusted to the ADCP velocity in the 190-274 m layer provided a better description of the mean flow field than the sections of geostrophic velocity using a level of no motion of 500 dbar, or the sections of ADCP velocity alone.

The transport was observed to be out of balance in an offshore box across a cold filament, due primarily to the non-synopticity of the sampling. The onshore-offshore

transport along Line 3 was out of balance, with more flow offshore due to the contribution of a strong jet-like flow to the north of the meander which was included in the transect. The on-offshore transport was approximately balanced along Line 4, further seaward, where the offshore flow in the jet and the offshore portion of the meander nearly equalled the net onshore transport of the meander.

B. RECOMMENDATIONS

The use of ADCP and CTD together and in conjunction with other instruments is desirable in oceanographic surveys. Each sensor employed by the scientist has its own unique capabilities and limitations. Integrated and coordinated use of all available sensors can provide much more information than each used independently. In the case of ADCP and CTD surveys, CTDs provide accurate information about the density structure of the ocean, to depths far below the range of hull-mounted acoustic Doppler current profilers, and can be used to infer density-driven motion or to detect phenomena affecting the density structure. The ADCP is capable of measuring motions which are not density-driven, such as tides, internal waves, inertial oscillations, the Ekman transport, and nonlinear effects. Properly sampled and accounted for, these motions, rather than being troublesome noise, may be filtered out or be studied for their own sake. The use of the two instruments in conjunction allows geostrophic reference levels to be more accurately chosen, or as was done herein, to adjust geostrophy to a level of known motion. It further allows the resolution of the ageostrophic velocity component from the total field.

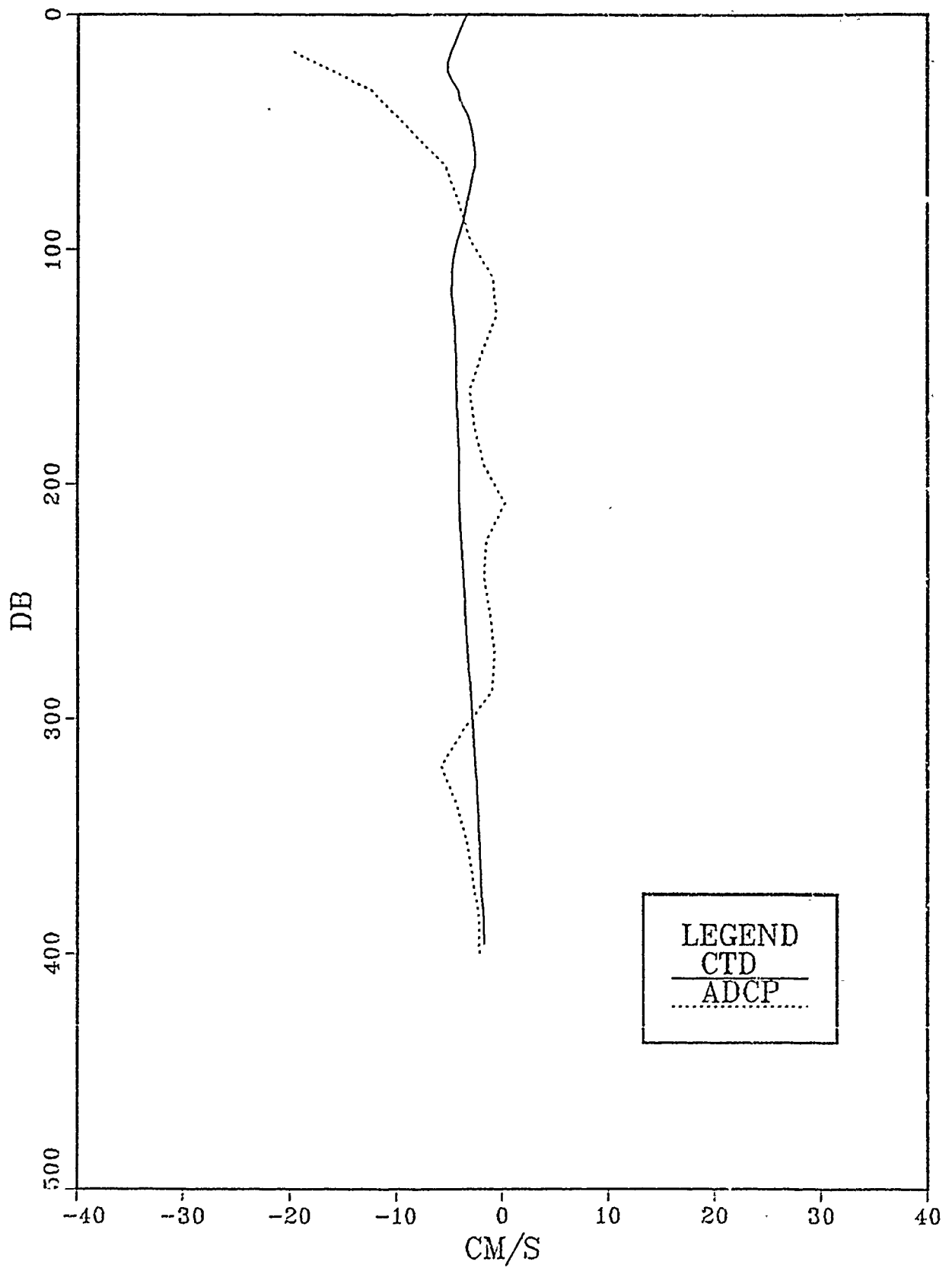
Increasingly accurate and detailed descriptions of the ocean velocity field will be required for use in initializing and evaluating numerical models, and to verify dynamical theories. Future surveys should continue to use multiple sensors and the best available navigation methods, and future research should continue to solve the problems associated with optimal integration of the various data obtained.

APPENDIX A. VERTICAL PROFILES OF HORIZONTAL VELOCITY CALCULATED FROM CTD DYNAMIC HEIGHT (REF TO 500 DB) AND ADCP DATA

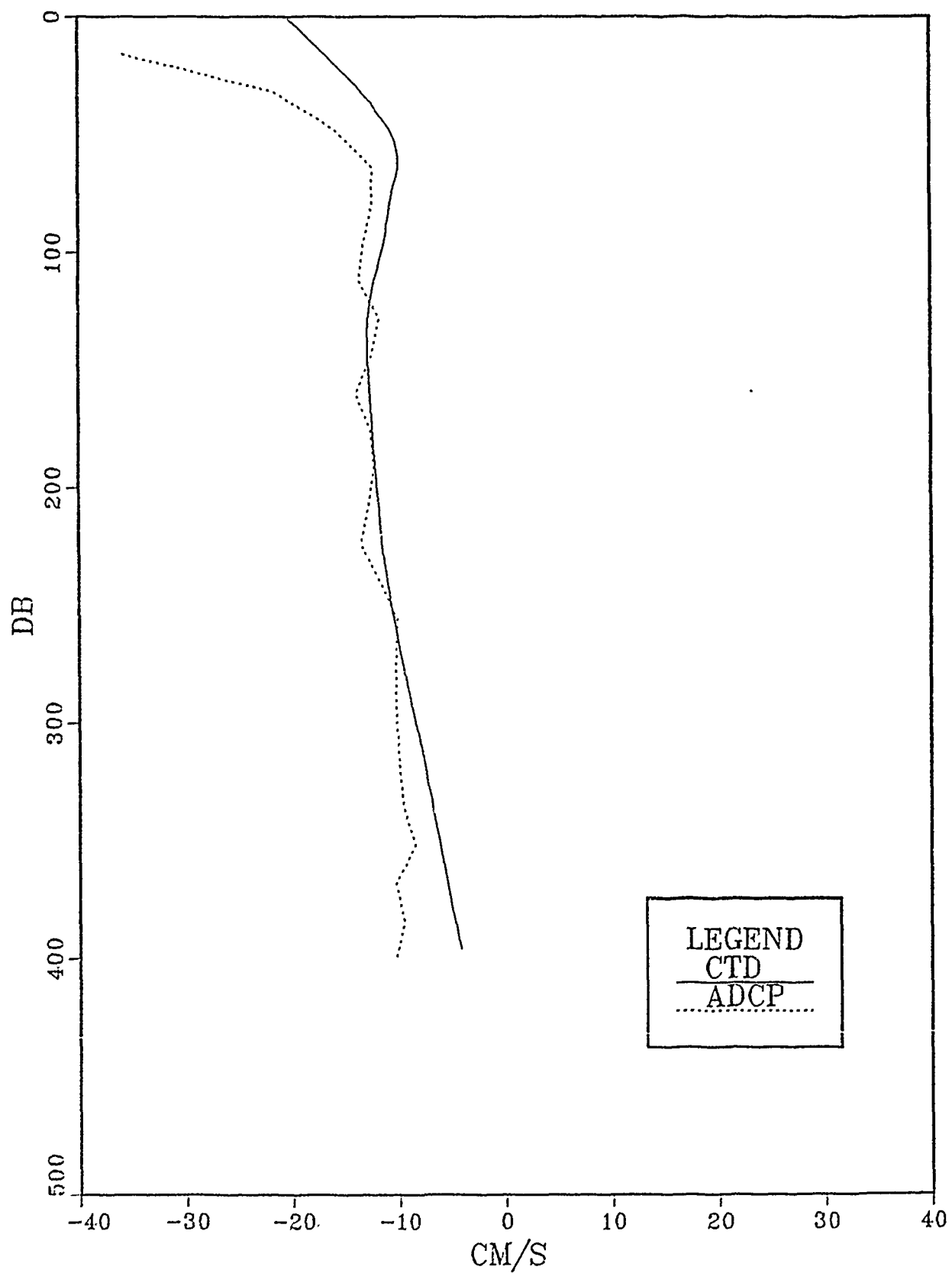
To prepare the profiles in this appendix, ADCP velocity was averaged horizontally between the corresponding CTD station pair, approximately 15 km in the mean. The actual distance between stations was used. Vertical averaging was 16 m, over four 4 m bins. Geostrophic velocity was calculated every 4 m using assuming a level of no motion at 500 db.

Due to an interface malfunction during the cruise, ADCP data was not available between stations 47 and 48. For this profile, three-minute ADCP profiles from 30 minutes before arrival at station 47 and from the 30 minute period after departure from station 48 were averaged to synthesize a profile to fill the gap. For this station pair only, vertical averaging is over a 4 m bin depth.

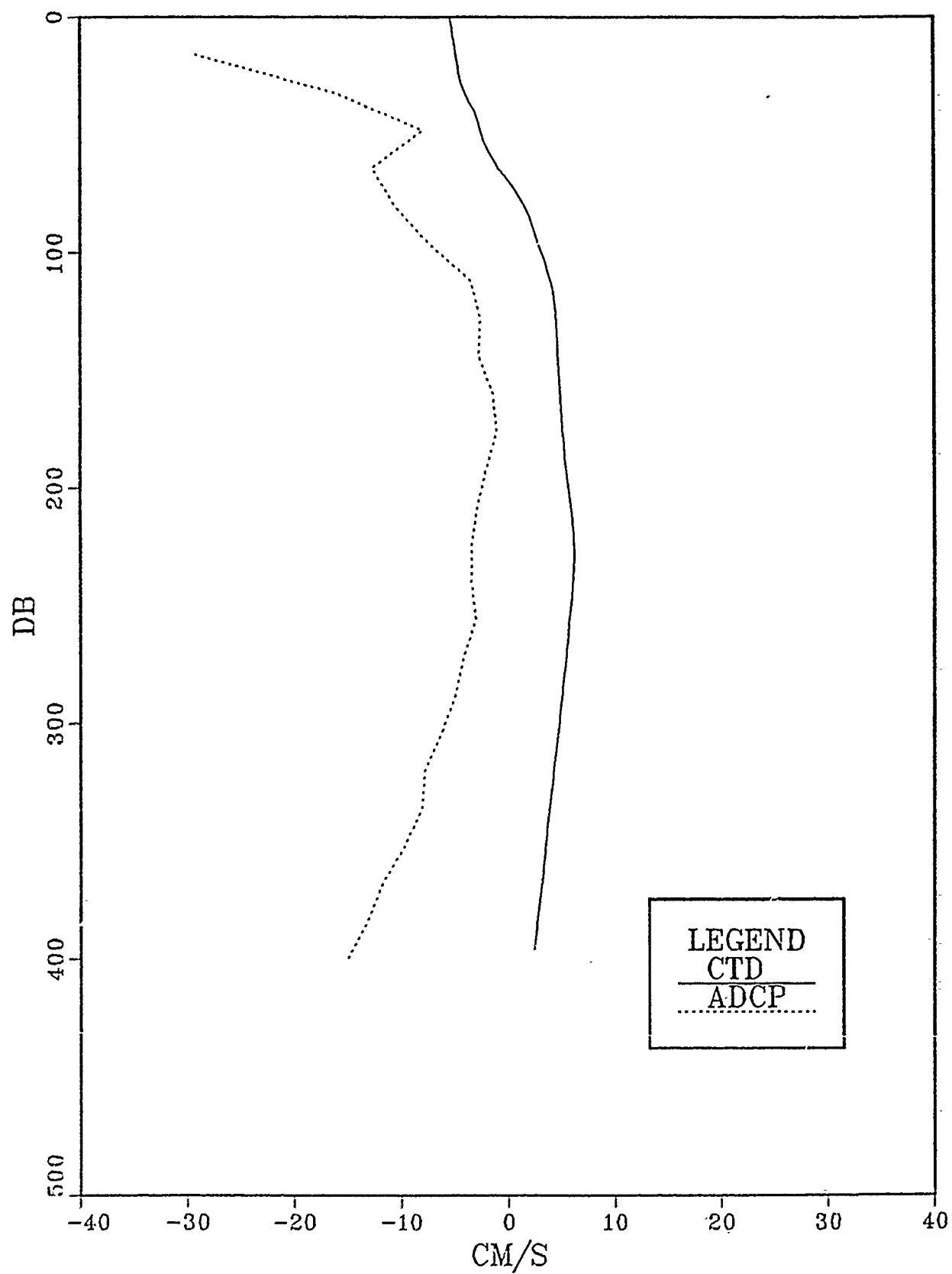
22-23



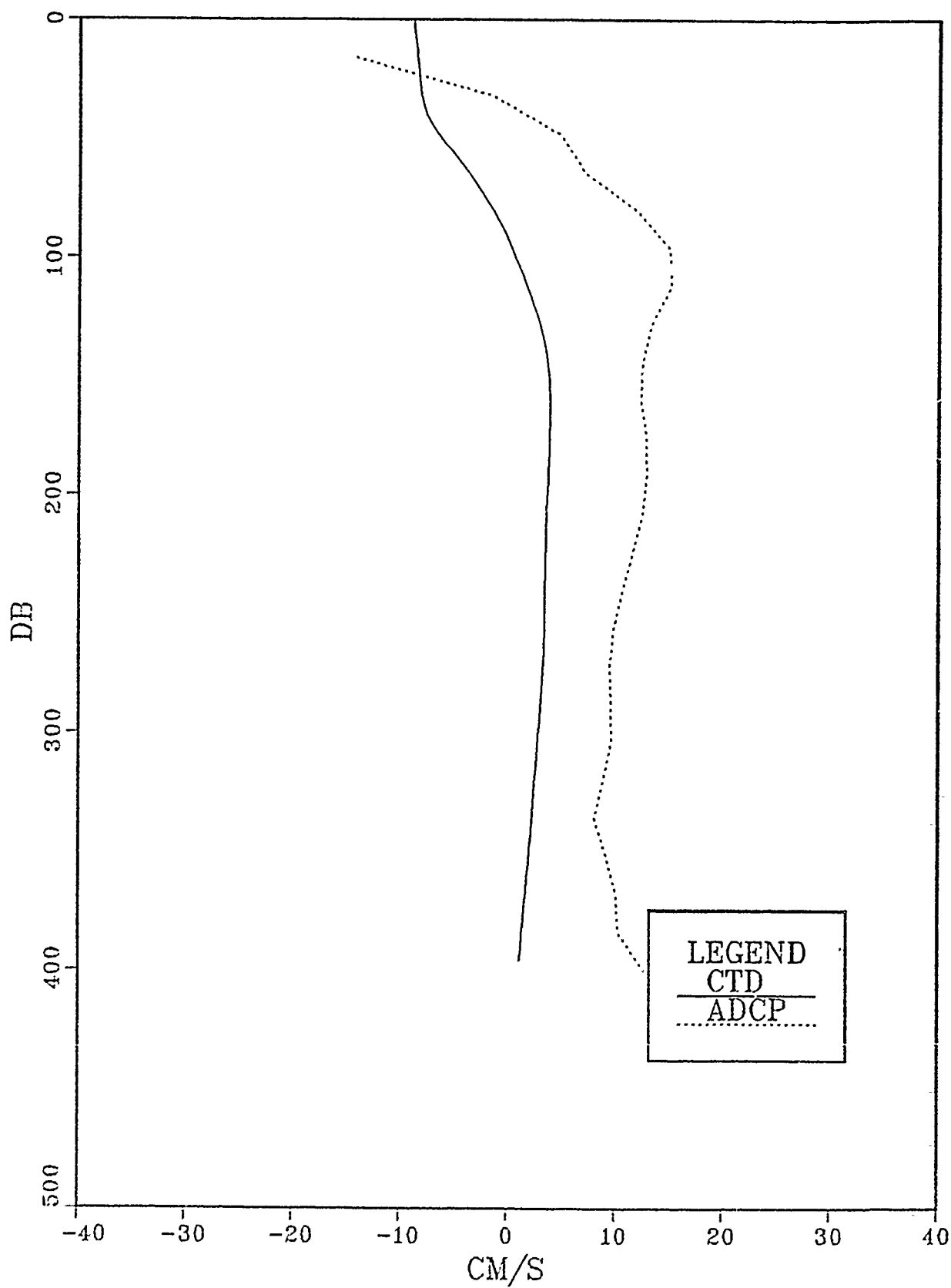
23-24



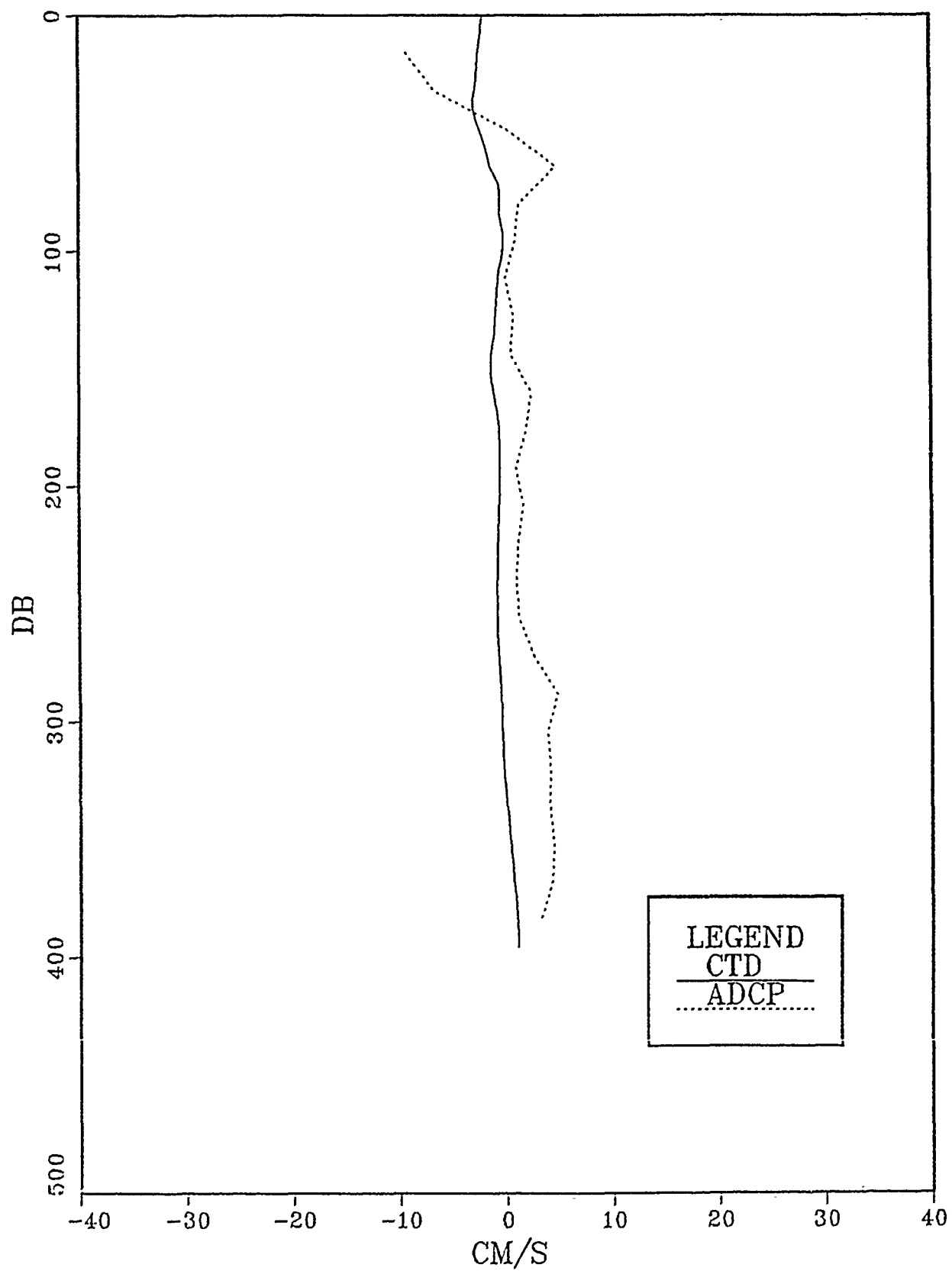
24-25



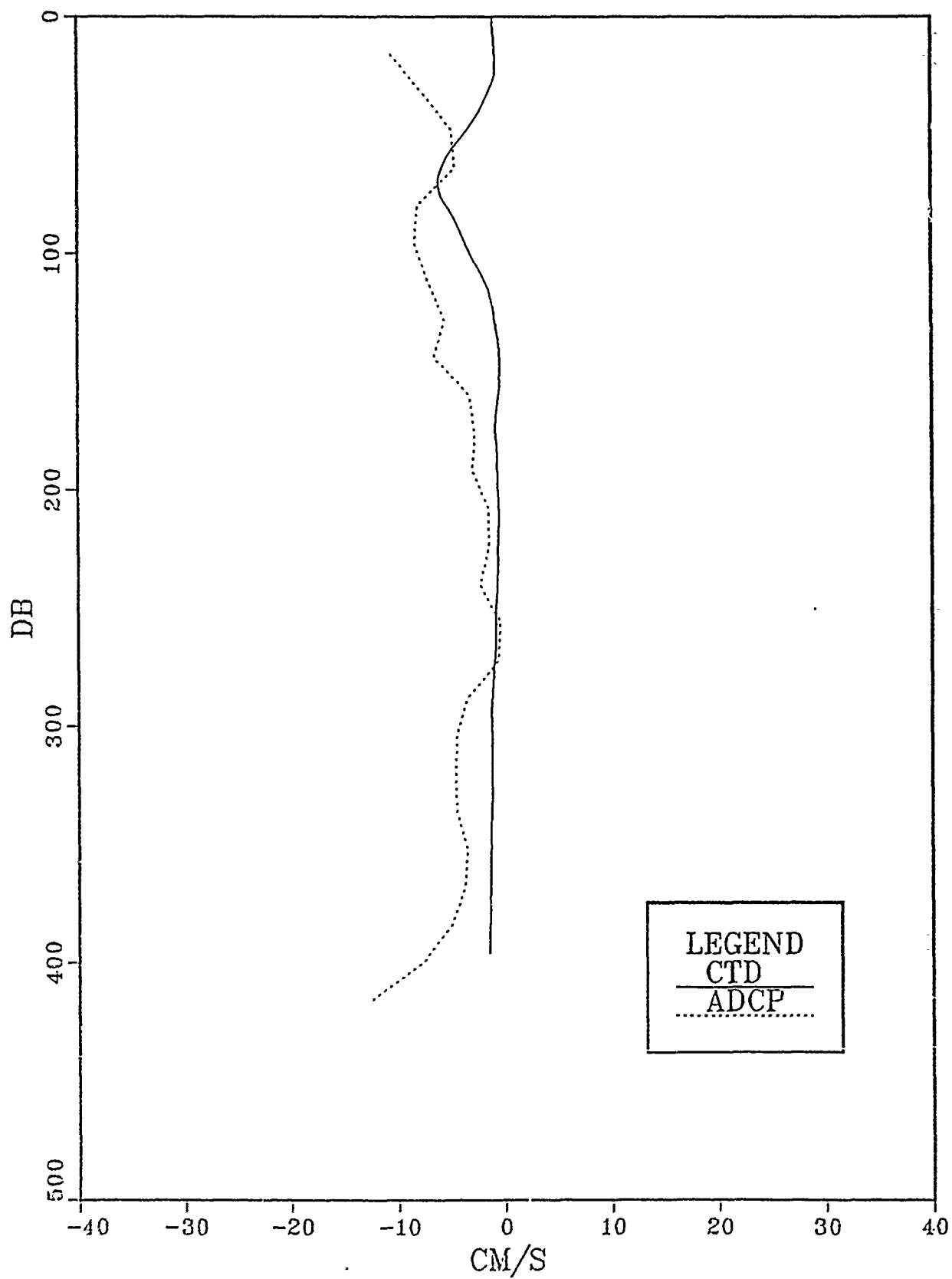
25-27



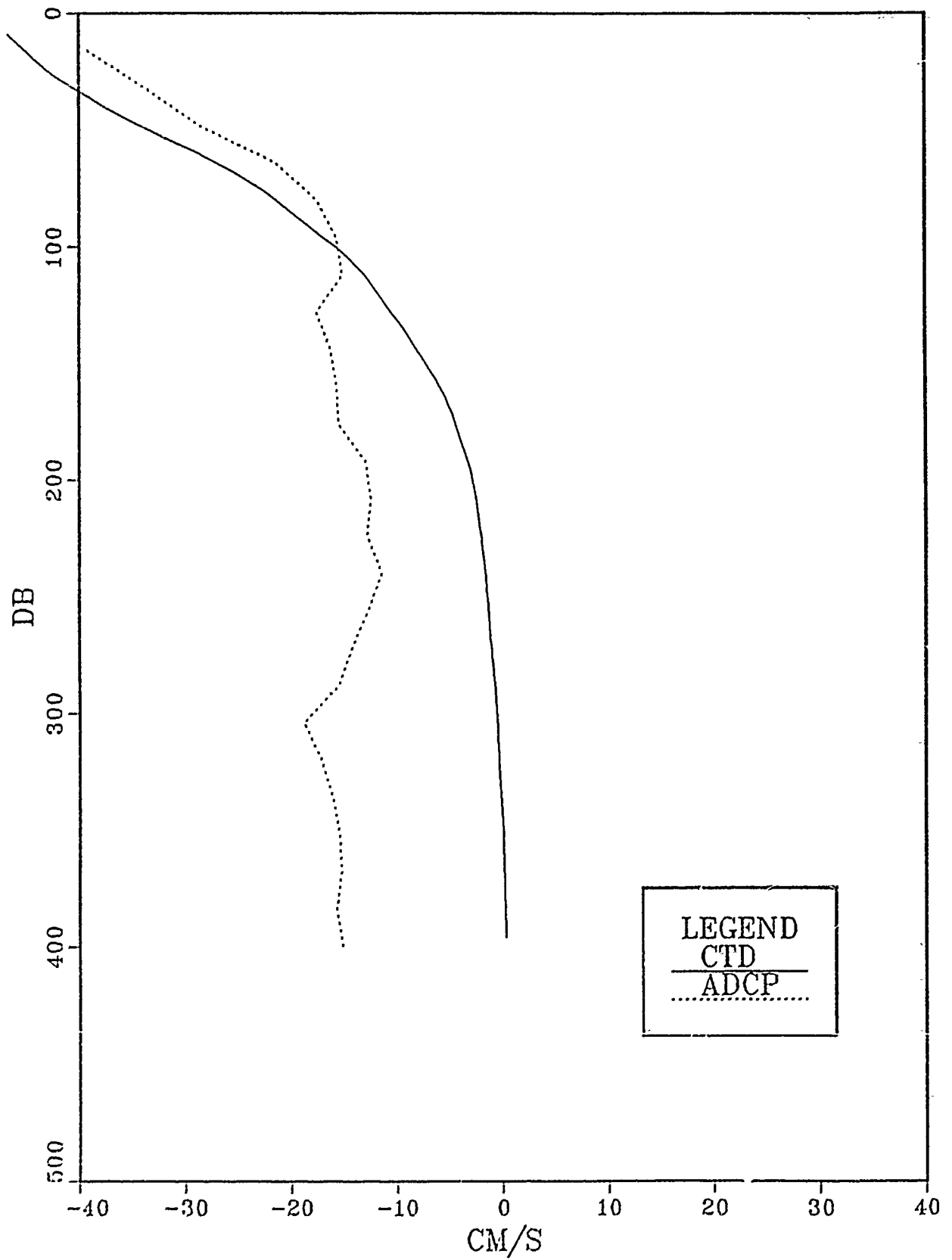
27-28



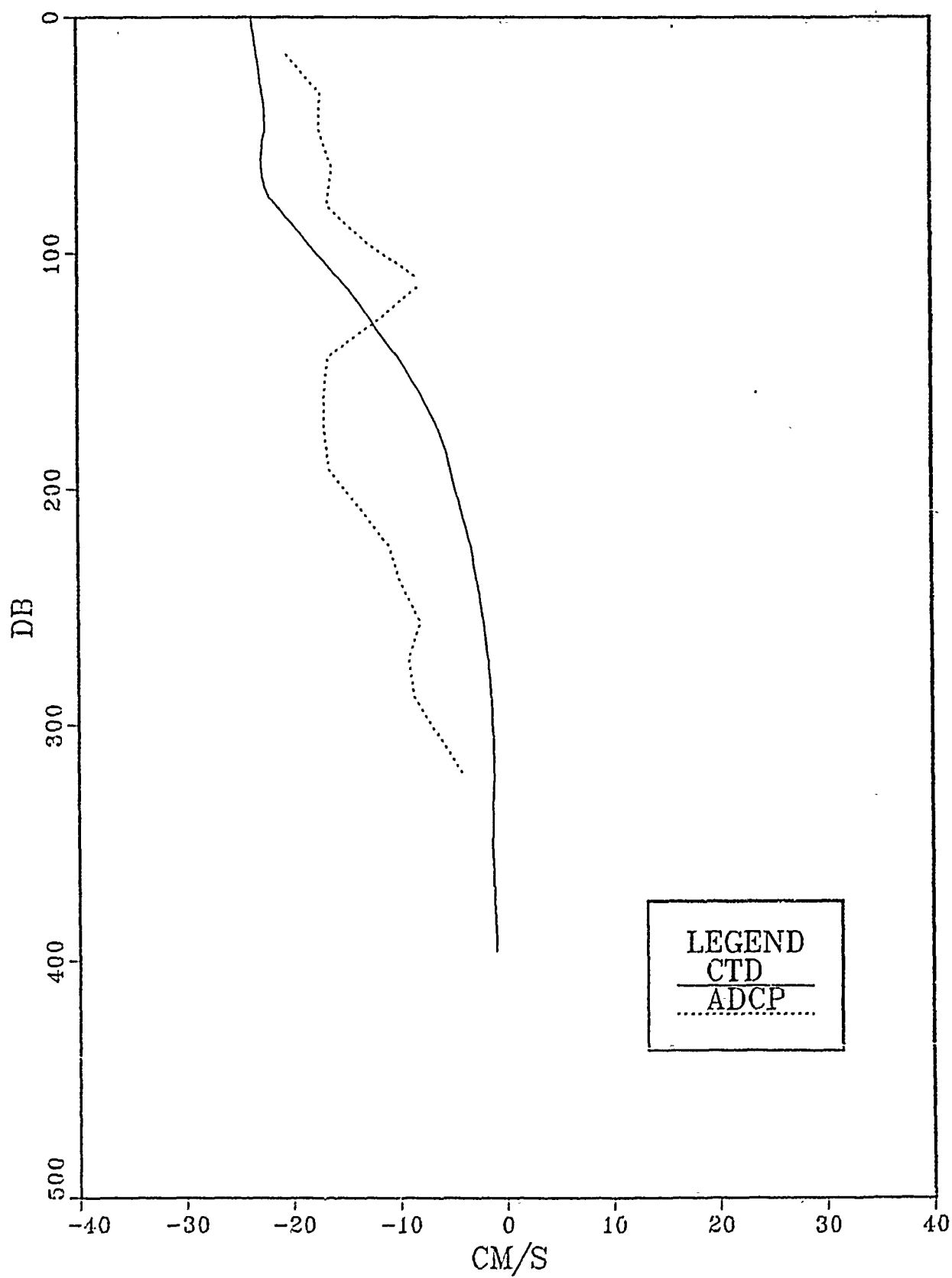
28-29



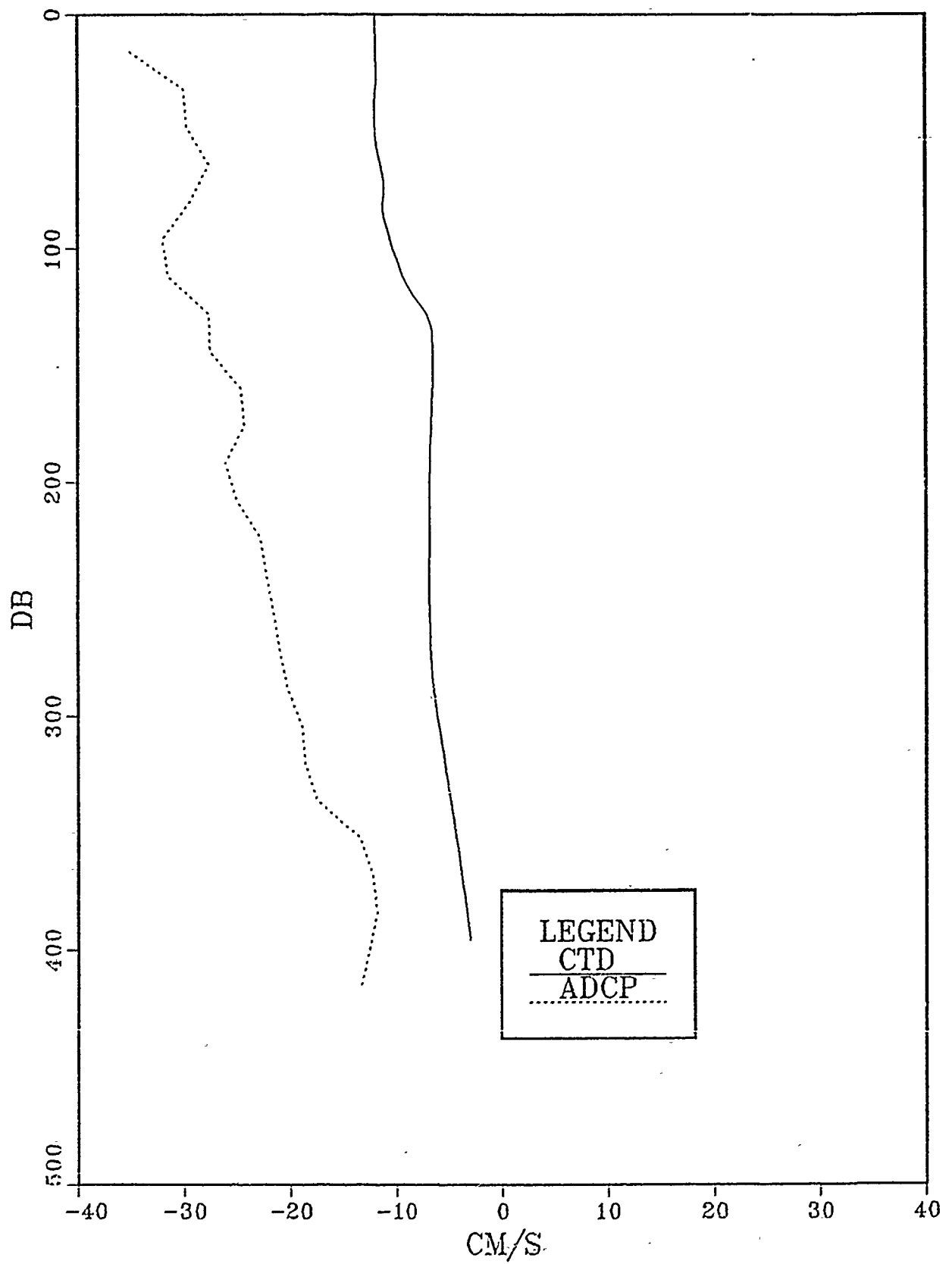
29-30



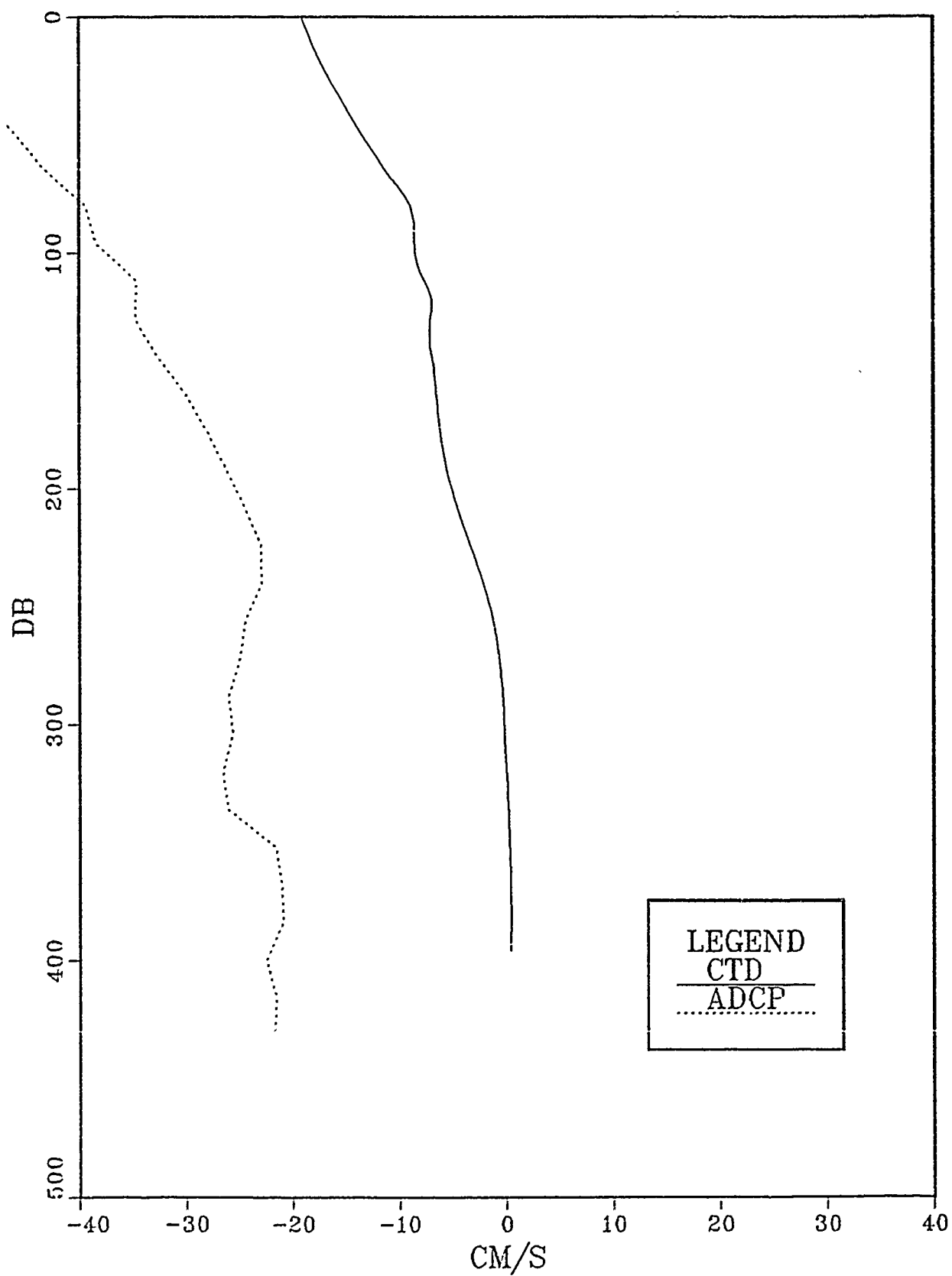
30-31



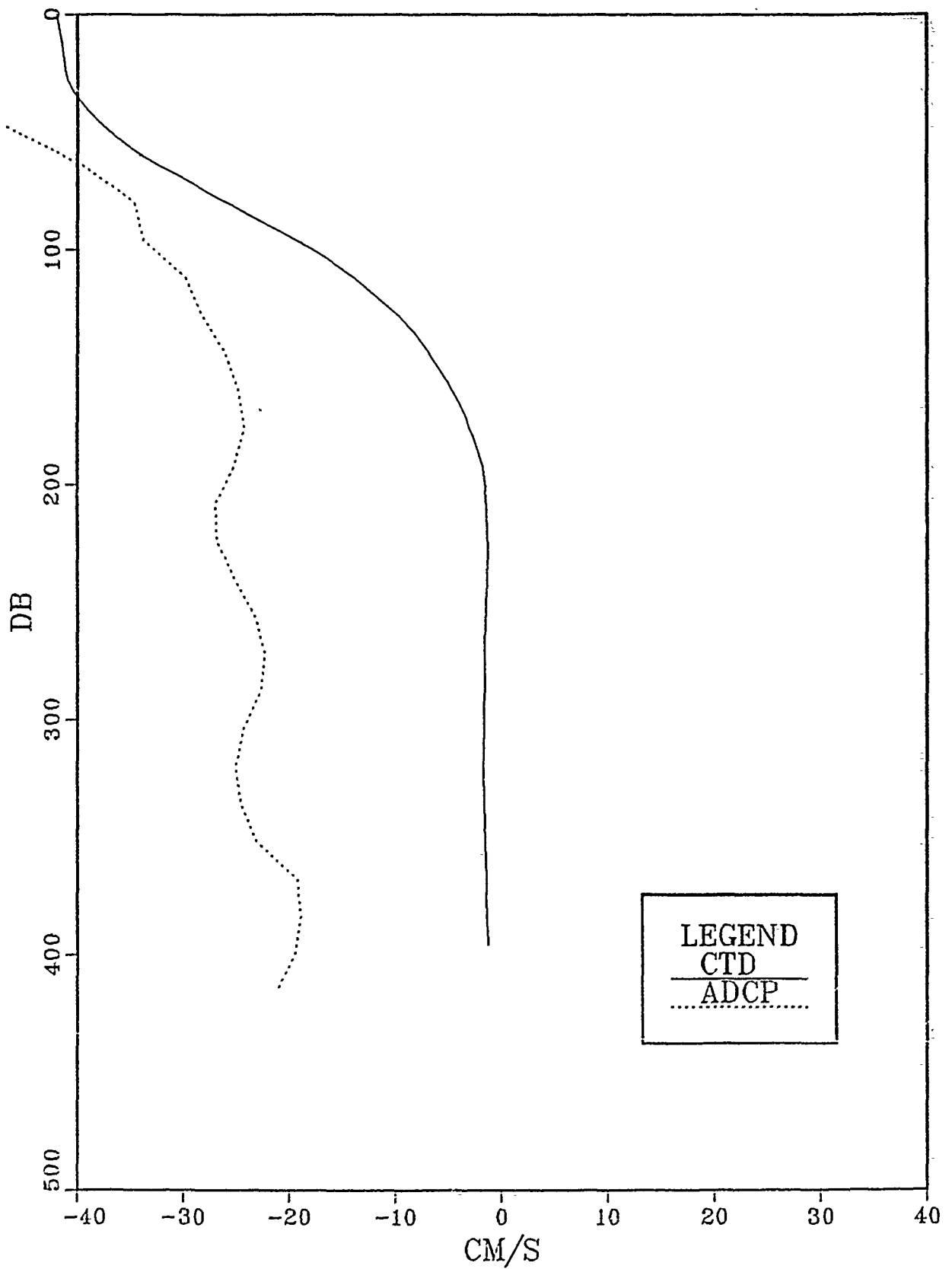
33-34



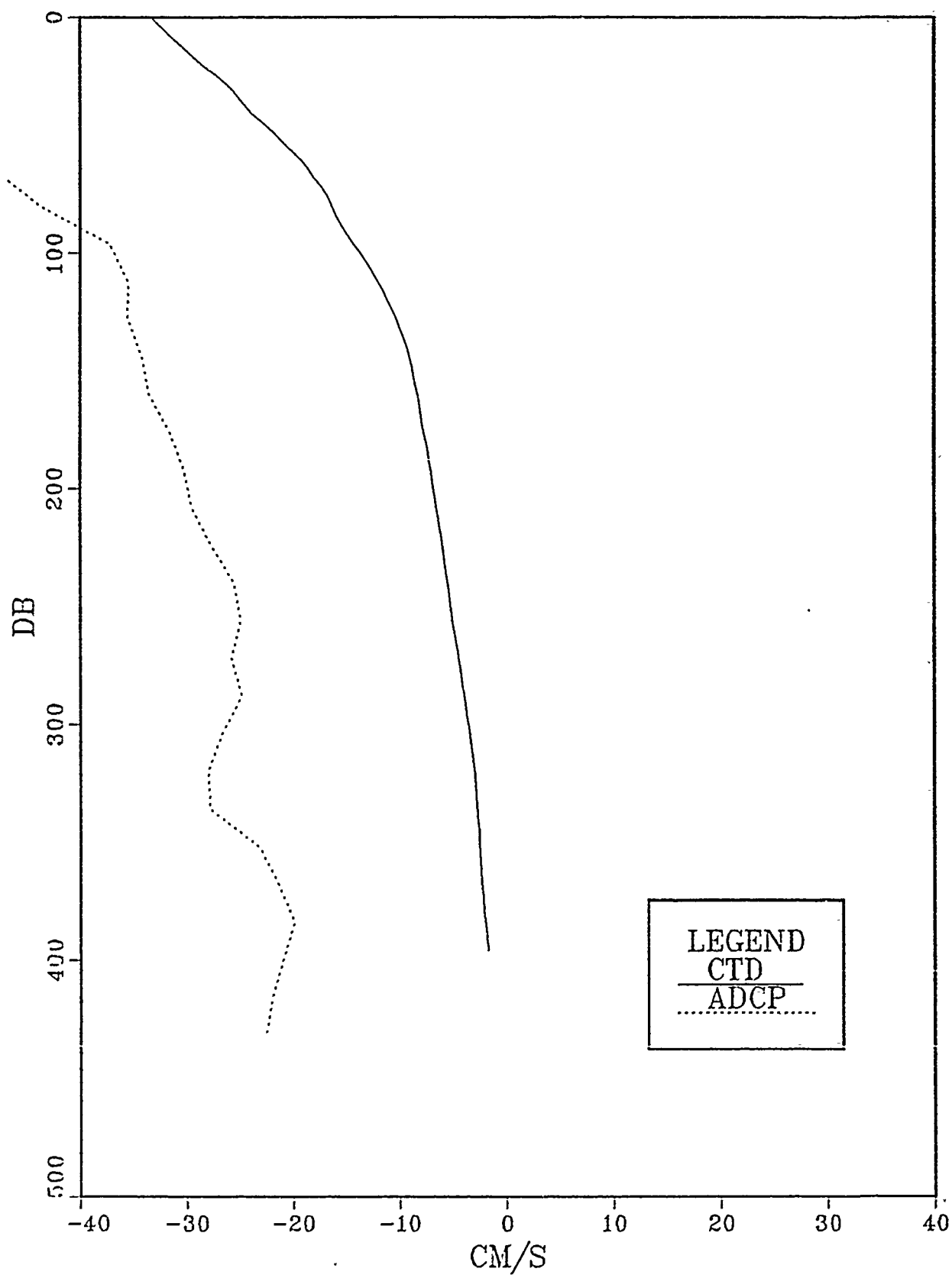
34-35



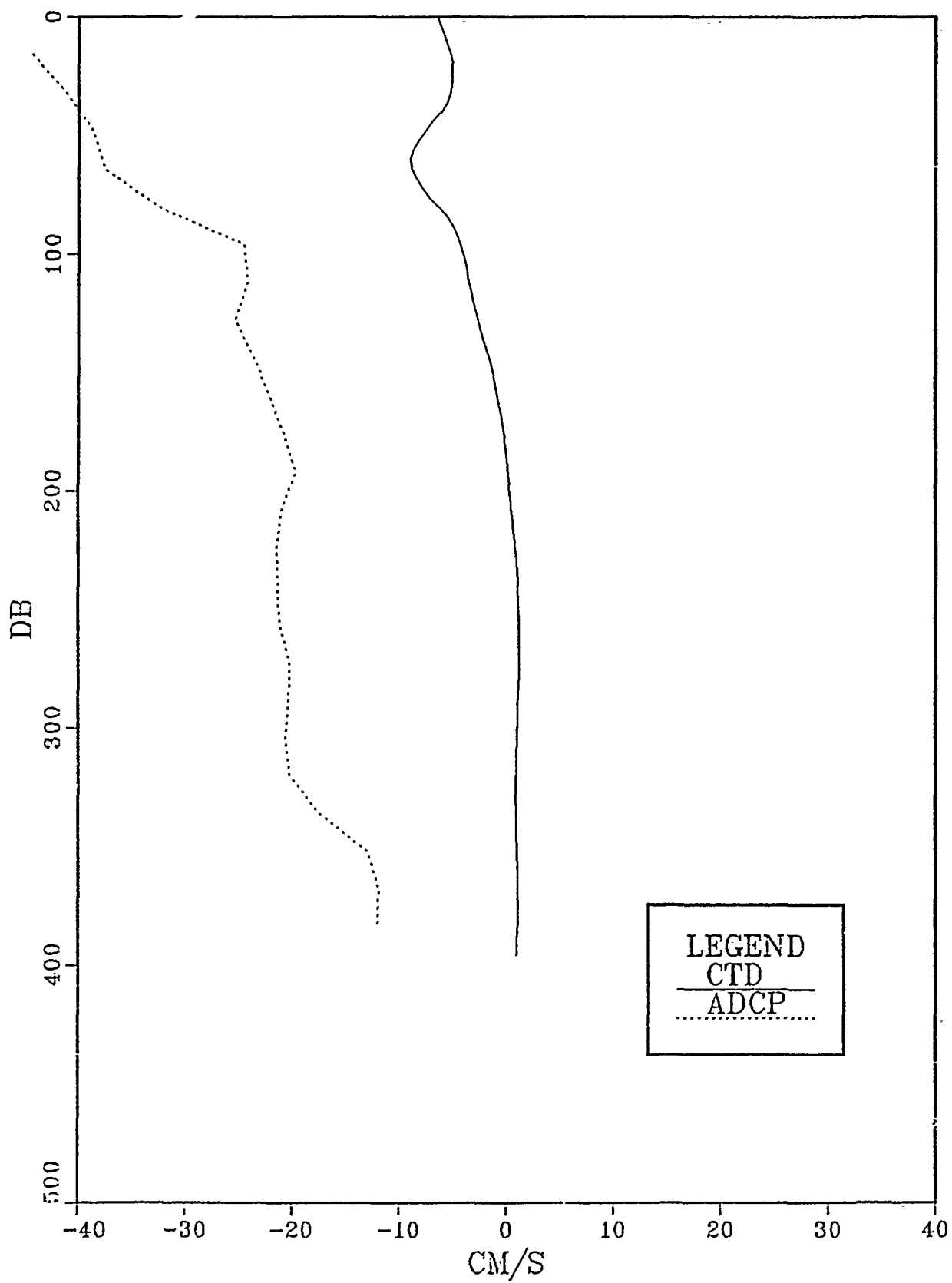
35-36



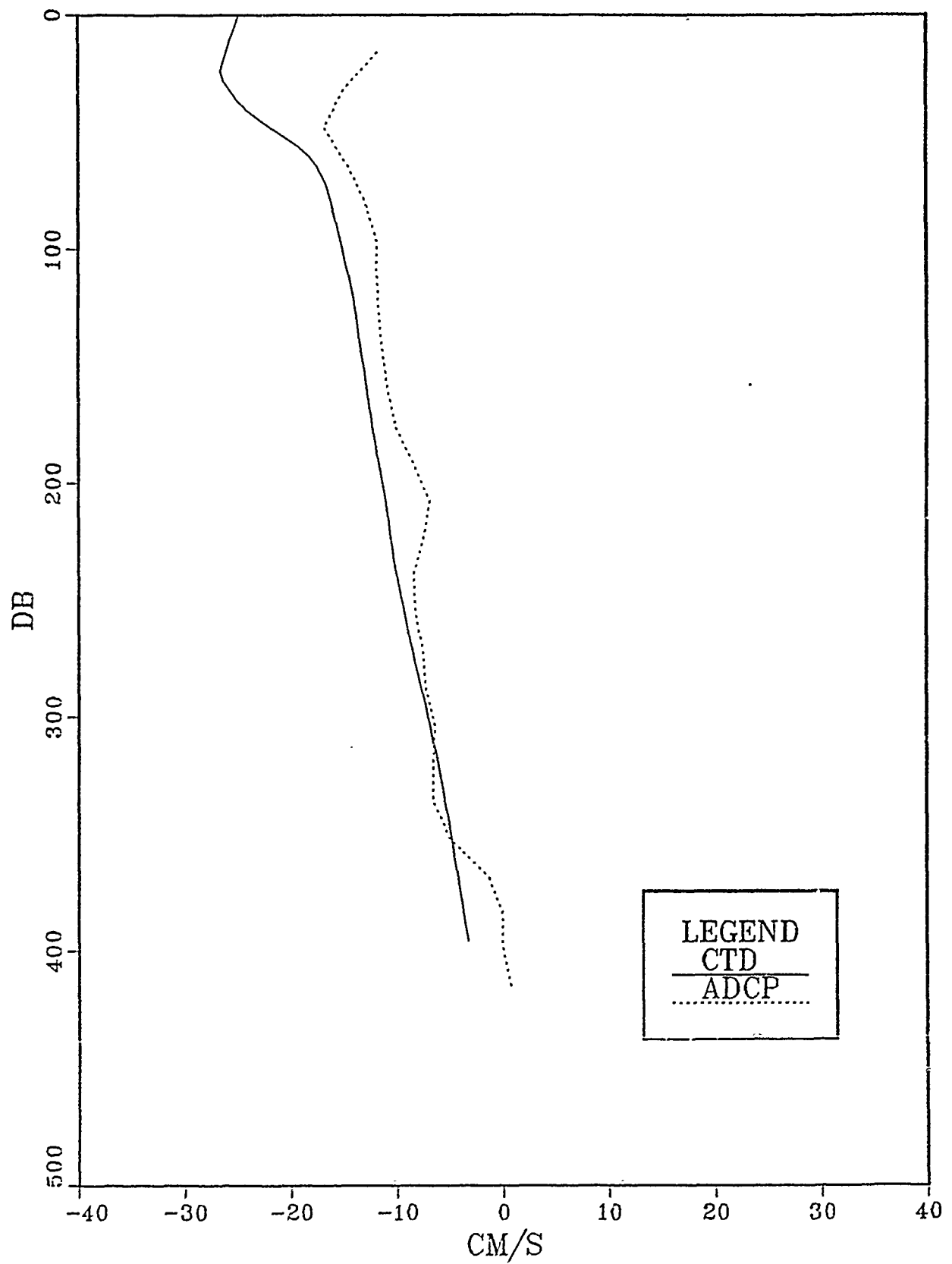
36-37



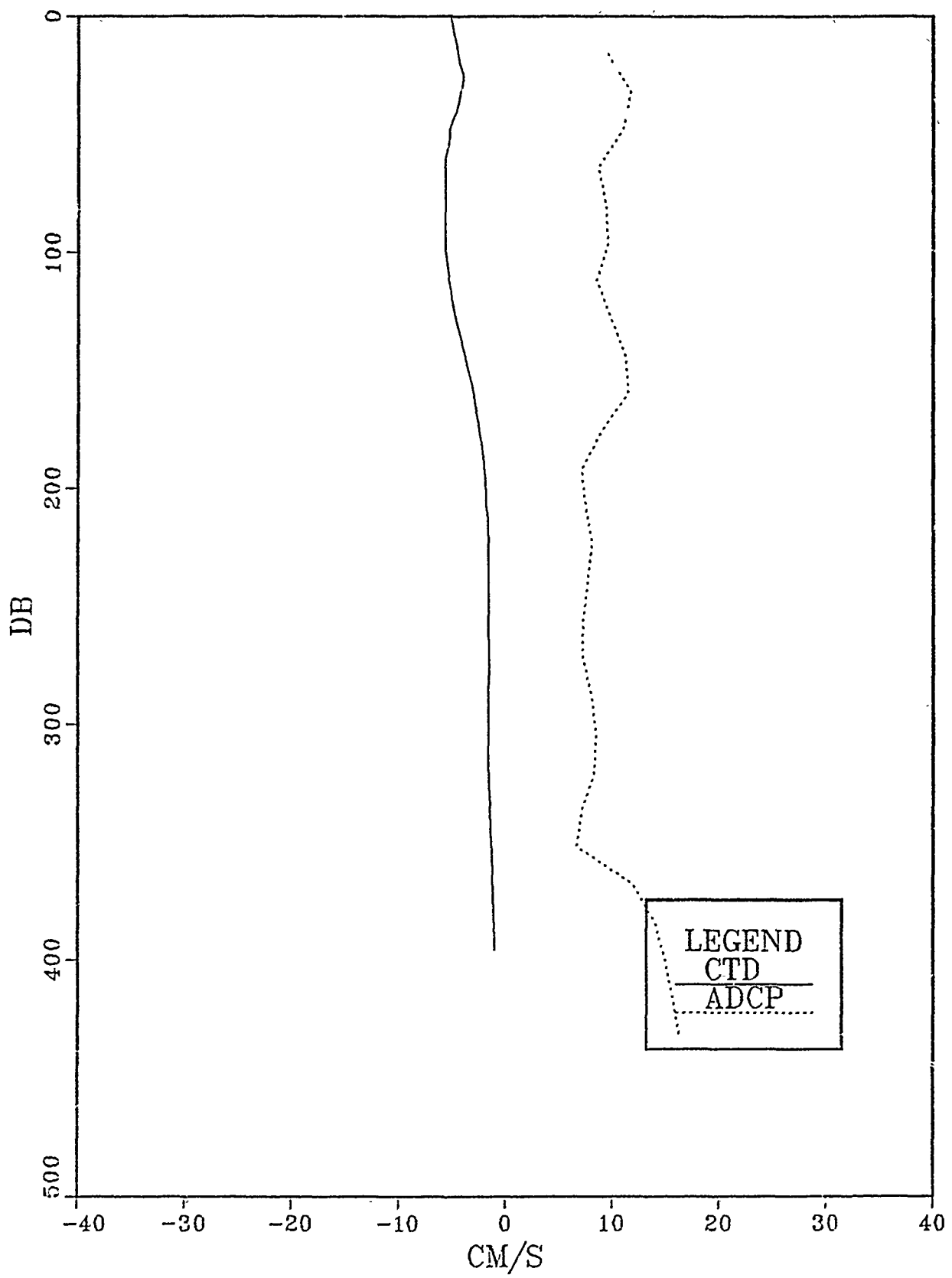
37-38



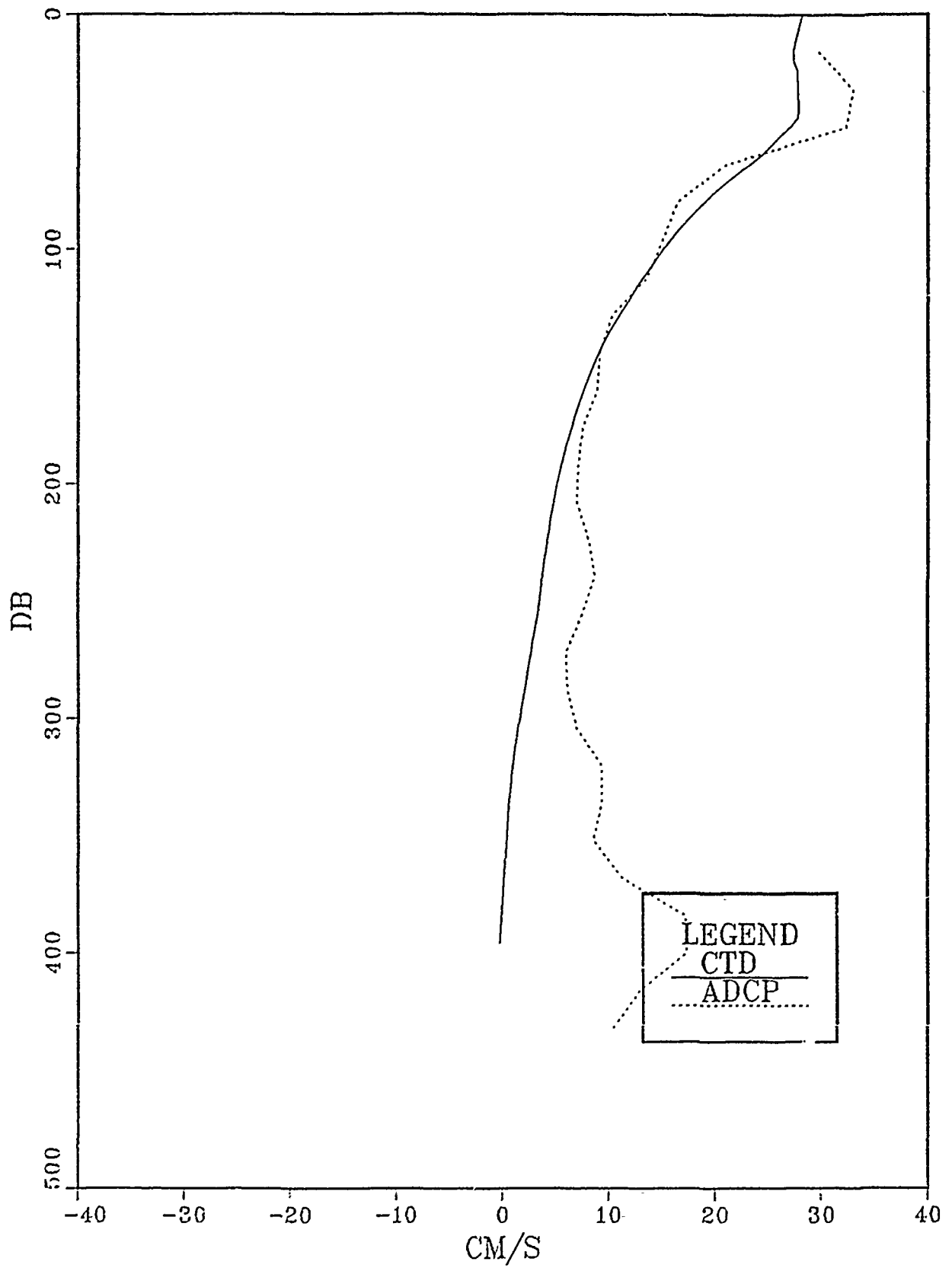
38-39



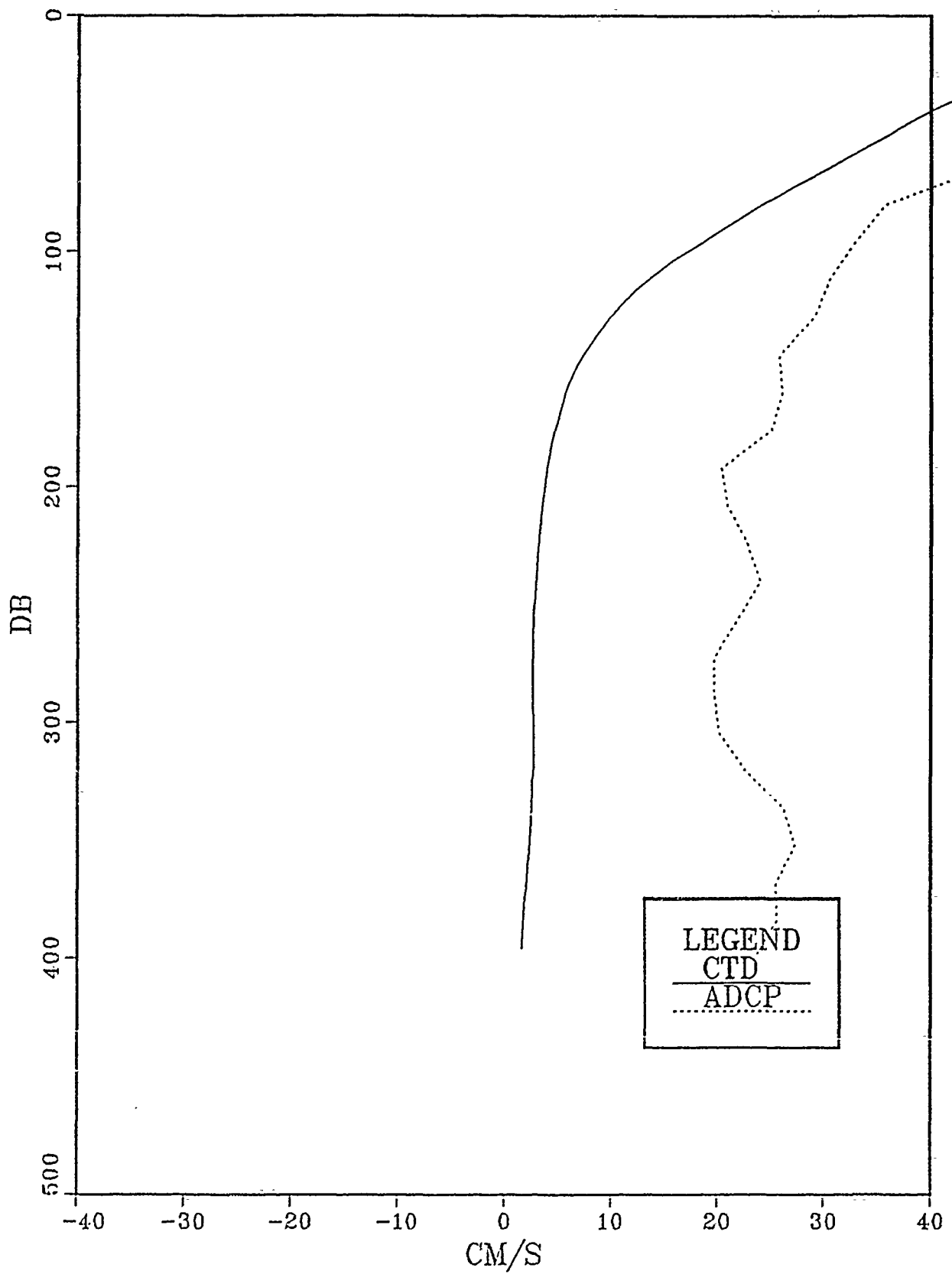
39-40



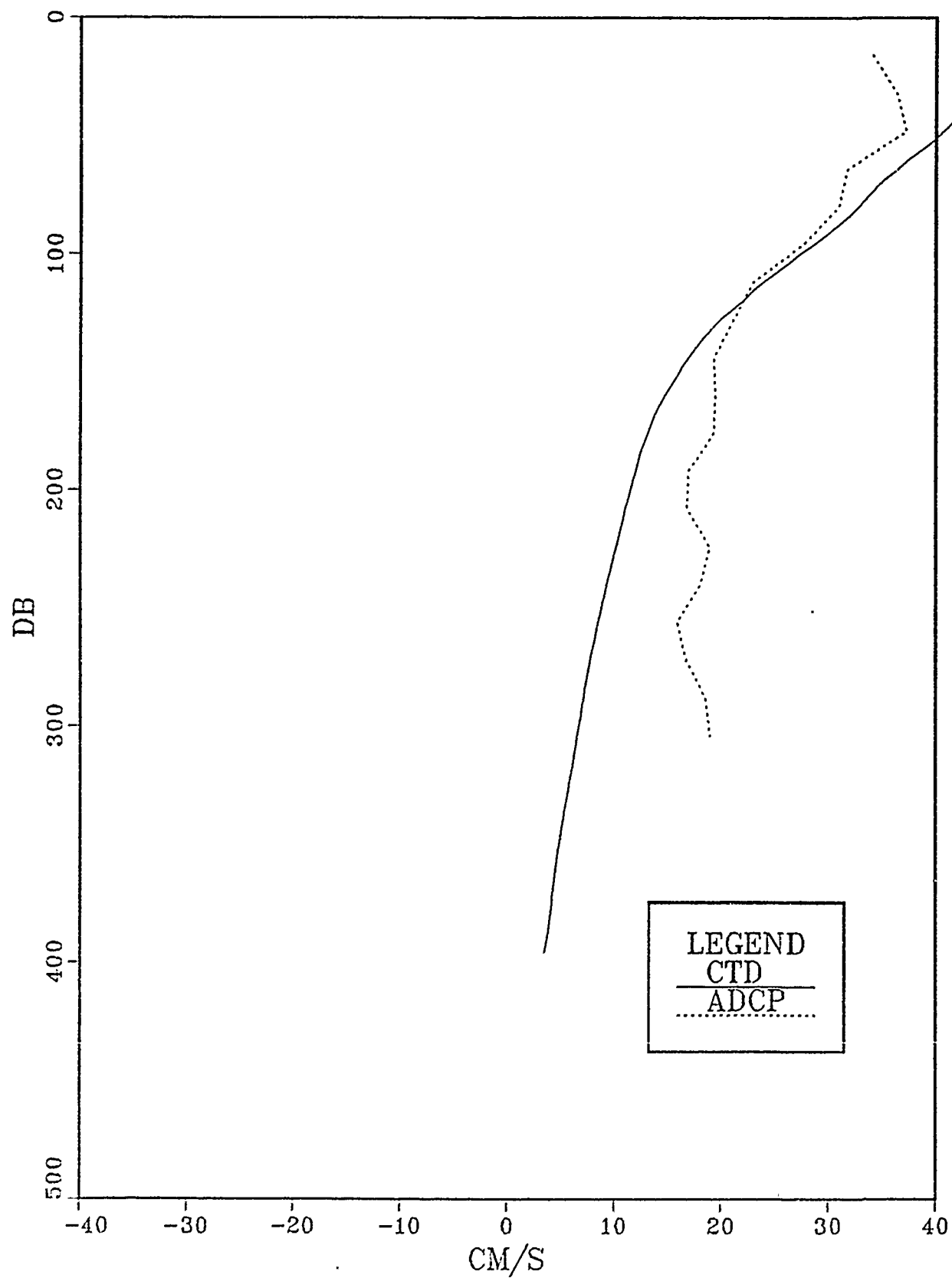
40-41



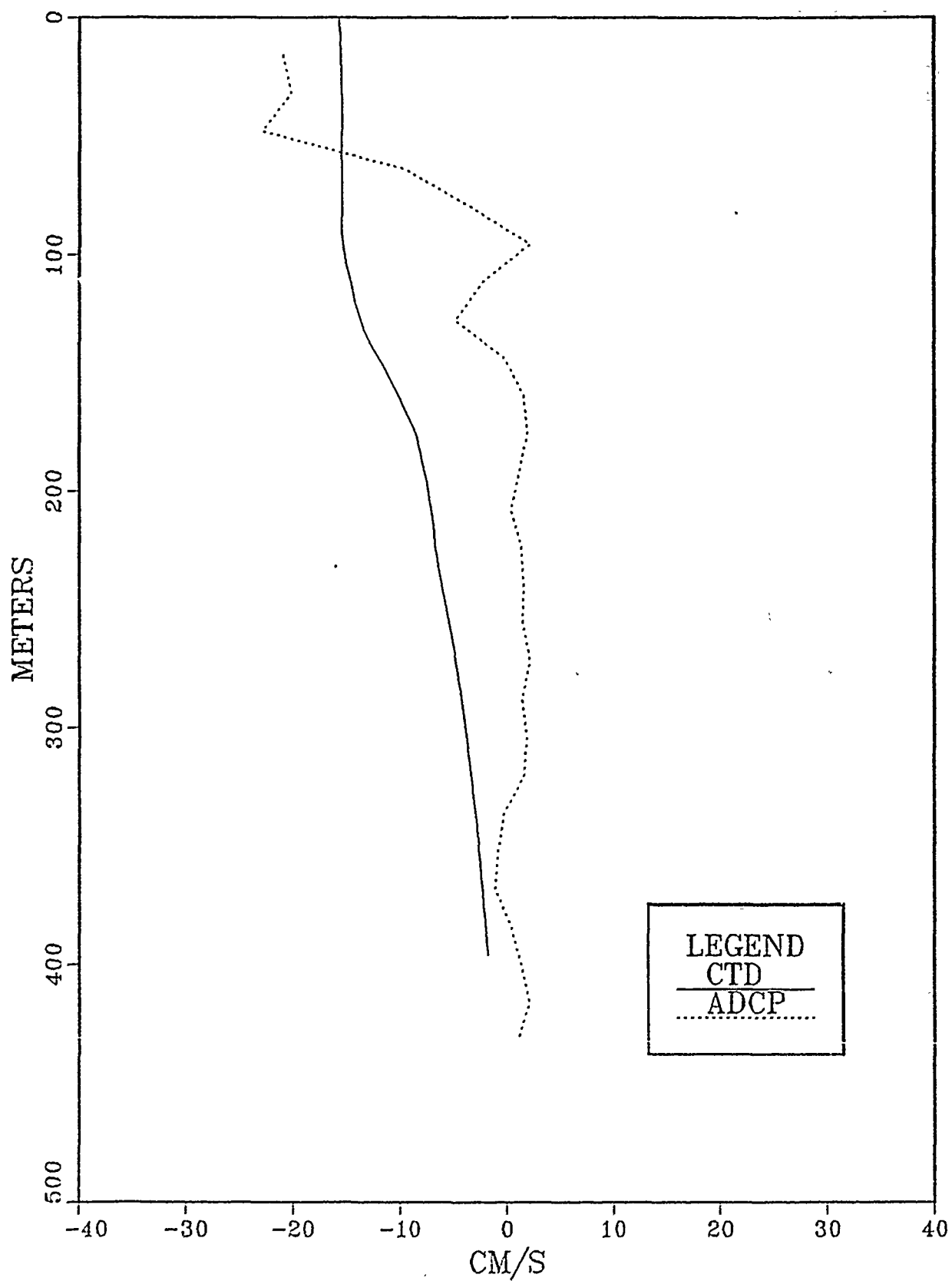
41-42



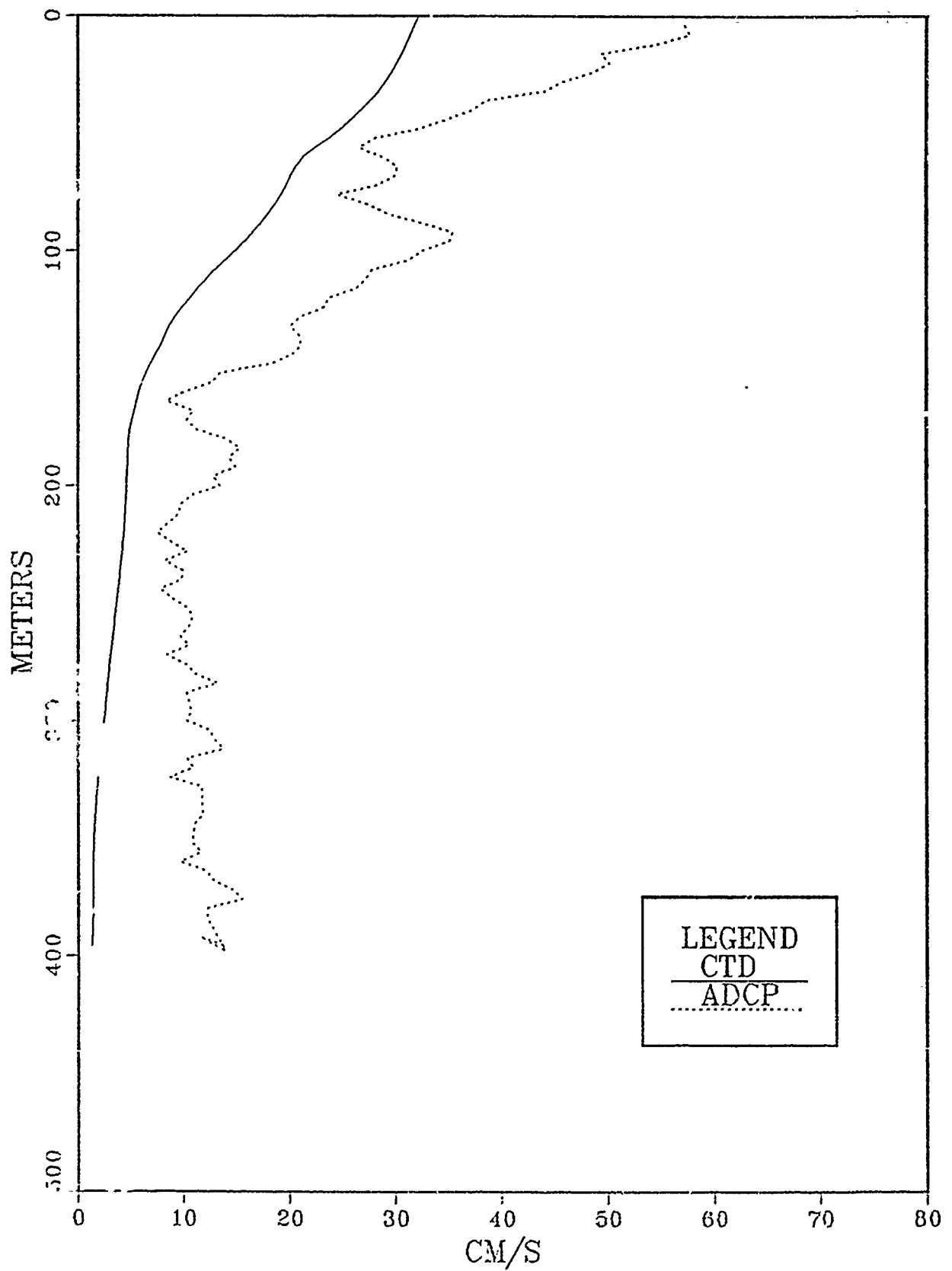
42-43



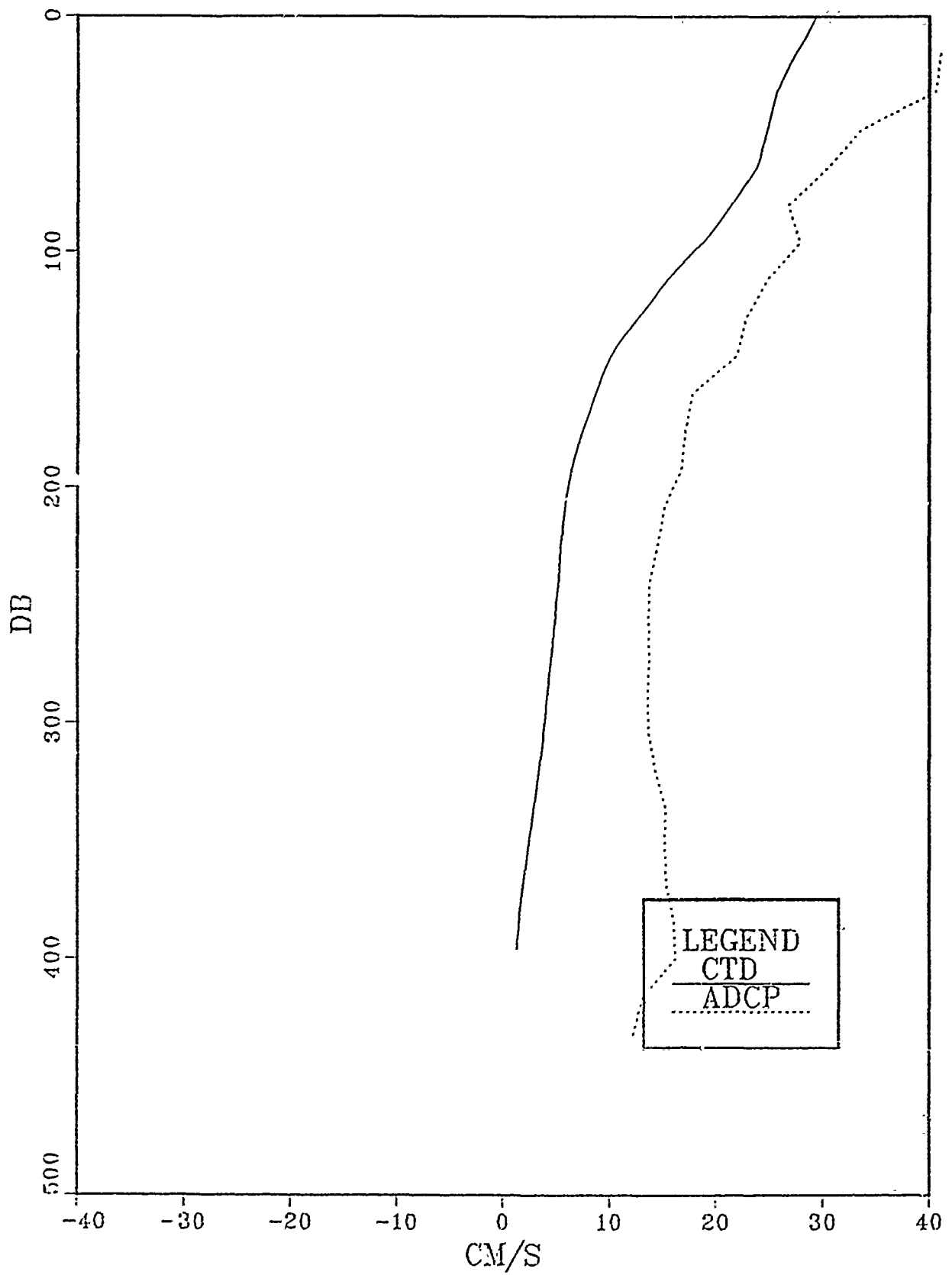
46-47



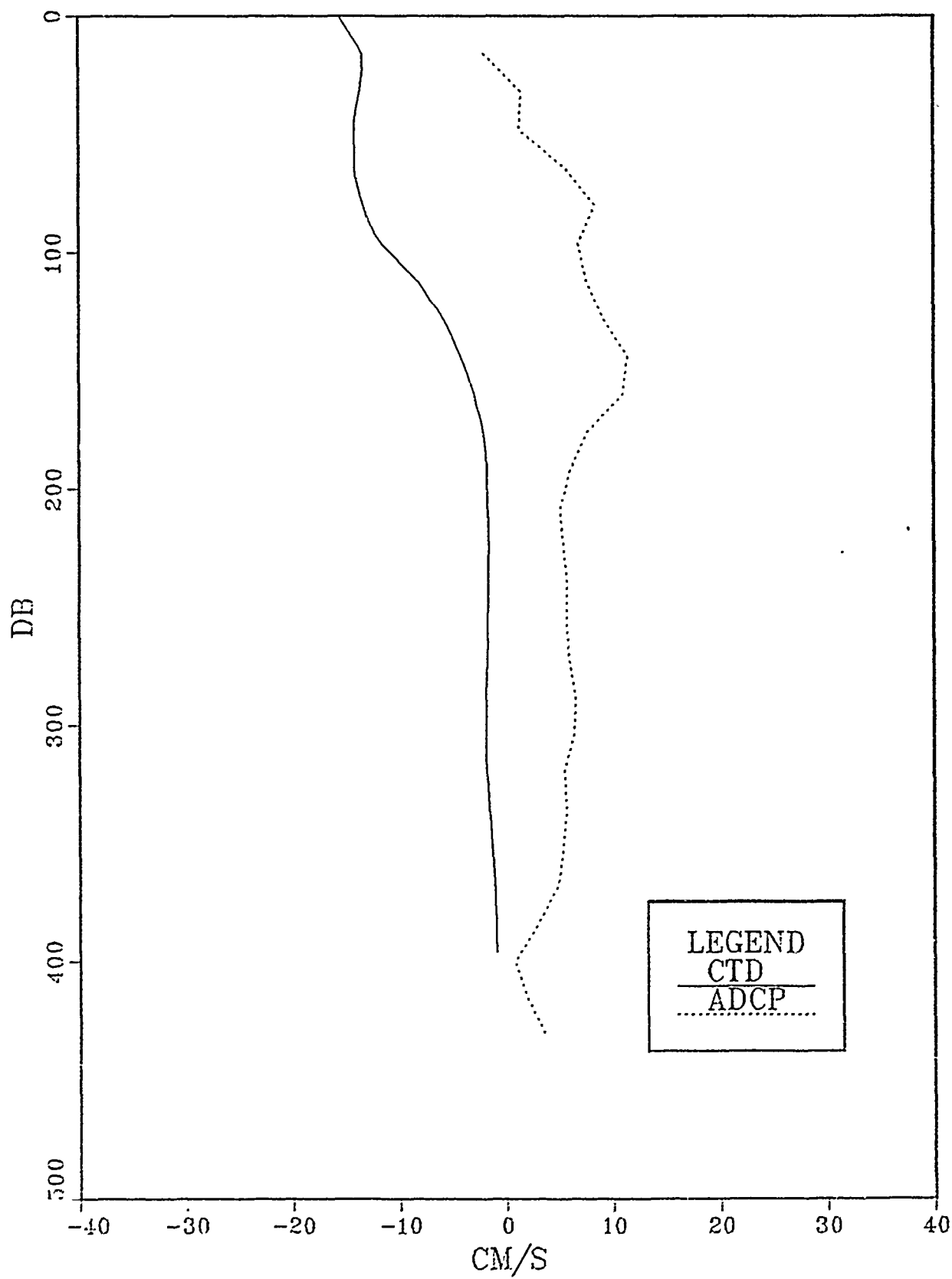
47-48



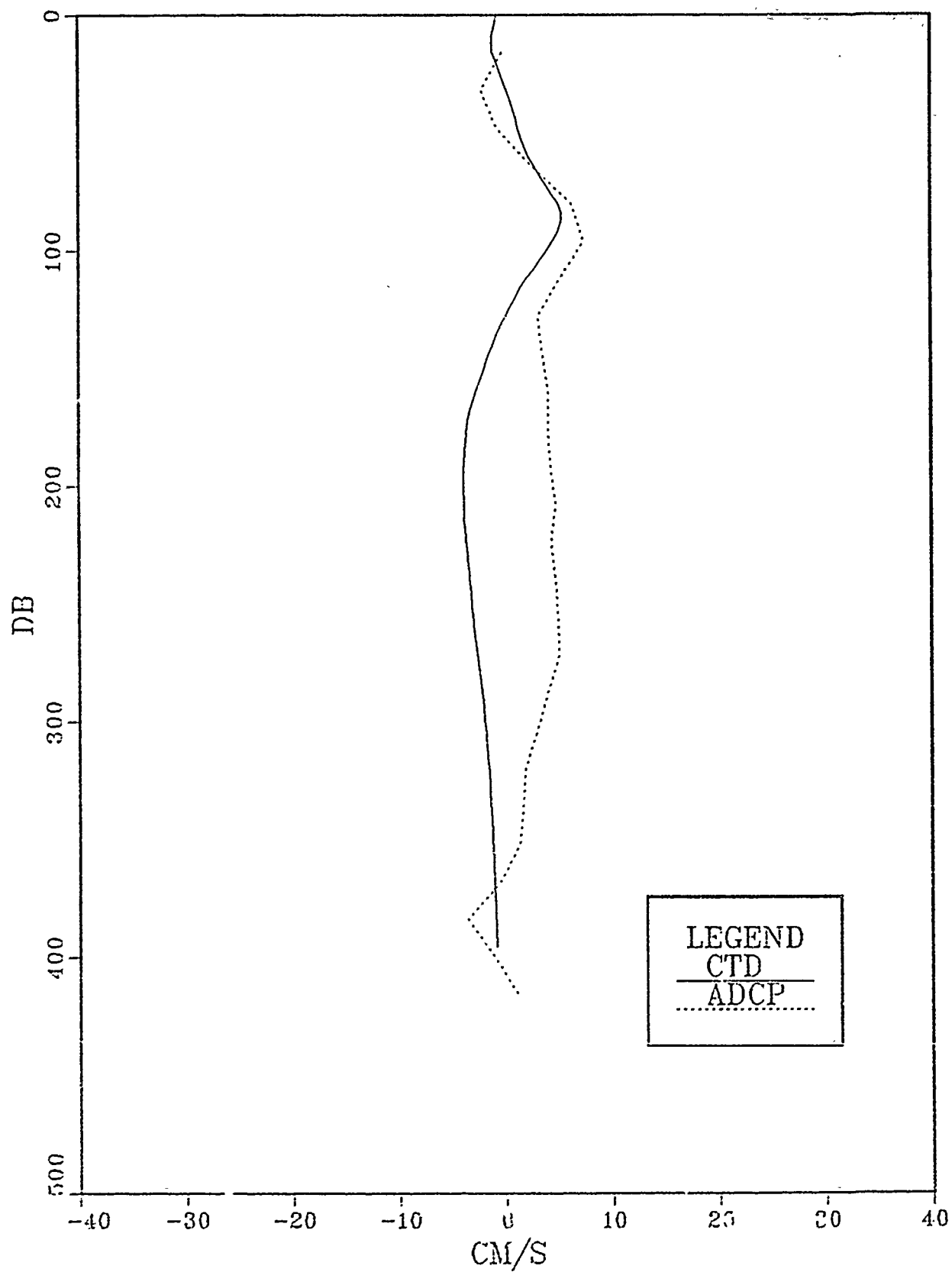
48-49



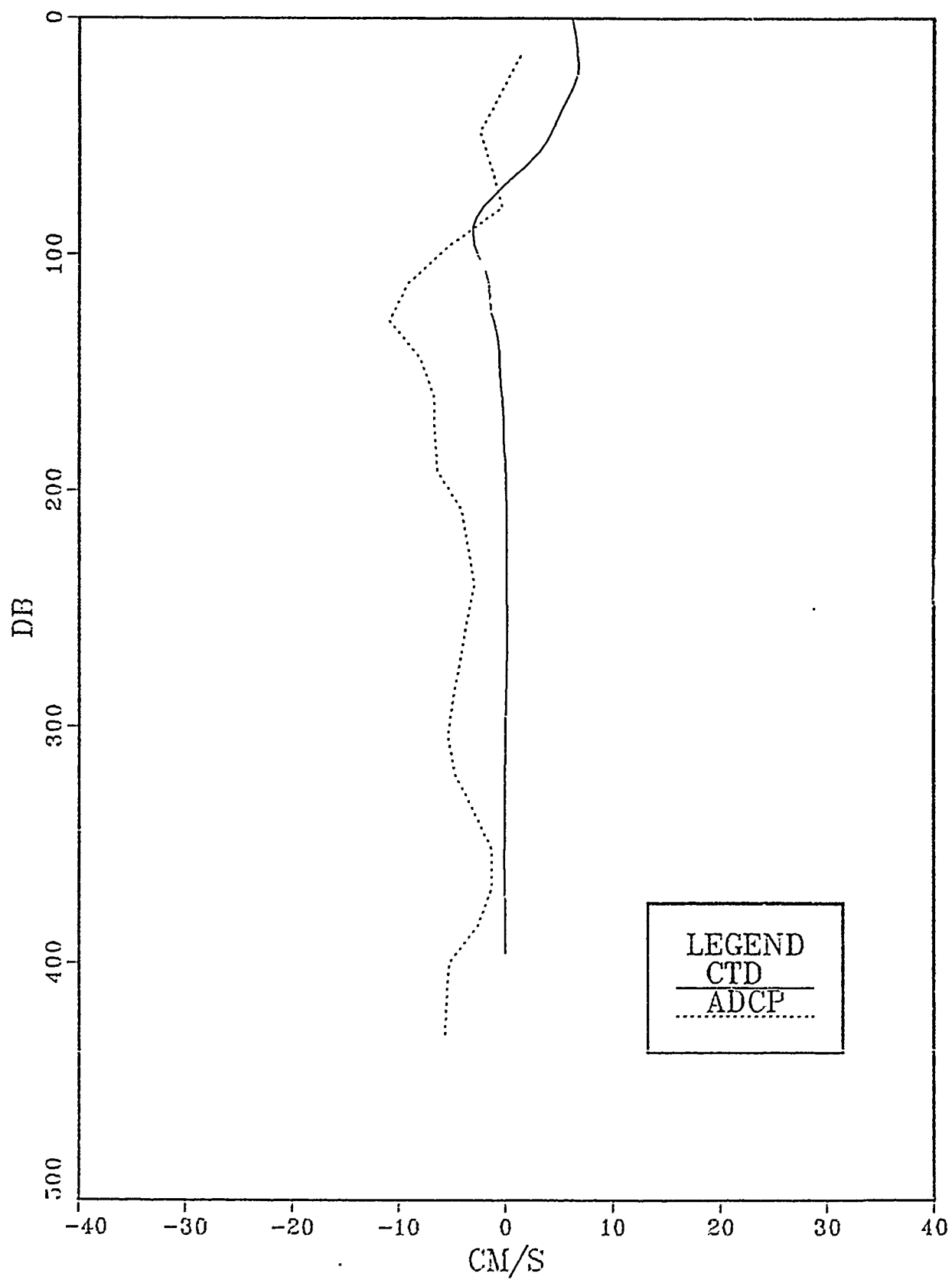
49-50



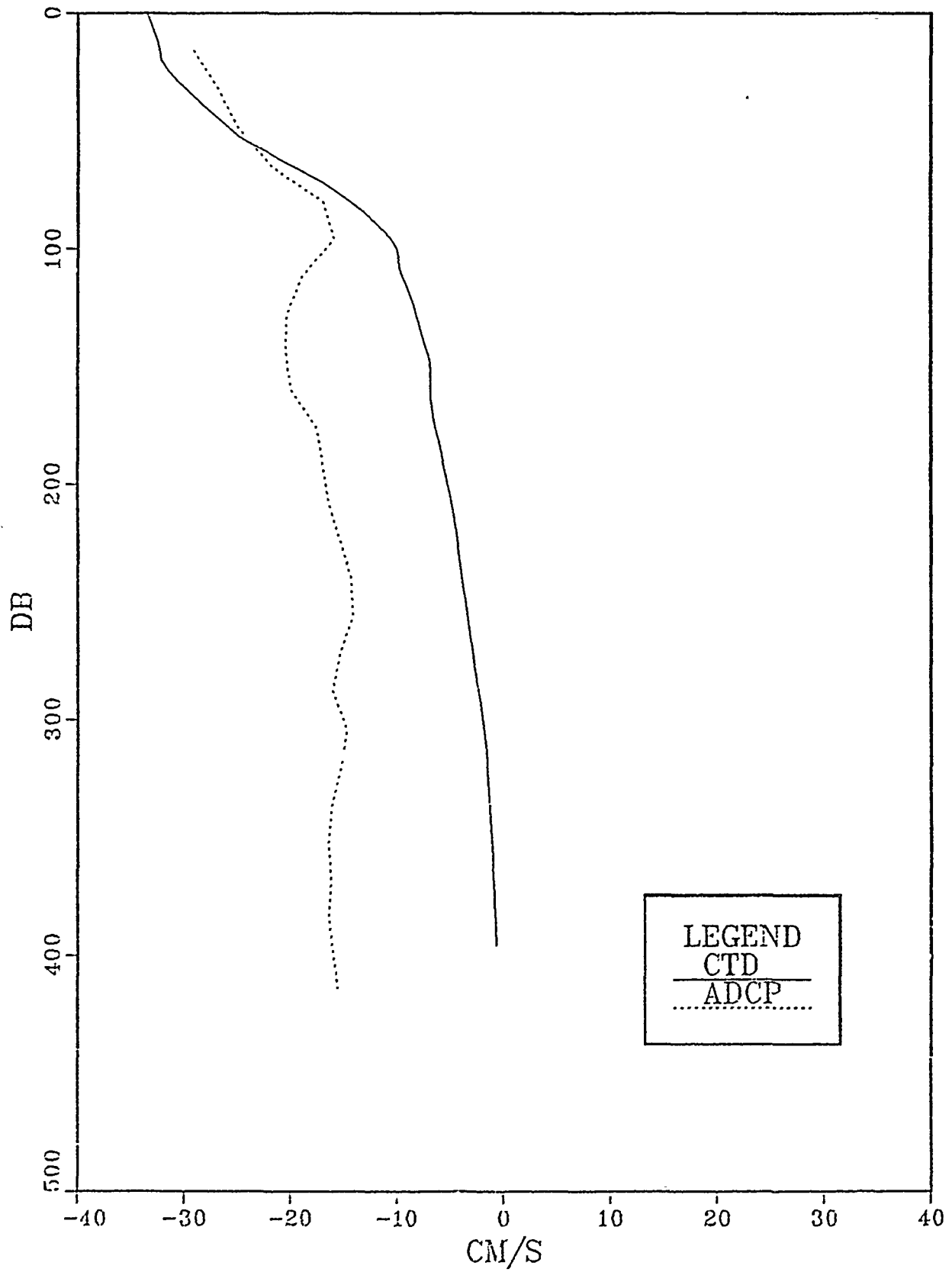
50-51



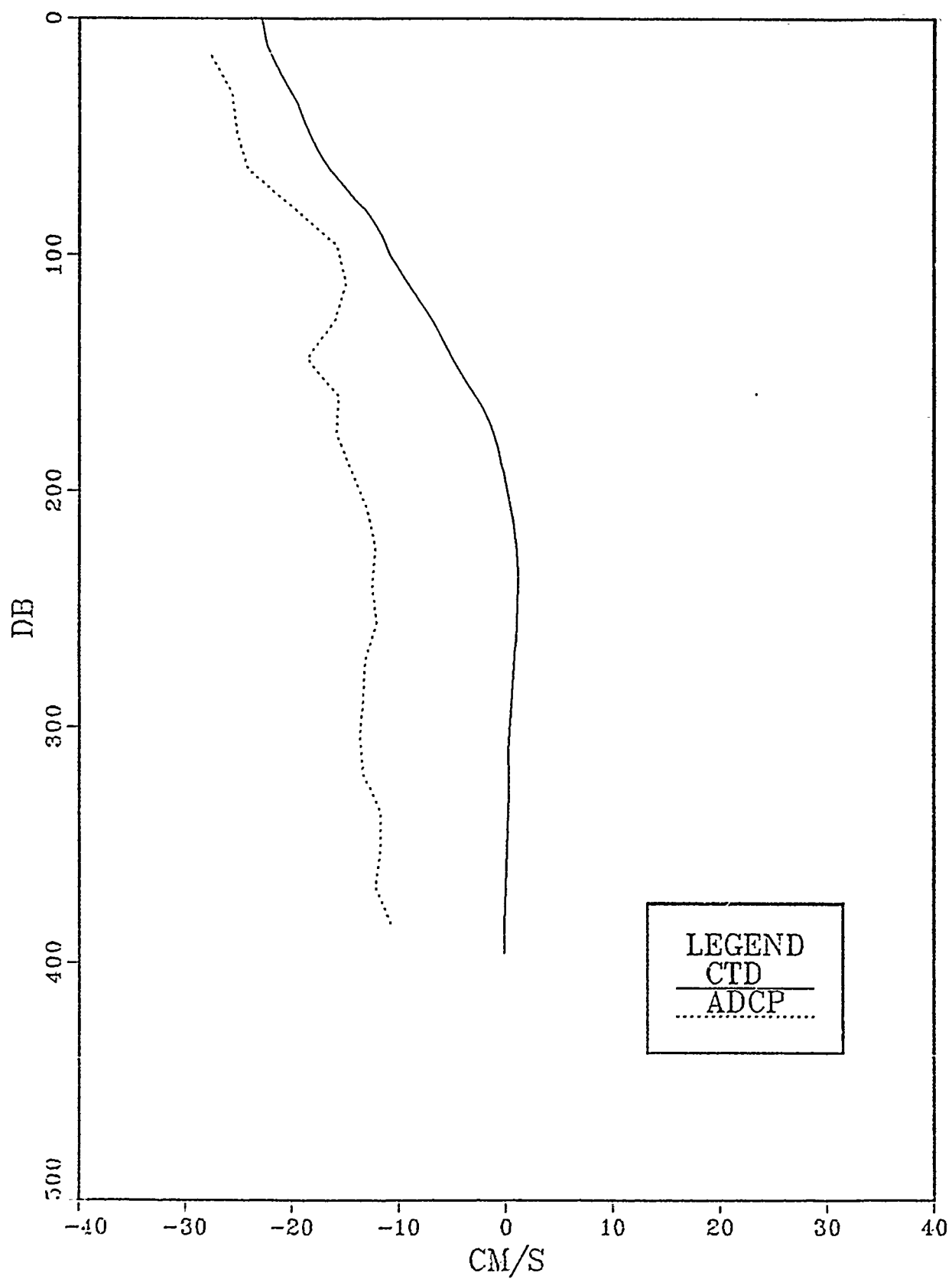
51-52



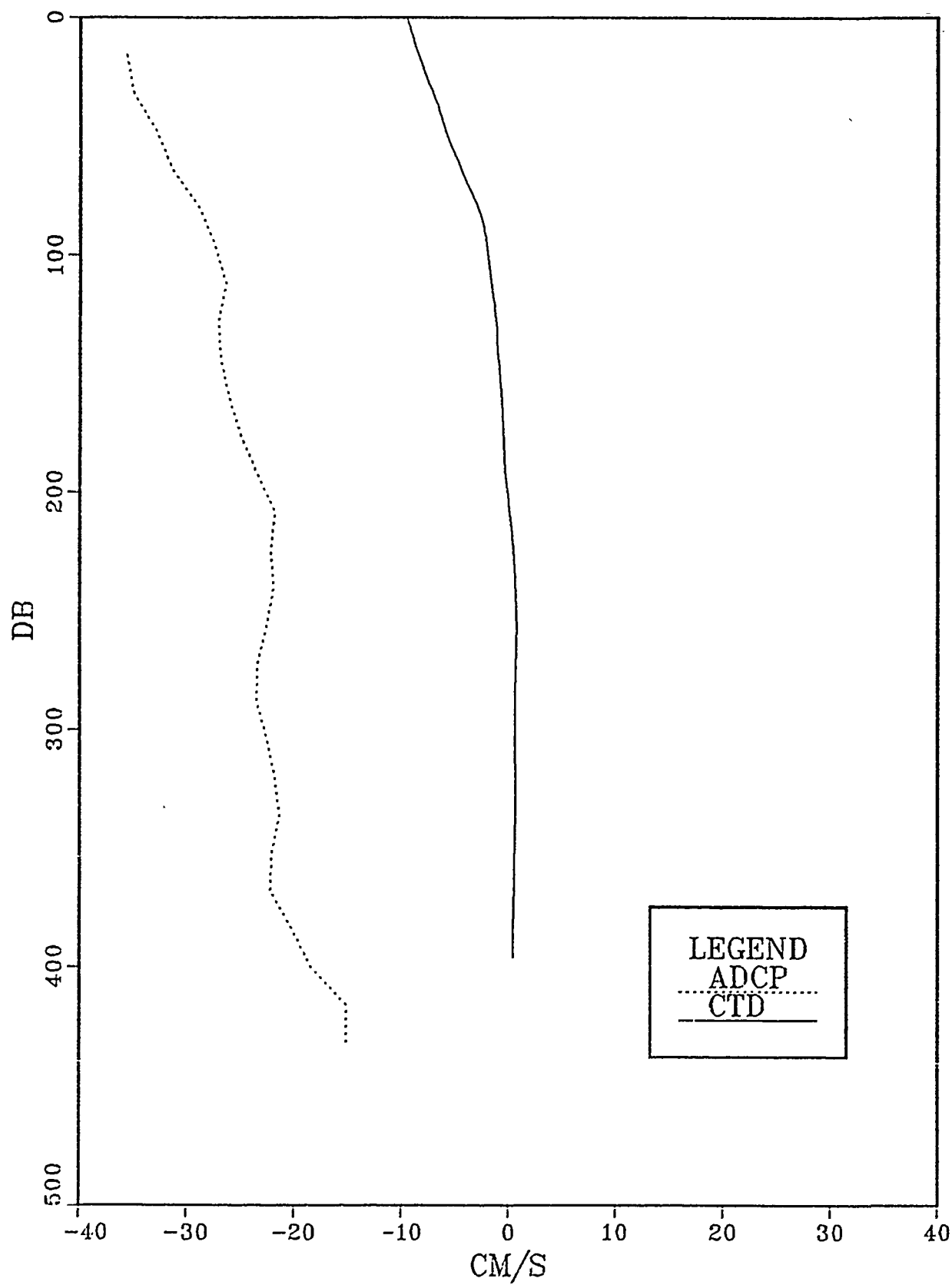
52-53



53-54



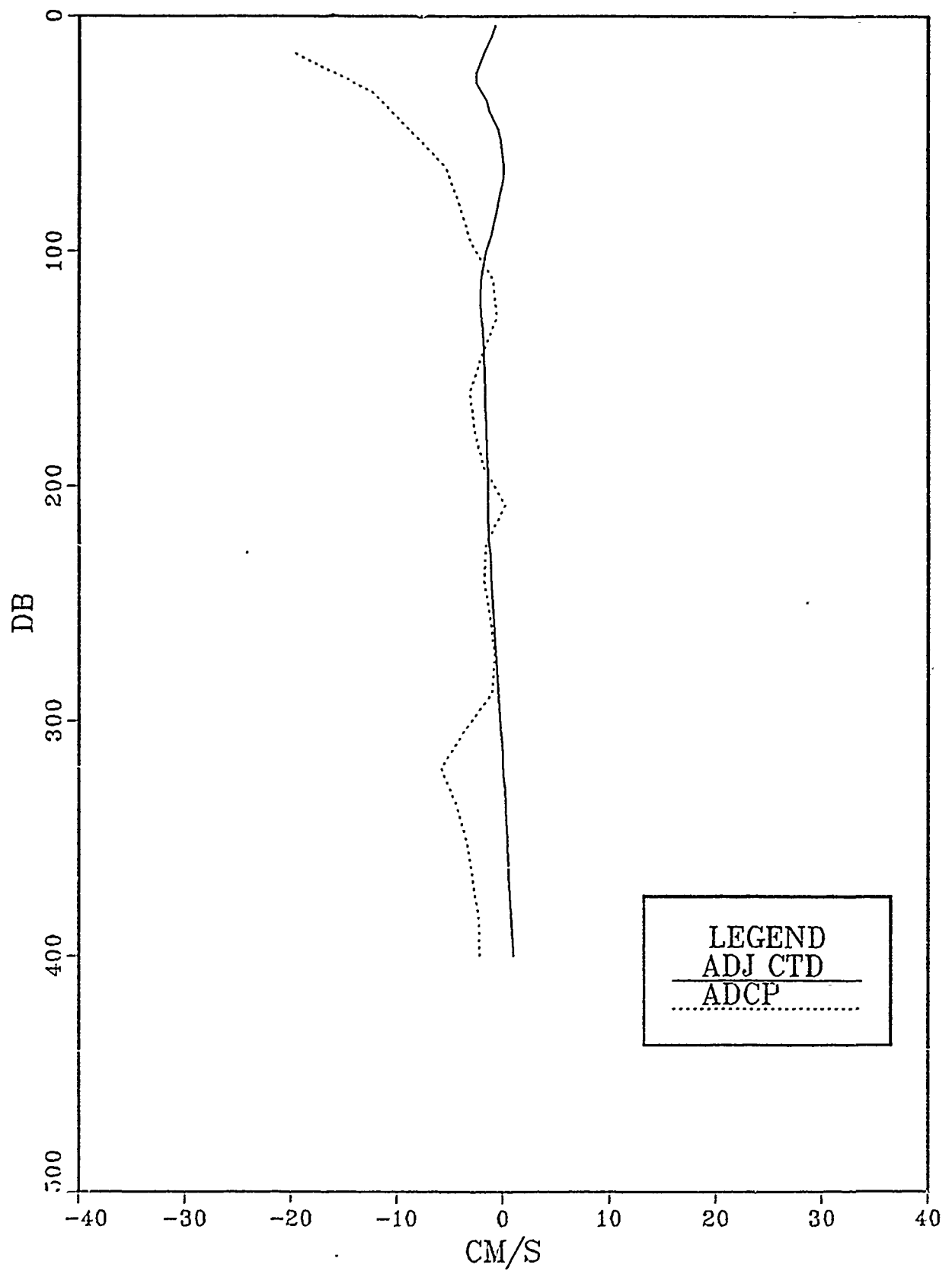
54-35



APPENDIX B. PROFILES OF ADCP AND ADJUSTED GEOSTROPHIC VELOCITY

For the profiles in this appendix, geostrophic profiles, calculated using a 500 db reference level, were then adjusted as described in the text to a reference layer defined by ADCP measurements averaged over the 190-274 m layer. See Appendix A and the text for further detail regarding these profiles.

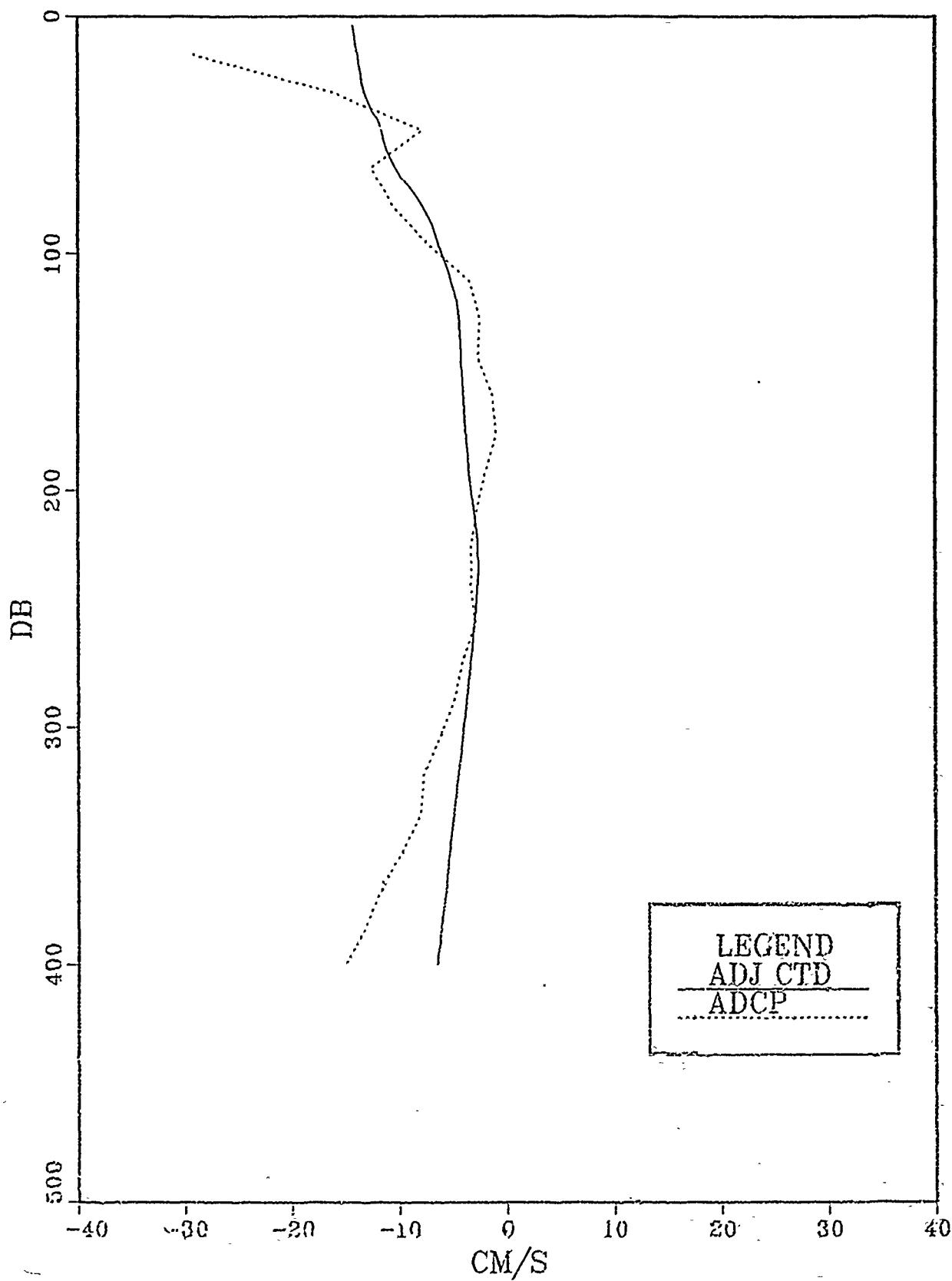
22-23



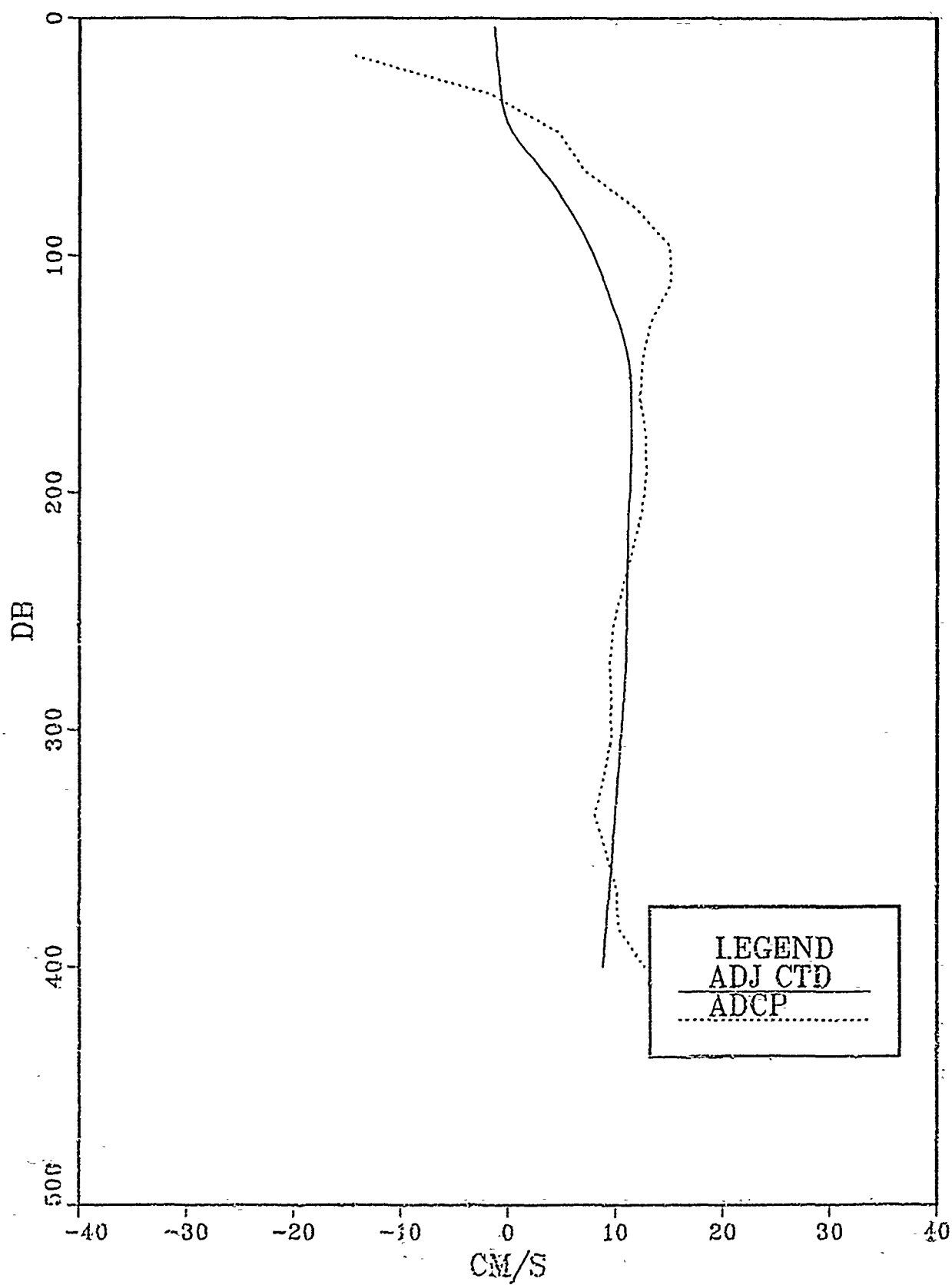
23-24



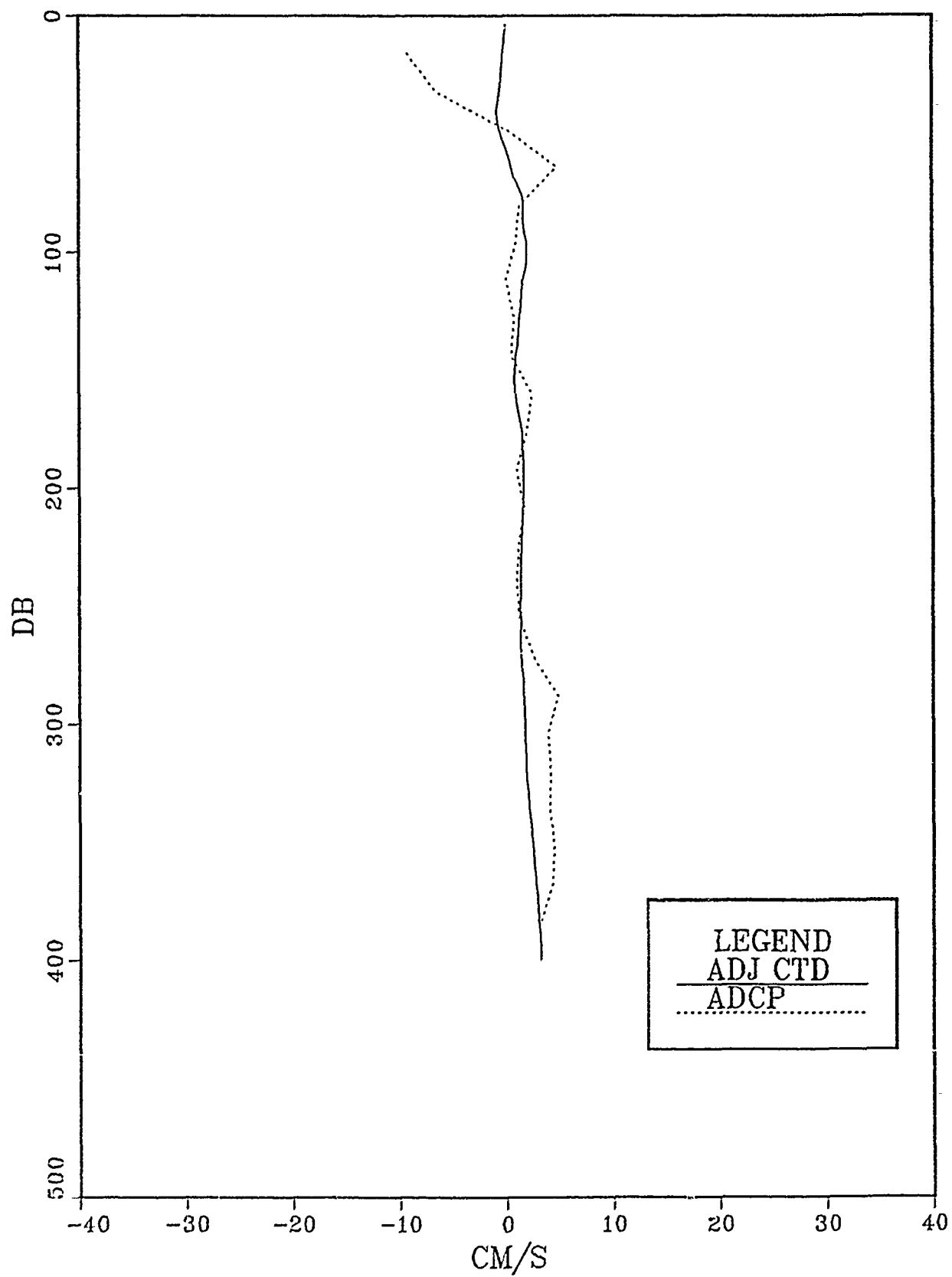
24-25



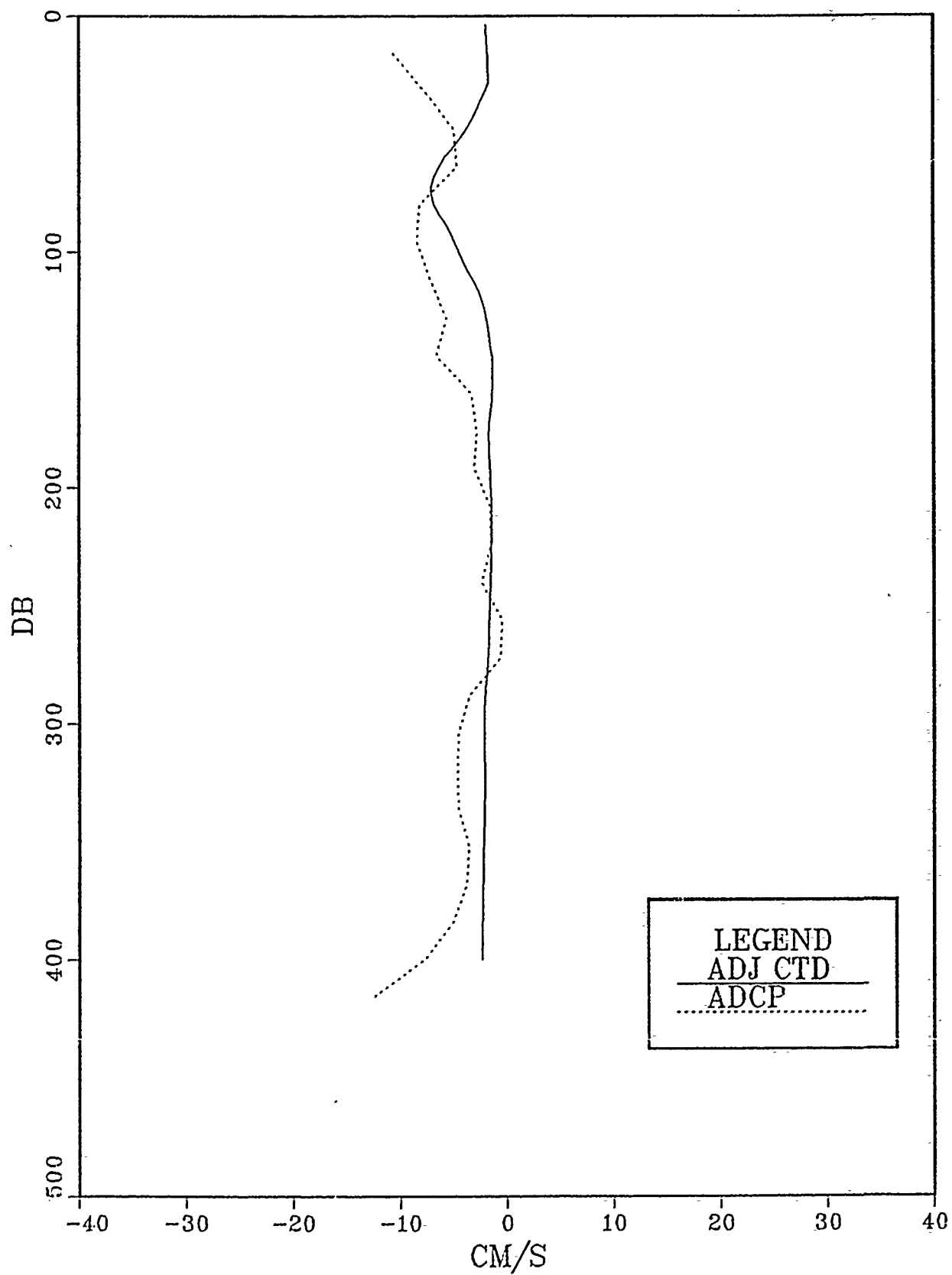
25-27



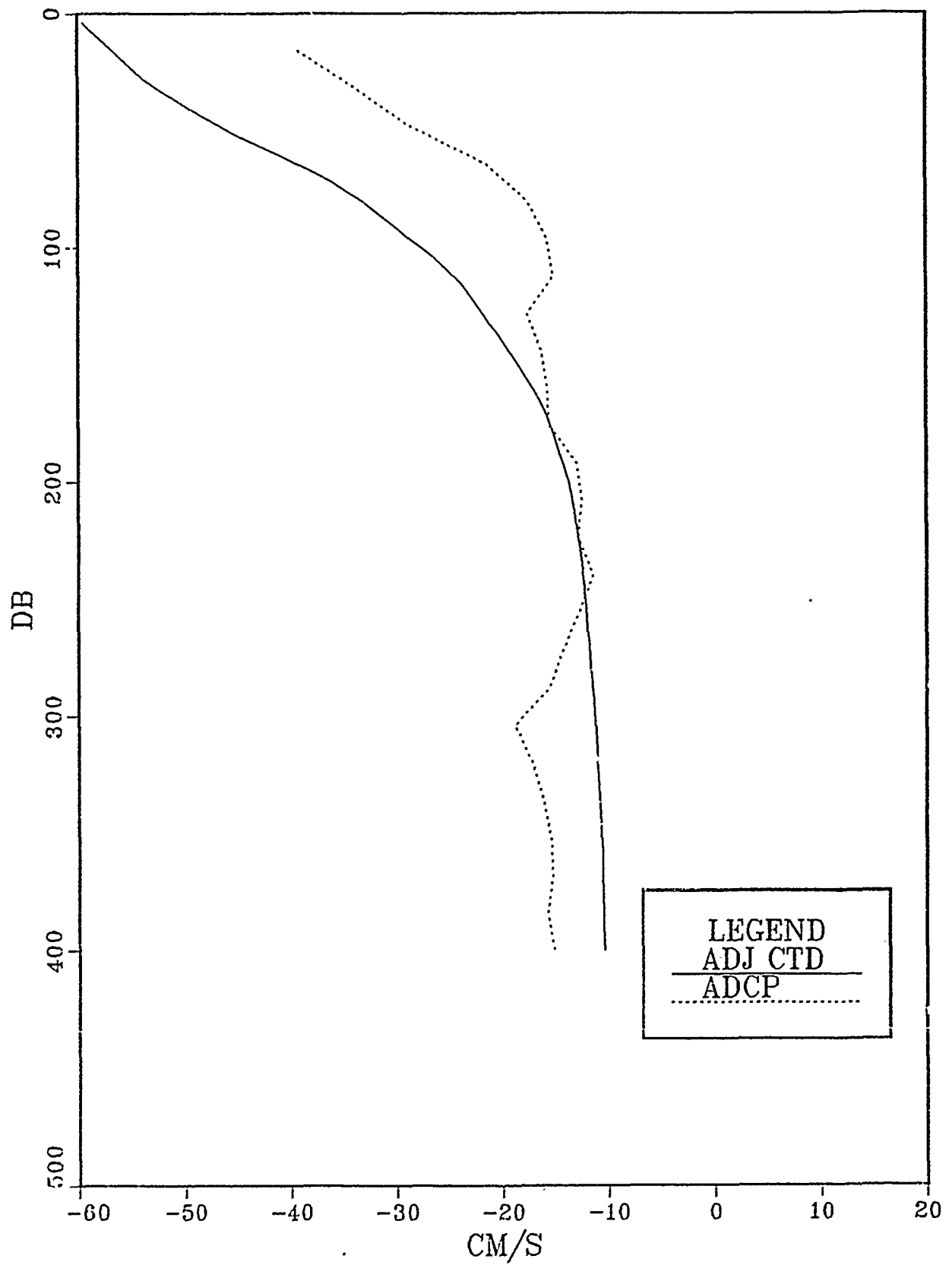
27-28



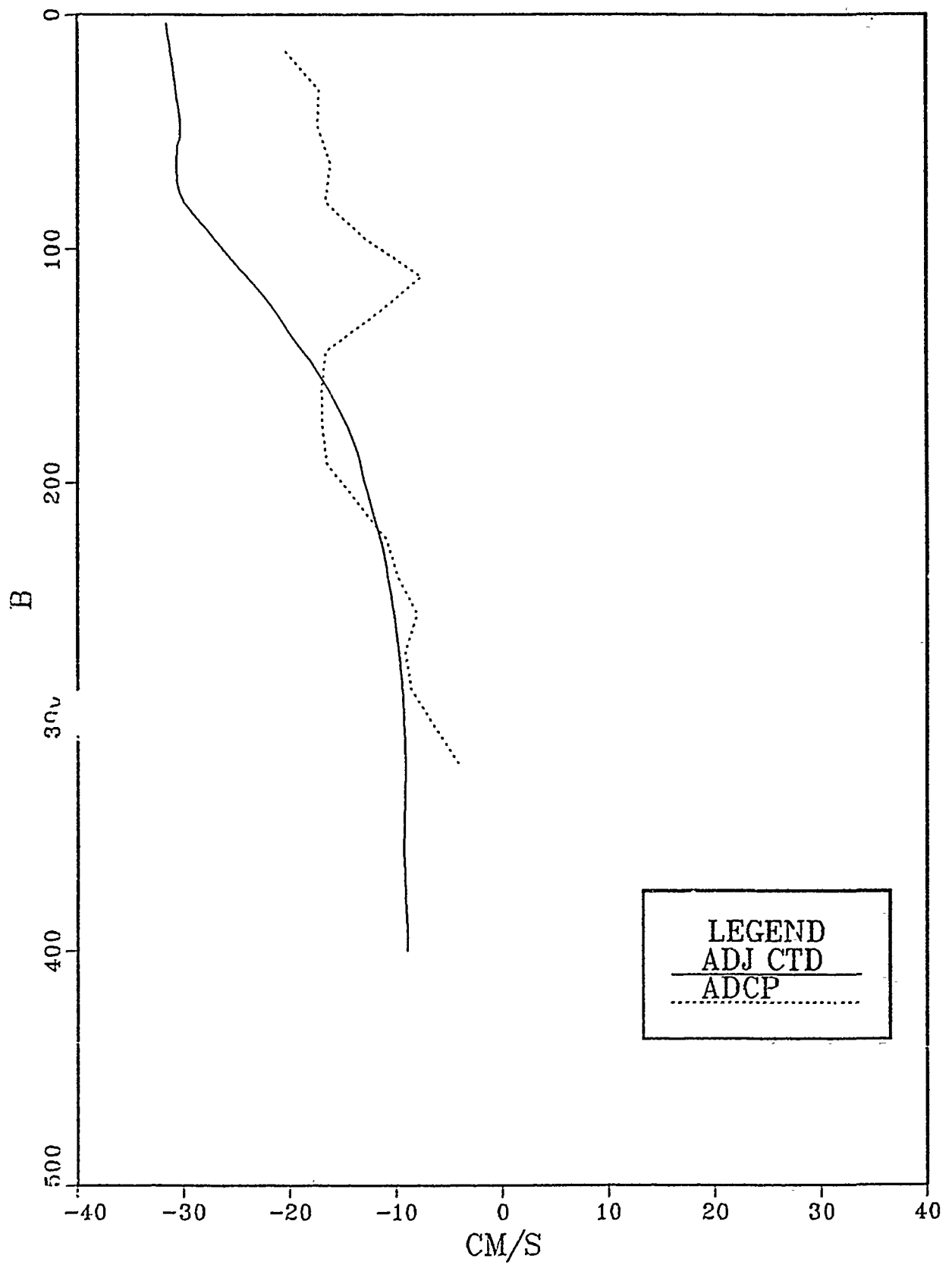
28-29



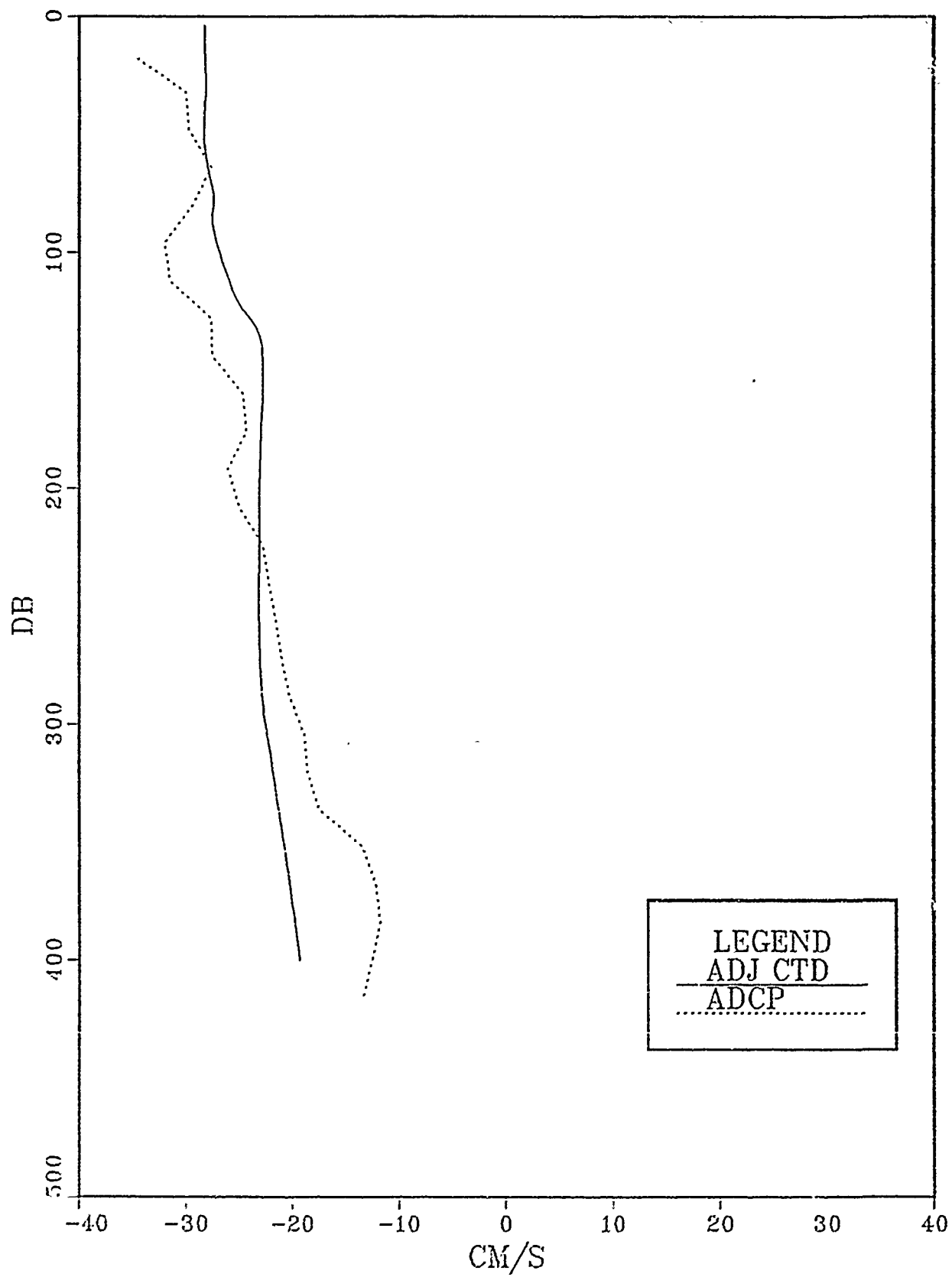
29-30



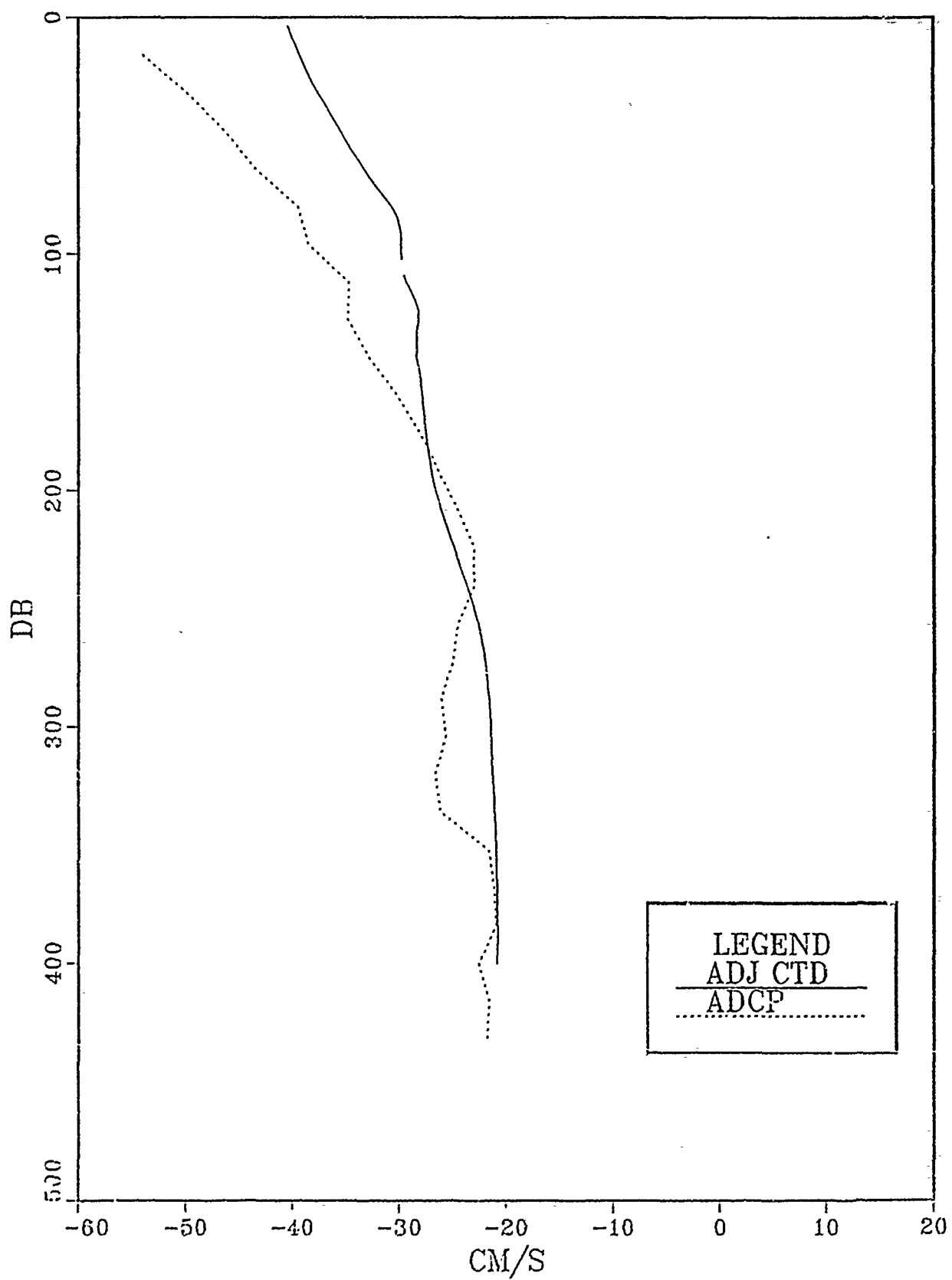
30-31



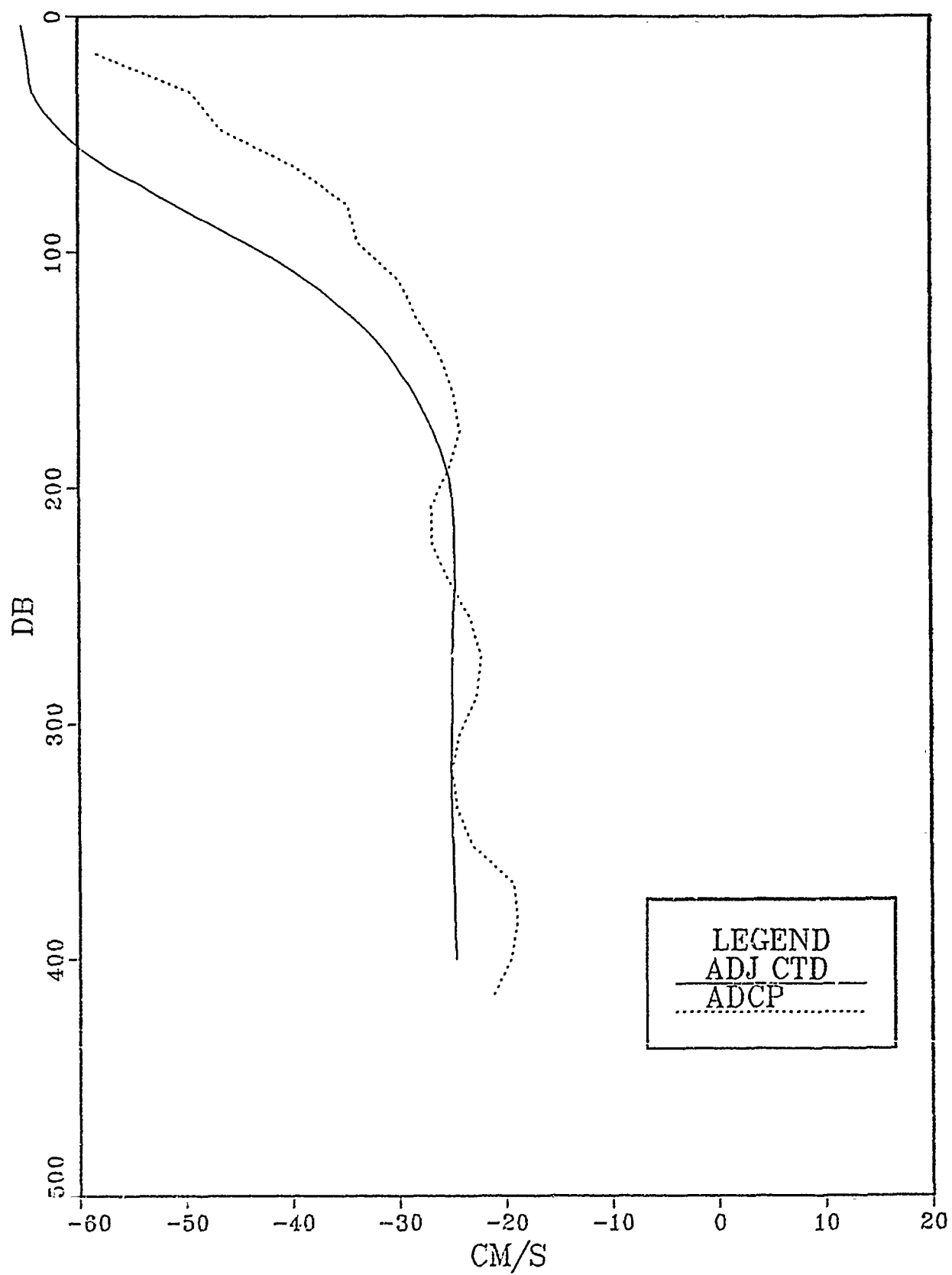
33-34



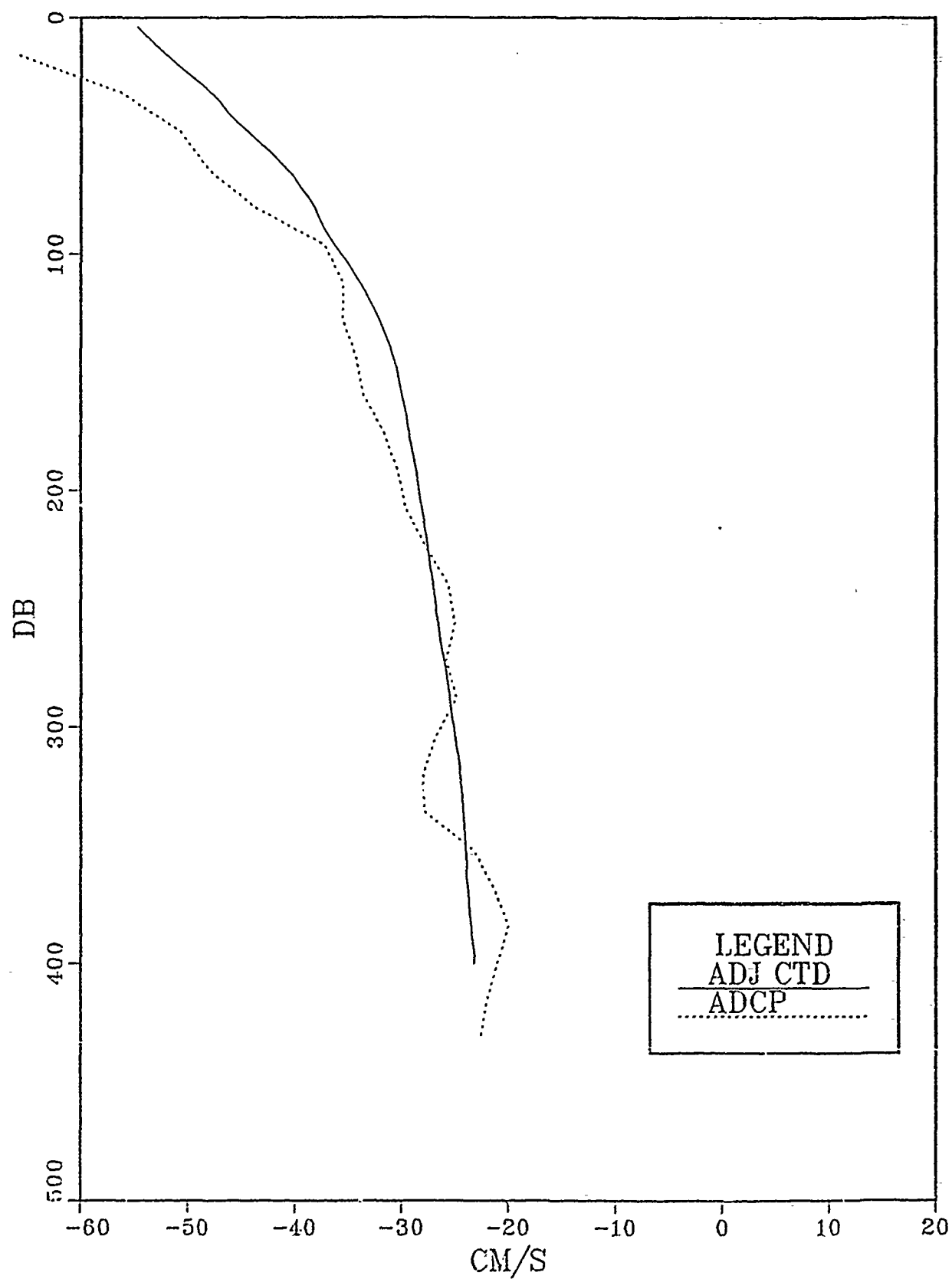
34--35



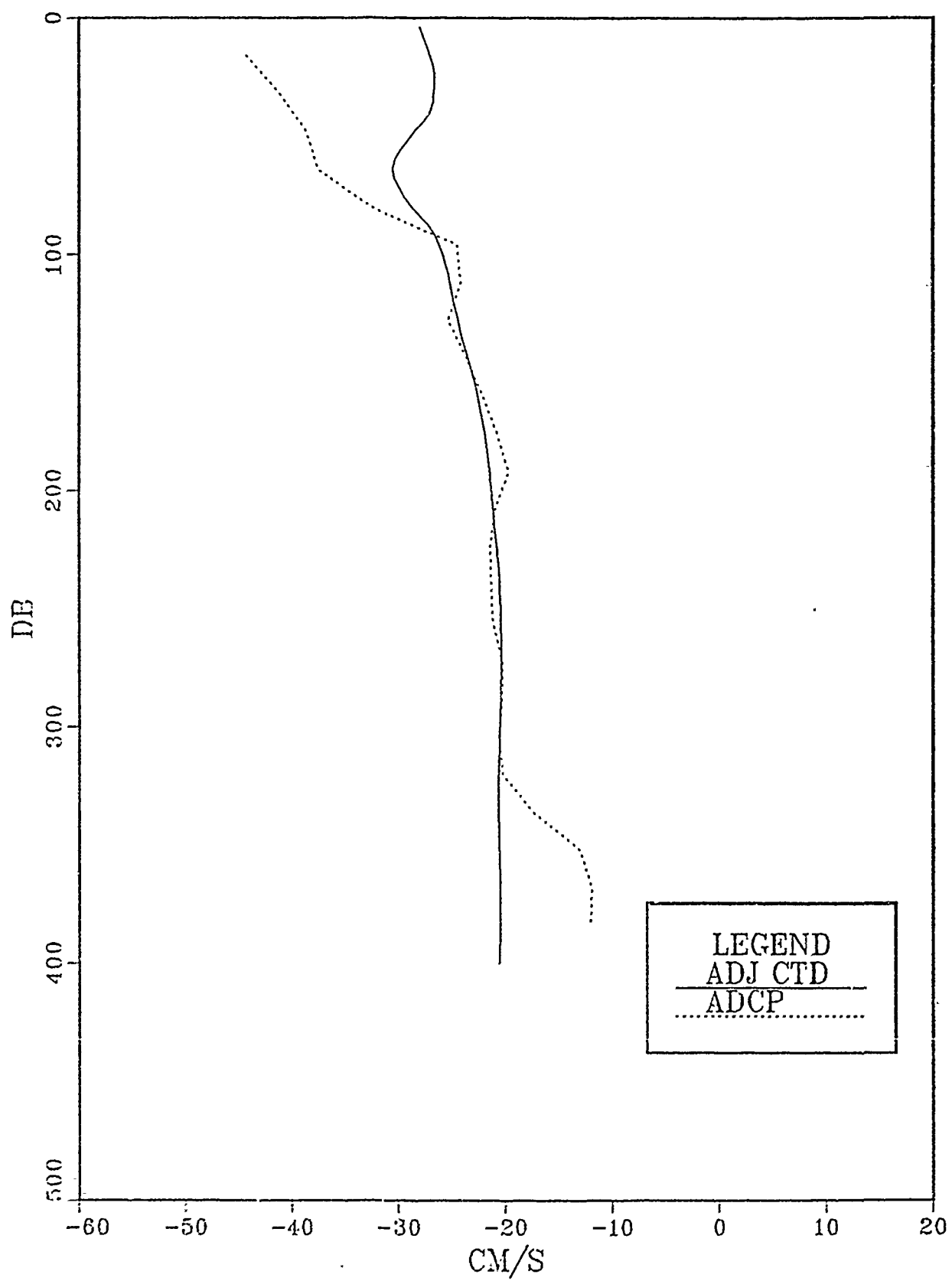
35-36



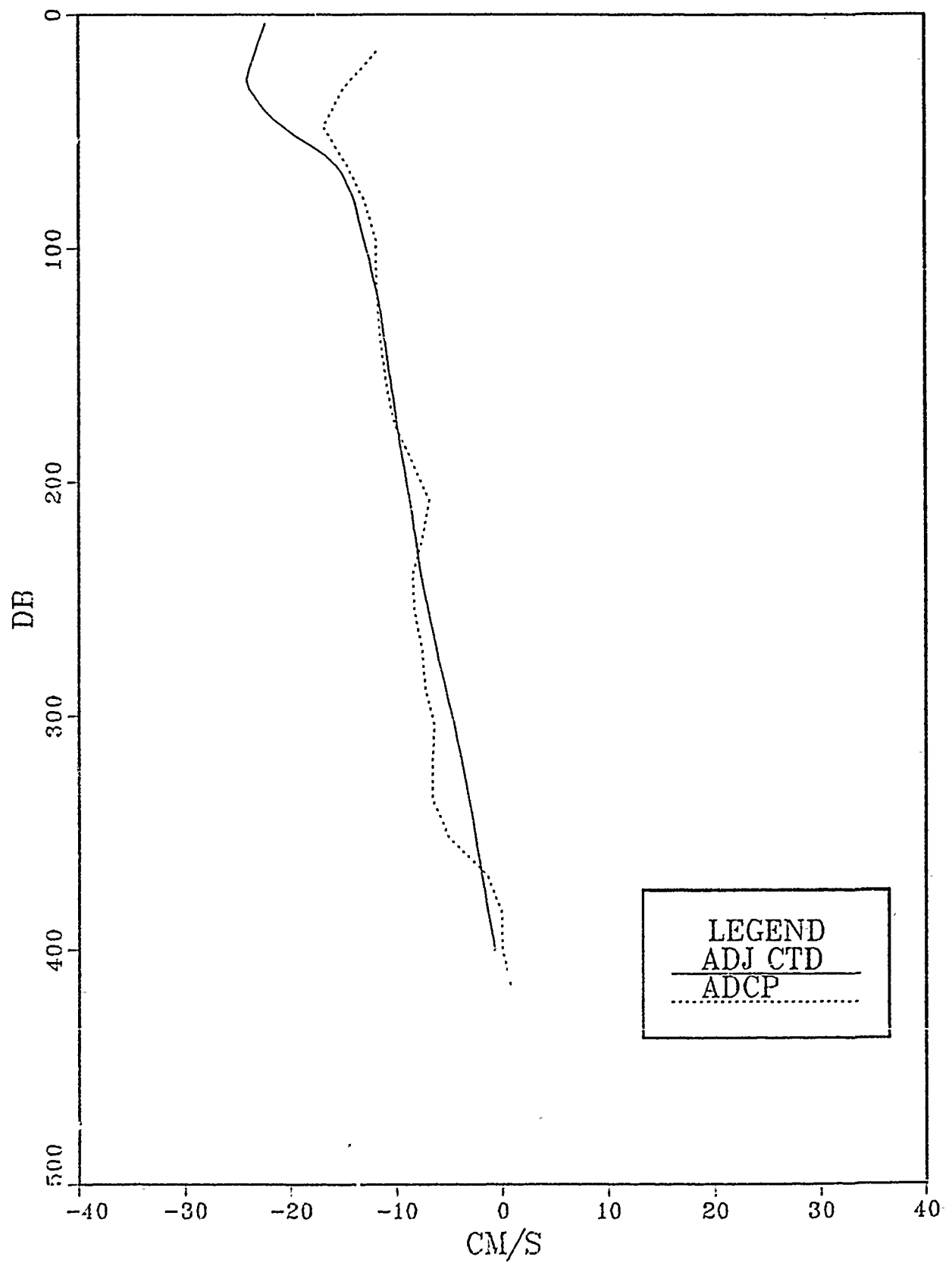
36-37



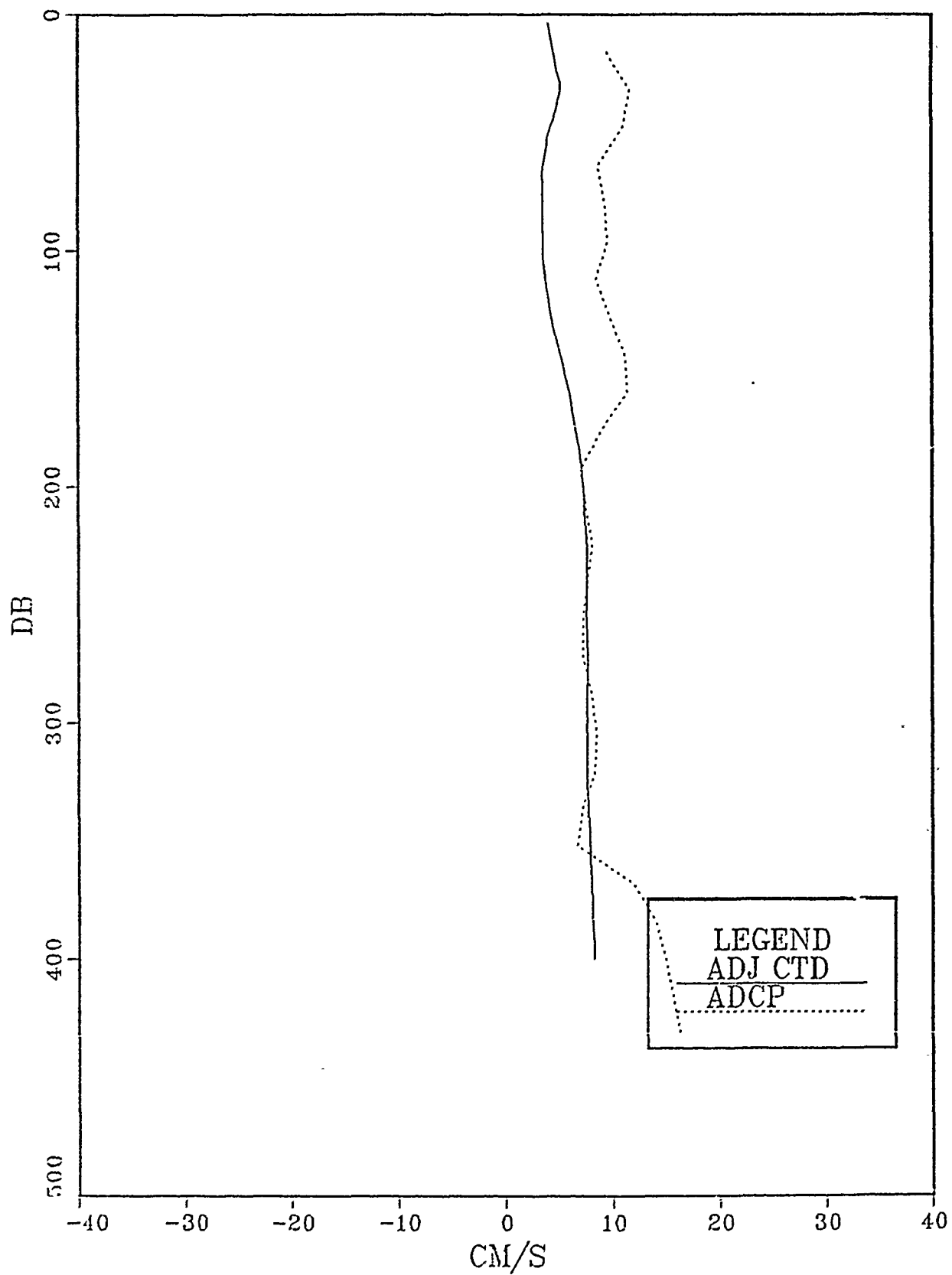
37-38



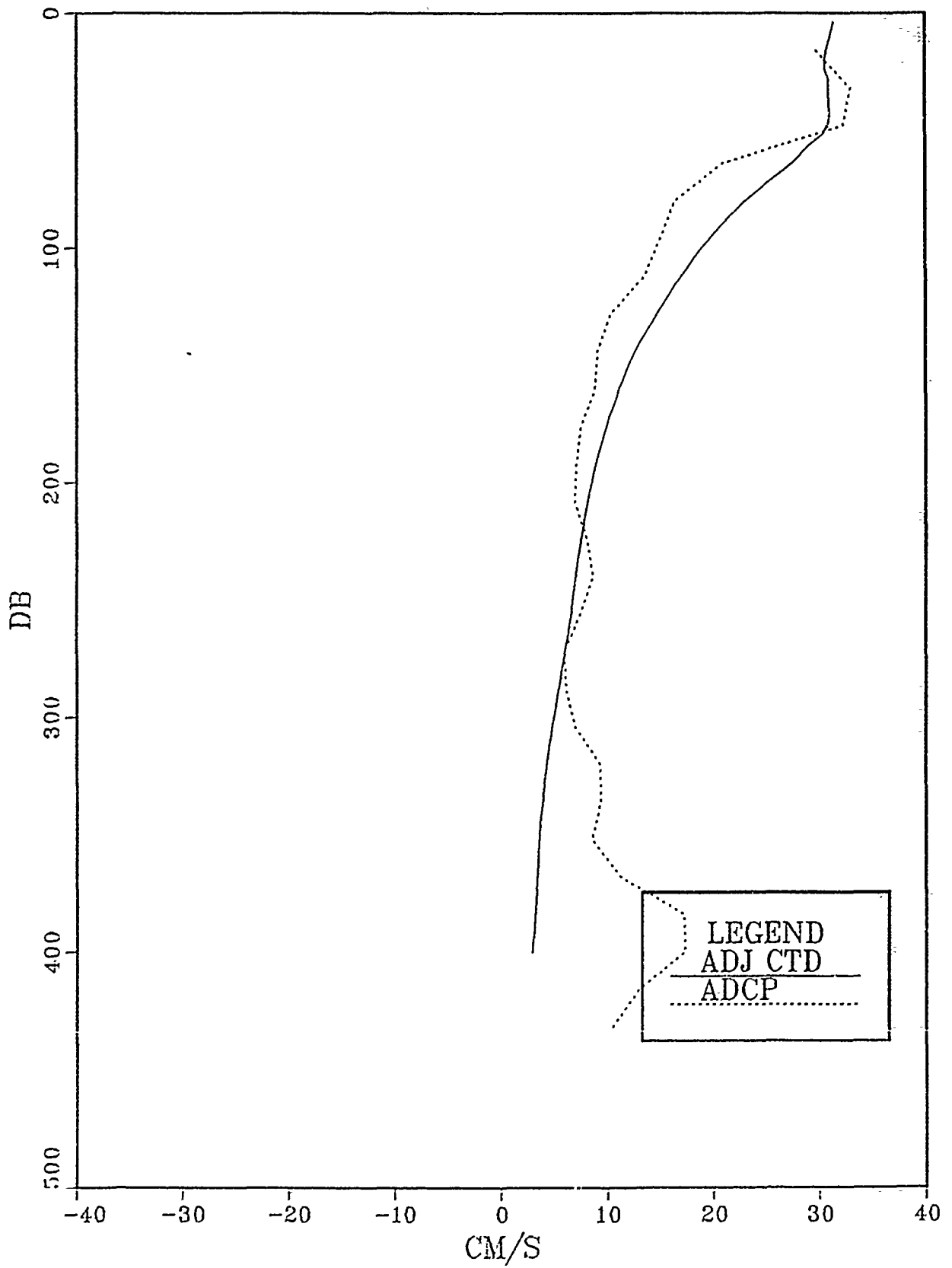
38-39



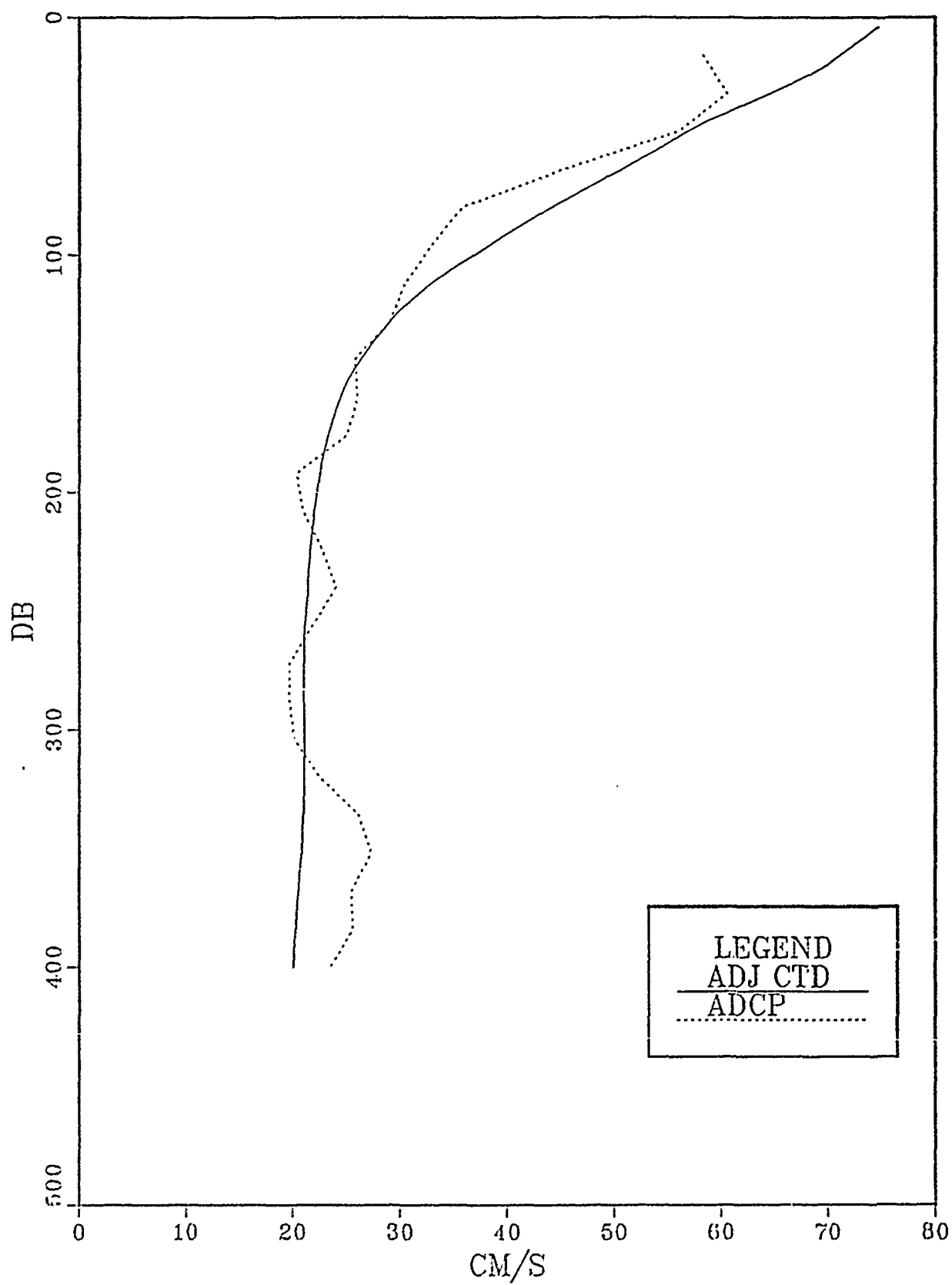
39-40



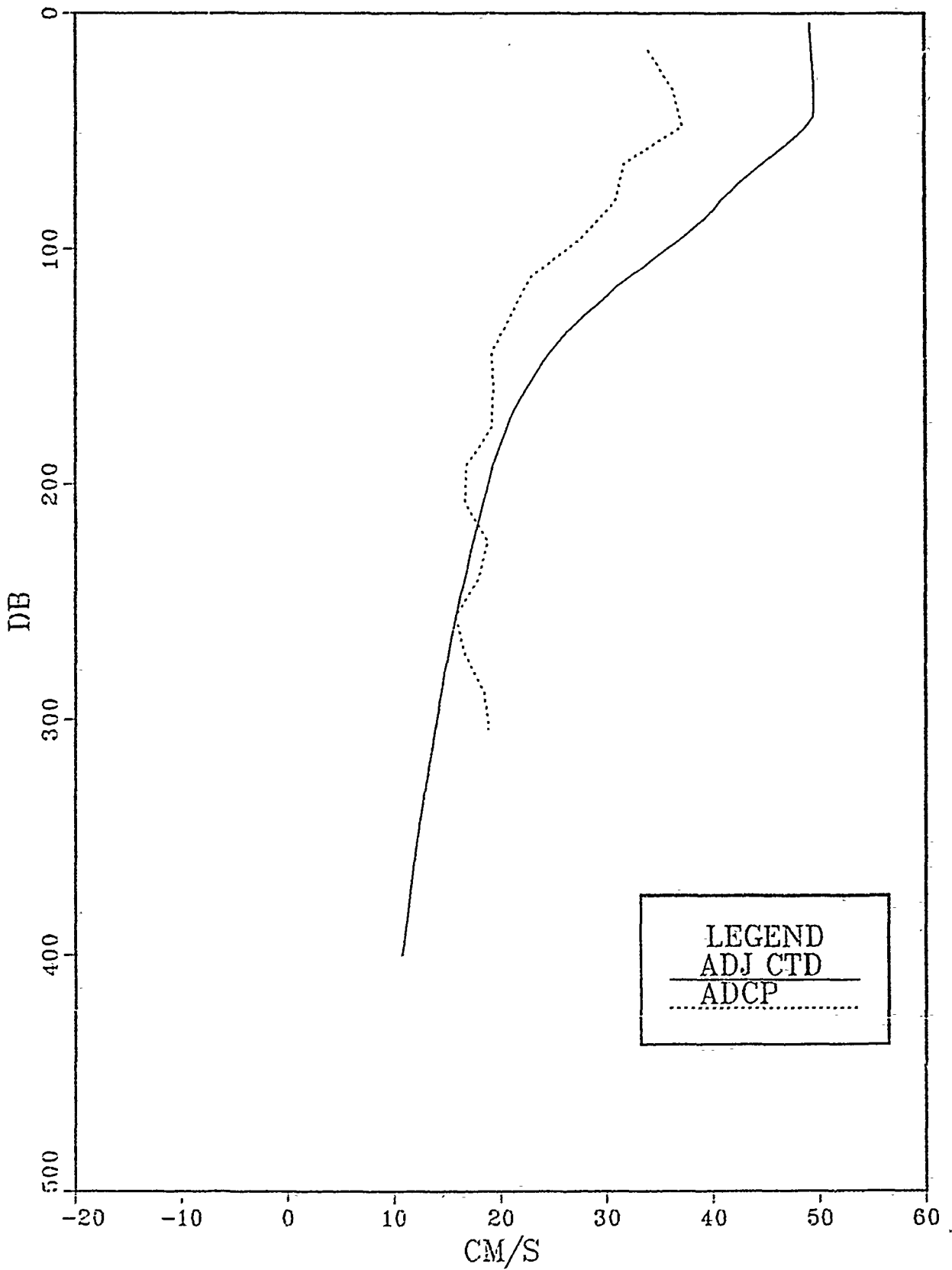
40-41



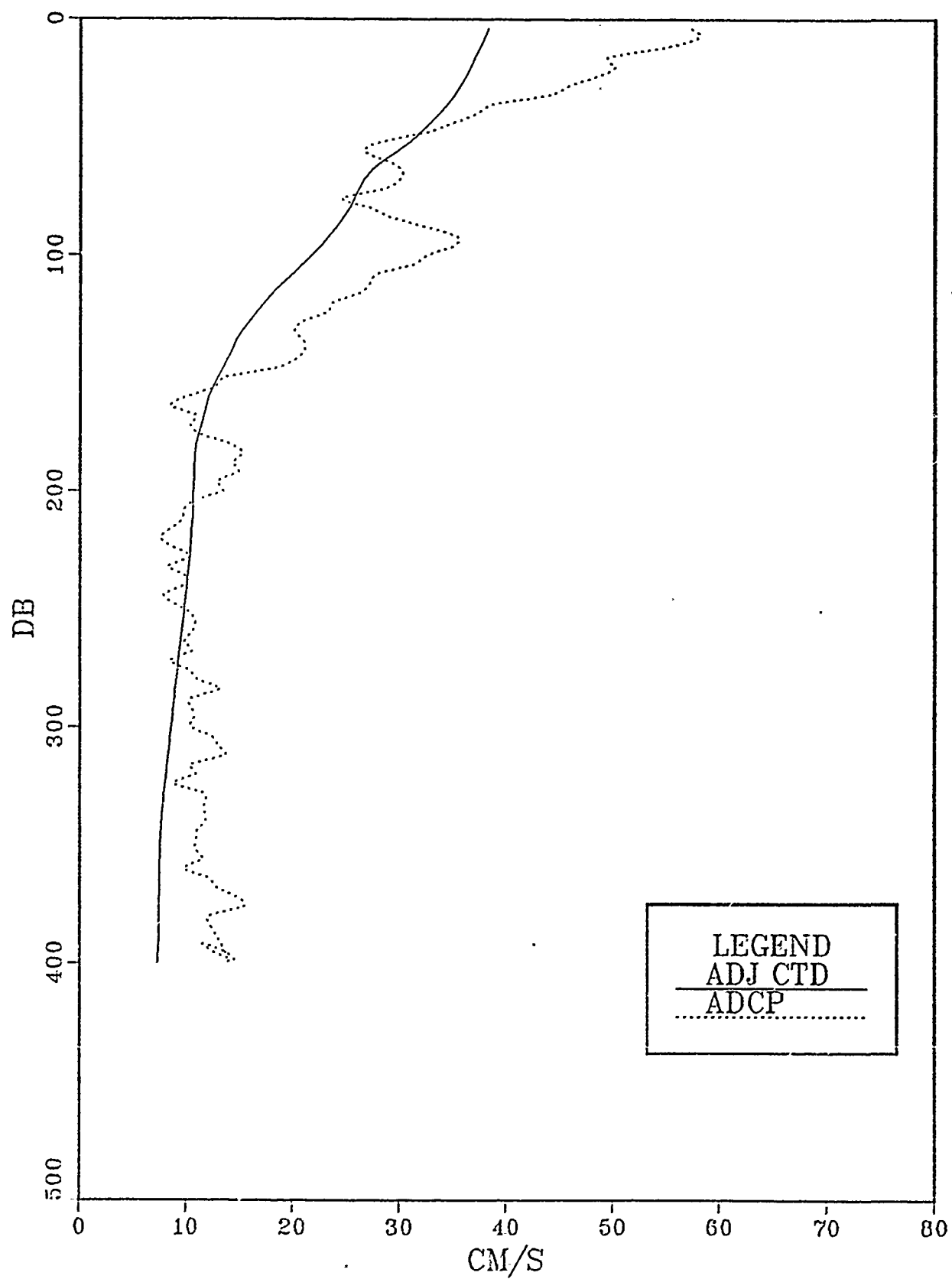
41-42



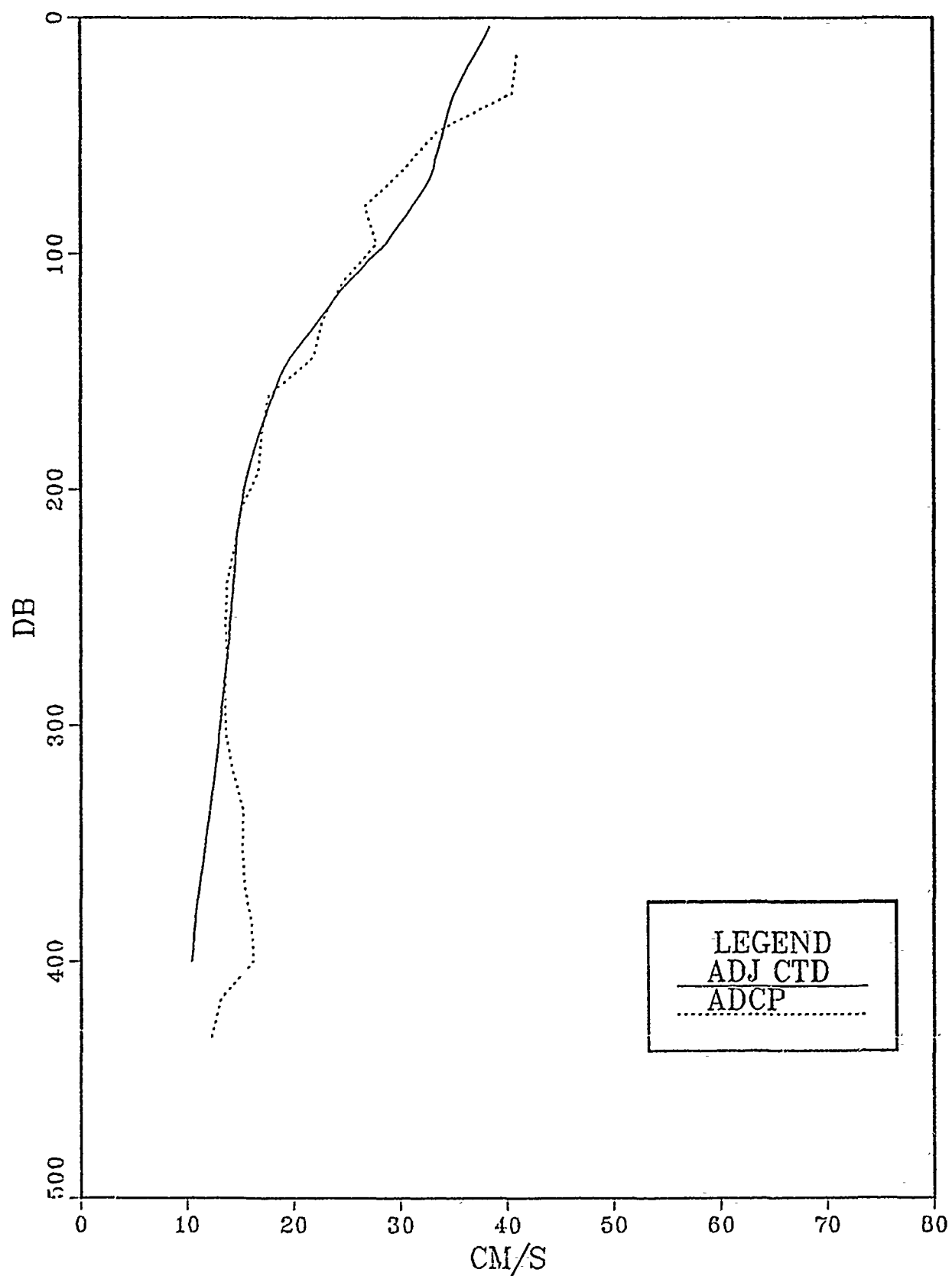
42-43



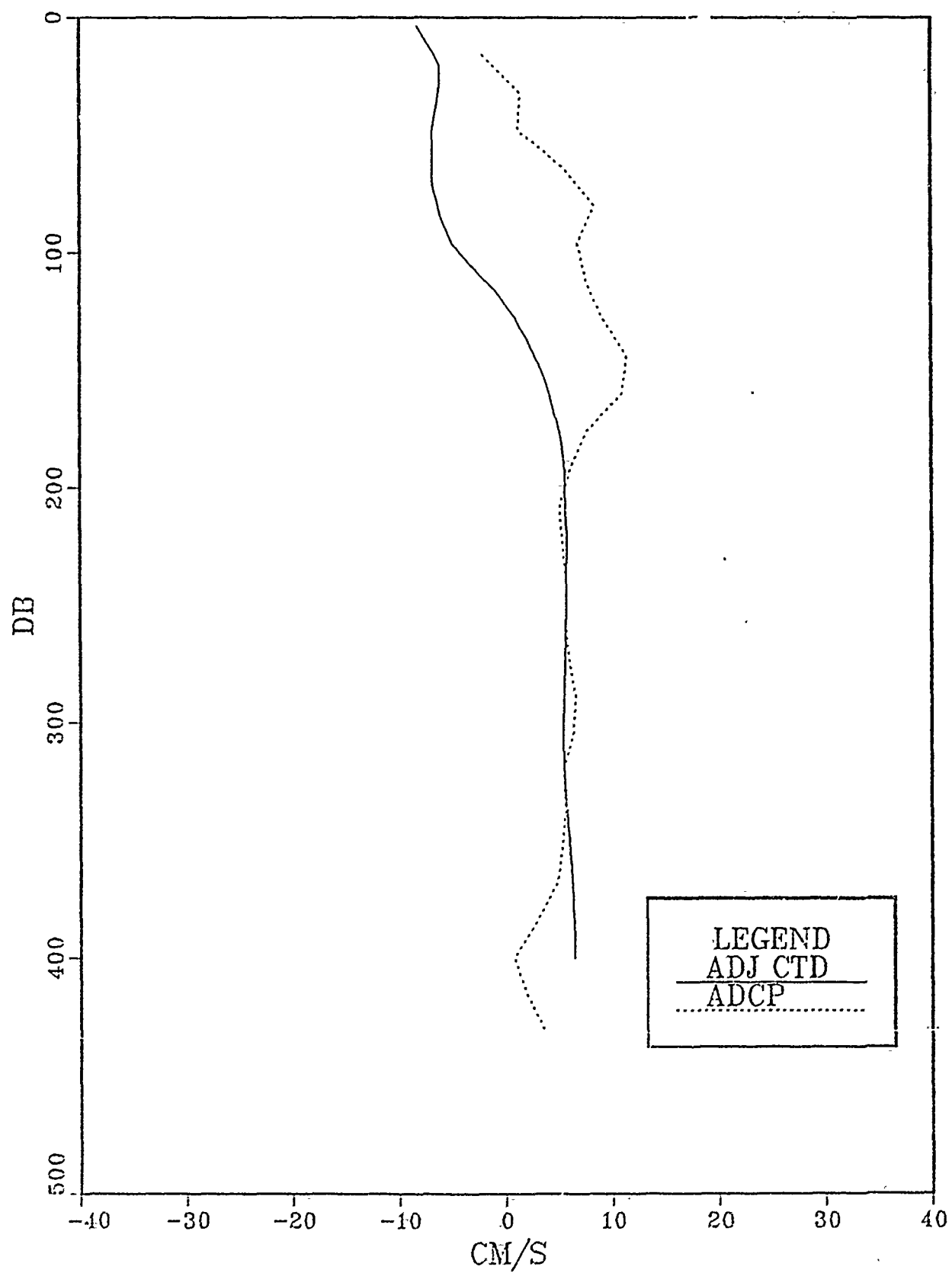
47-48



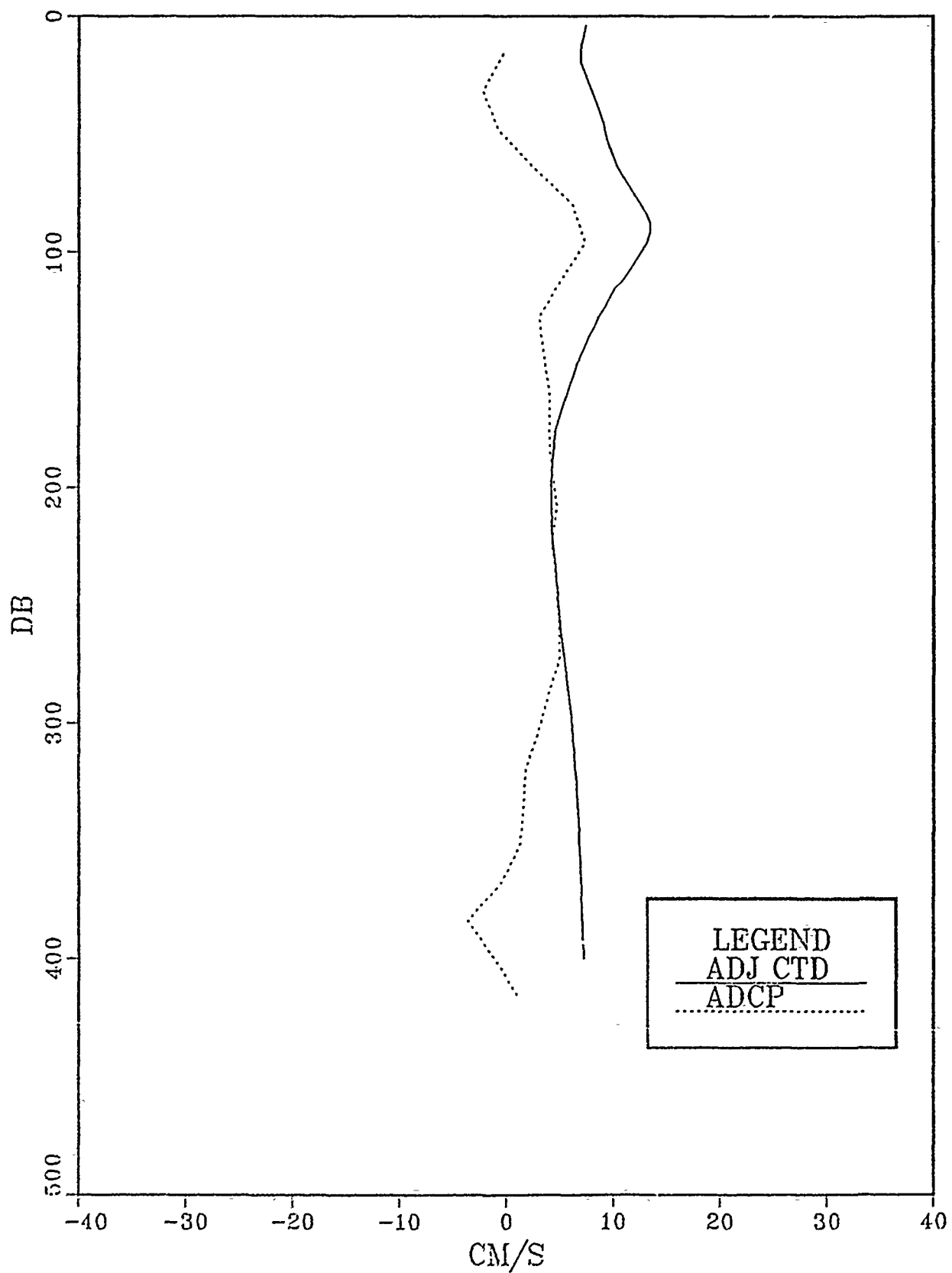
48-49



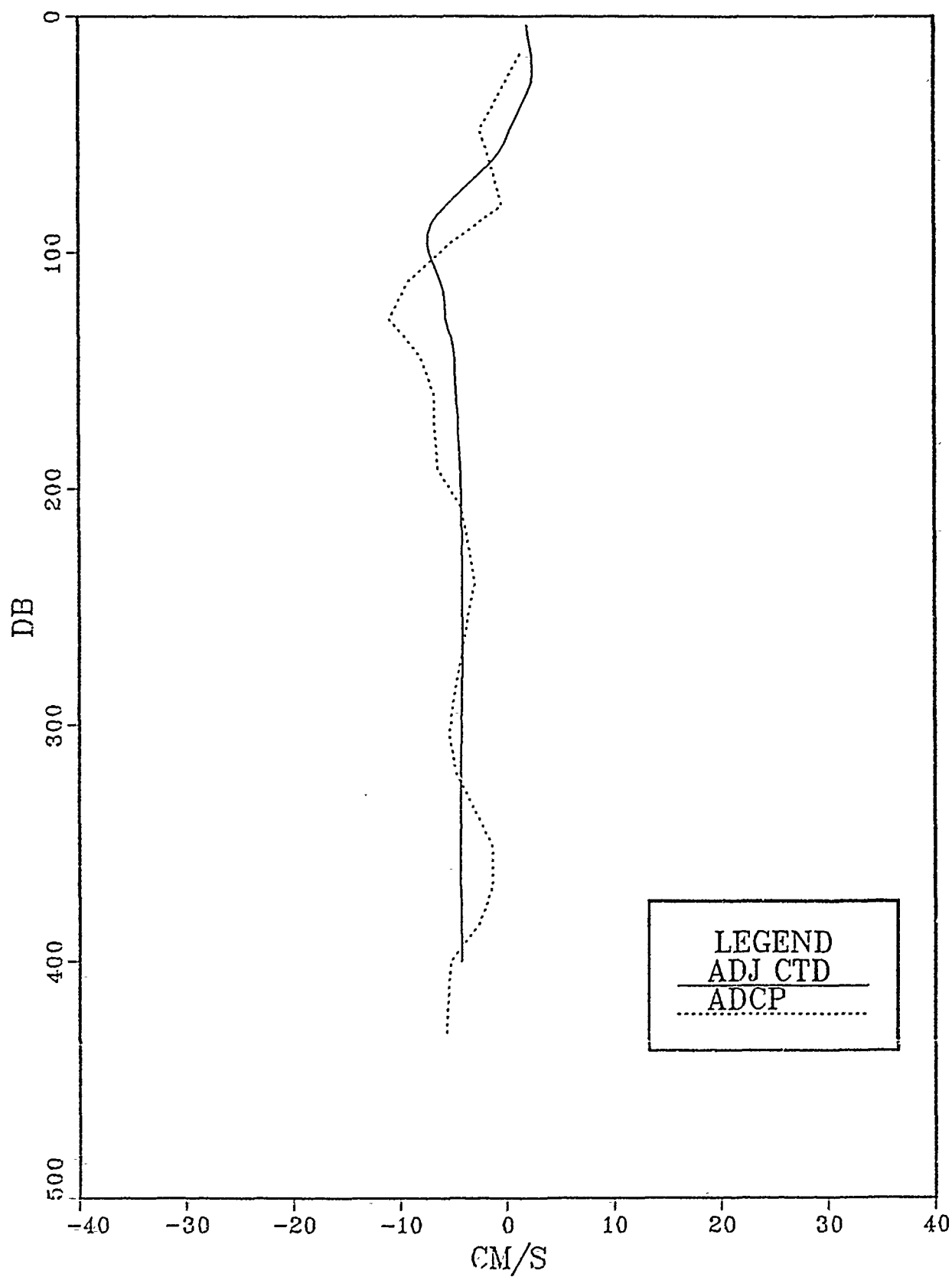
49-50



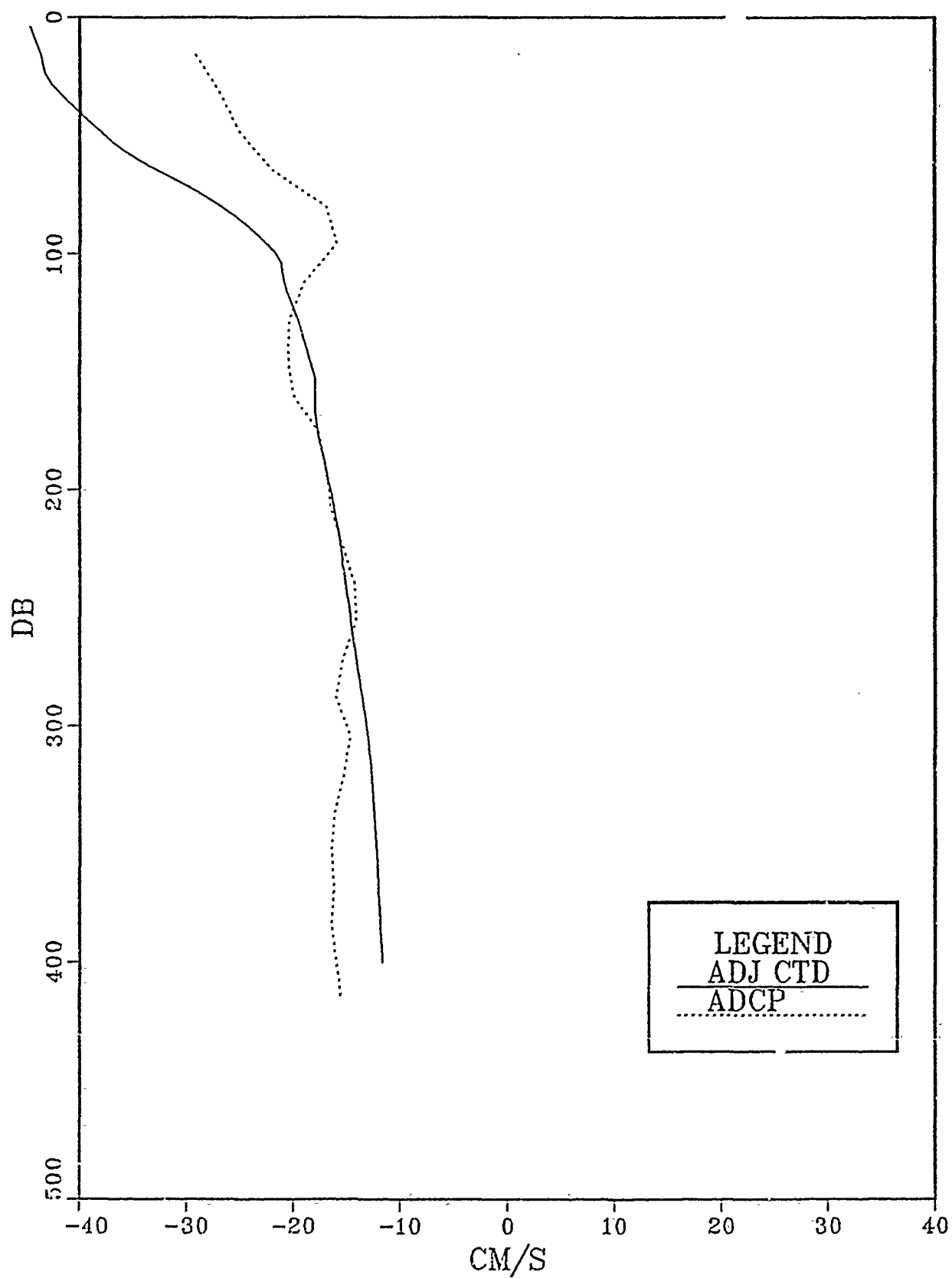
50-51



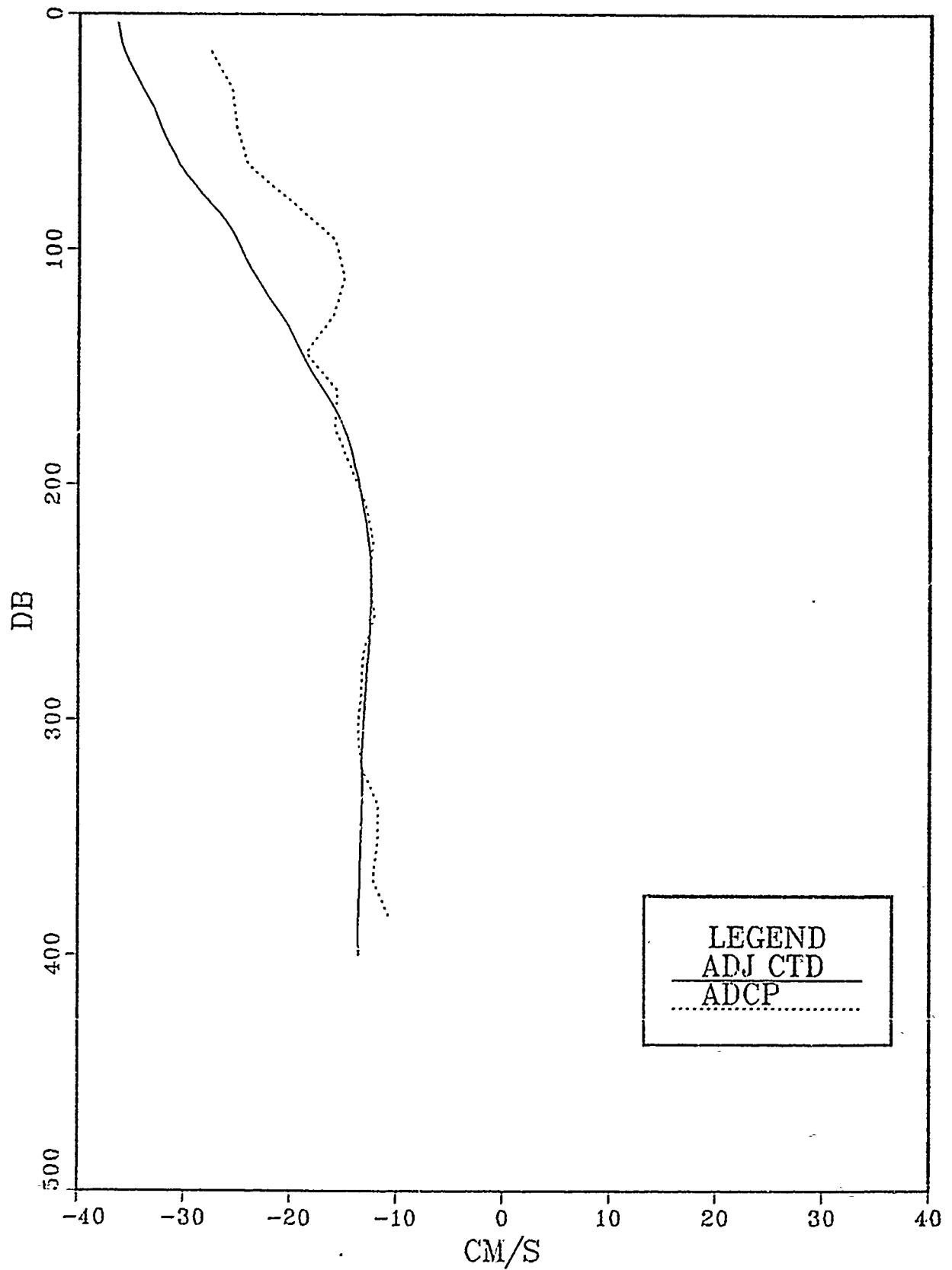
51-52



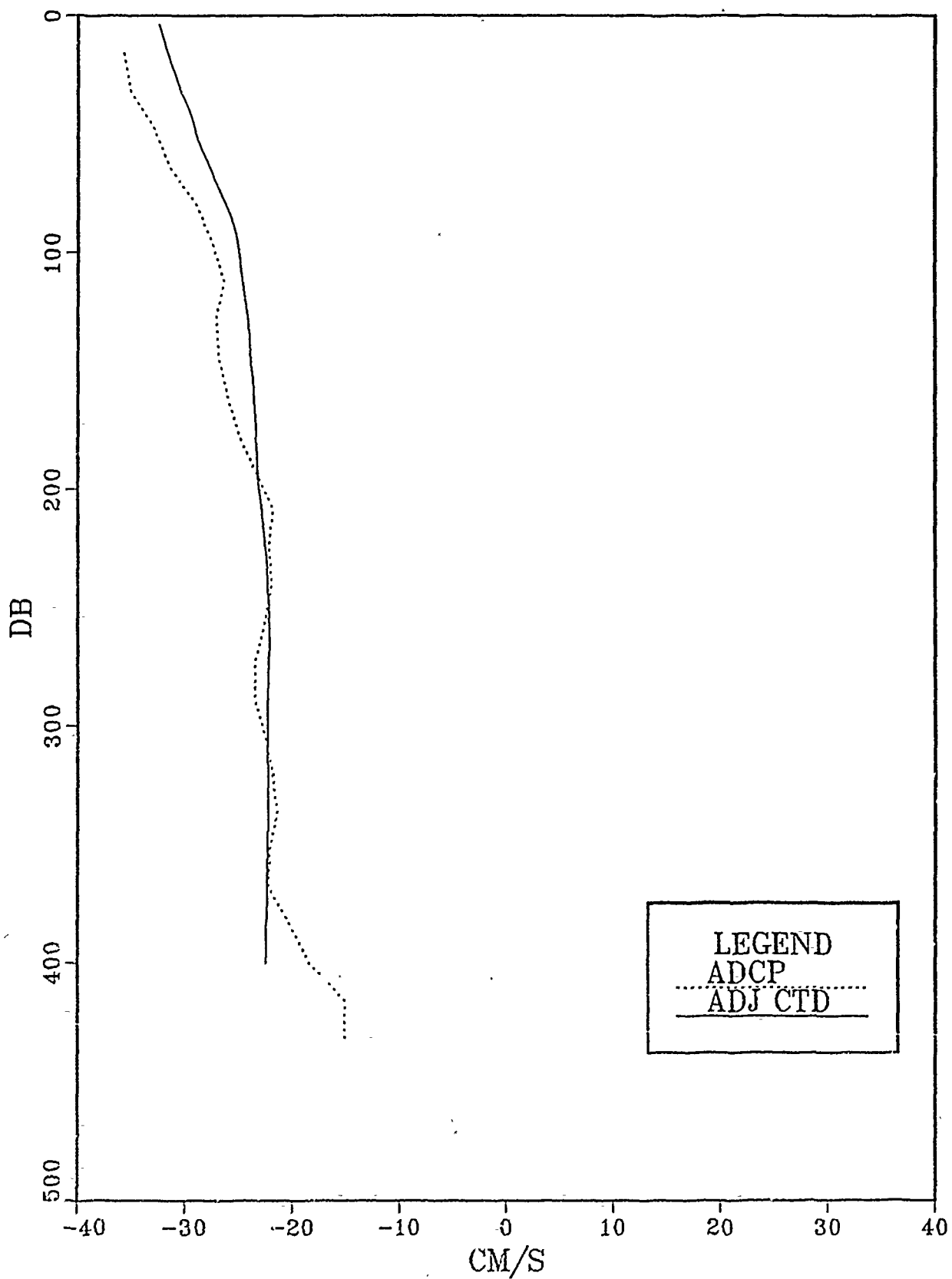
52-53



53-54



54-35



LIST OF REFERENCES

- Batteen, M. L., R. L. Haney, T. A. Tielking, and P. G. Renaud, A numerical study of wind forcing of eddies and jets in the California Current System, *J. Mar. Res.*, 47, 493-523, 1989.
- Best, J. S., Correlation of AVHRR imagery with sub-surface features in the California Current, M.S. thesis, Naval Postgraduate Sch., Monterey, Calif., 1989.
- Brink, K. H., The near-surface dynamics of coastal upwelling, *Prog. in Oceanogr.*, 12, 227-257, 1983.
- Brink, K. H., Coastal ocean physical processes, *Rev. Geophys.*, 25, 204-216, 1987.
- Chereskin, T.K., E. Firing, and J.A. Gast, On identifying and screening filter skew and noise bias in acoustic Doppler current profiler measurements, *J. Atmos. Ocean. Technol.*, submitted.
- Firing, E., Report from the WOCE/NOAA workshop on ADCP measurements, held in Austin, Texas, March 1-2, 1988, U.S. WOCE Planning Report No. 13, 97 pp., U.S. Planning Office for WOCE, College Station, TX, 1988.
- Flament, P., L. Armi, and L. Washburn, The evolving structure of an upwelling filament, *J. Geophys. Res.*, 90, 11765-11778, 1985.
- Huyer, A. and P. M. Kosro, Mesoscale surveys over the shelf and slope in the upwelling region near Point Arena, California, *J. Geophys. Res.*, 92, 1655-1681, 1987.
- Jessen, P. F., and S. R. Ramp, Velocity structure associated with a cold filament off Point Arena, California, during July 1988, *Eos Transactions*, 69, 1259, 1988 (abstract only).
- Jessen, P. F., S. R. Ramp, and C. A. Clark, Hydrographic data from the pilot study of the Coastal Transition Zone (CTZ) program, 15 - 28 June 1987, *NPS-69-89-004*, Naval Postgraduate Sch., Monterey, Calif., 1989.
- Kosro, P. M., Shipboard acoustic current profiling during the Coastal Ocean Dynamics Experiment, Ph.D thesis, *SIO Ref. 85-8*, 119 pp Scripps Inst. of Oceanogr., La Jolla, Calif. 1985.
- Kosro, P. M., and A. Huyer, CTD and velocity surveys of seaward jets off northern California, July 1981 and 1982, *J. Geophys. Res.*, 91, 7680-7690, 1986.
- McCreary, J. P., P. K. Kundu, and S.-Y. Chao, On the dynamics of the California Current system, *J. Mar. Res.*, 45, 1-32, 1987.

- Narimousa, S. and T. Maxworthy, On the effects of coastline perturbations on coastal currents and fronts, *J. Phys. Oceanogr.*, 17, 1296-1303, 1987.
- Narimousa, S. and T. Maxworthy, Two layer model of shear driven coastal upwelling in the presence of bottom topography, *J. Fluid Mech.*, 159, 503-531, 1985.
- Peffley, M. B., and J. J. O'Brien, A three-dimensional simulation of coastal upwelling off Oregon, *J. Phys. Oceanogr.*, 6, 164-180, 1976.
- Pierce, S. D., and T. M. Joyce, Gulf Stream velocity structure through inversion of hydrographic and acoustic Doppler data, *J. Geophys. Res.*, 93, 2227-2236, 1988.
- Preller, R., and J. J. O'Brien, The influence of bottom topography on upwelling off Peru, *J. Phys. Oceanogr.*, 10,, 1377-1398, 1980.
- RD Instruments, Acoustic Doppler current profilers, principles of operation, tech. man., San Diego, Calif., 1989.
- Stanton, T. P., and J. Stockel, Relaxation of the CTZ 88 domain, *Eos Transactions*, 69, 1260, 1988 (abstract only).

INITIAL DISTRIBUTION LIST

		No. Copies
1.	Defense Technical Information Center Cameron Station Alexandria, VA 22304-6145	2
2.	Library, Code 0142 Naval Postgraduate School Monterey, CA 93943-5002	2
3.	Chairman (Code 63Rd) Department of Meteorology Naval Postgraduate School Monterey, CA 93943-5000	1
4.	Chairman (Code 68Co) Department of Oceanography Naval Postgraduate School Monterey, CA 93943-5000	1
5.	Professor C. A. Collins (Code 68Co) Department of Oceanography Naval Postgraduate School Monterey, CA 93943-5000	1
6.	Professor Steven R. Ramp (Code 68Ra) Department of Oceanography Naval Postgraduate School Monterey, CA 93943-5000	2
7.	Professor Timothy P. Stanton Department of Oceanography Naval Postgraduate School Monterey, CA 93943-5000	1
8.	Director Naval Oceanography Division Naval Observatory 34th and Massachusetts Avenue NW Washington, DC 20390	1
9.	Commander Naval Oceanography Command Naval Oceanography Command Stennis Space Center, MS 39529-5000	1
10.	Commanding Officer Fleet Numerical Oceanography Center Monterey, CA 93943	1

- | | | |
|-----|--|---|
| 11. | Commanding Officer
Naval Oceanographic Office
Stennis Space Center, MS 39522-5001 | 1 |
| 12. | Commanding Officer
Naval Ocean Research and Development Activity
Stennis Space Center, MS 39522-5001 | 1 |
| 13. | Commanding Officer
Naval Environmental Prediction Research Facility
Monterey, CA 93943-5006 | 1 |
| 14. | Chairman, Oceanography Department
U. S. Naval Academy
Annapolis, MD 21402 | 1 |
| 15. | Chief of Naval Research
800 North Quincy Street
Arlington, VA 22217 | 1 |
| 15. | Office of Naval Research (Code 420)
Naval Ocean Research and Development Activity
800 North Quincy Street
Arlington, VA 22217 | 1 |
| 16. | Office of Naval Research
Code 1122PO
800 North Quincy Street
Arlington, VA 22217
Attn: Dr. David Evans | 1 |
| 17. | Office of Naval Research
Code 1122PO
800 North Quincy Street
Arlington, VA 22217
Attn: Dr. Tom Kinder | 1 |
| 18. | Lt. Francis L. Daggett
SWOSCOLCOM
NETC
Newport RI 02841 | 2 |
| 19. | Prof. Robert L. Haney
Department of Meteorology
Naval Postgraduate School
Monterey, CA 93943-5000 | 1 |
| 20. | Mr. Paul Jessen
Department of Oceanography
Naval Postgraduate School
Monterey, CA 93943-5000 | 1 |

- | | | |
|-----|---|---|
| 21. | Dr. John Allen
College of Oceanography
Oregon State University
Corvallis, OR 97331 | 1 |
| 22. | Dr. Leonard Walstad
College of Oceanography
Oregon State University
Corvallis, OR 97331 | 1 |
| 23. | Dr. P. Michael Kosro
College of Oceanography
Oregon State University
Corvallis, OR 97331 | 1 |
| 24. | Dr. A. Huyer
College of Oceanography
Oregon State University
Corvallis, OR 97331 | 1 |
| 24. | Dr. Robert Smith
College of Oceanography
Oregon State University
Corvallis, OR 97331 | 1 |
| 25. | Lt. A. Negron, USN (Code 35)
Air-Ocean Sciences Programs
Naval Postgraduate School
Monterey, CA 93943-5000 | 1 |